INFORMATION TO USERS

This manuscript has been reproduced from the microfilm master. UMI films the text directly from the original or copy submitted. Thus, some thesis and dissertation copies are in typewriter face, while others may be from any type of computer printer.

The quality of this reproduction is dependent upon the quality of the copy submitted. Broken or indistinct print, colored or poor quality illustrations and photographs, print bleedthrough, substandard margins, and improper alignment can adversely affect reproduction.

In the unlikely event that the author did not send UMI a complete manuscript and there are missing pages, these will be noted. Also, if unauthorized copyright material had to be removed, a note will indicate the deletion.

Oversize materials (e.g., maps, drawings, charts) are reproduced by sectioning the original, beginning at the upper left-hand corner and continuing from left to right in equal sections with small overlaps. Each original is also photographed in one exposure and is included in reduced form at the back of the book.

Photographs included in the original manuscript have been reproduced xerographically in this copy. Higher quality 6" x 9" black and white photographic prints are available for any photographs or illustrations appearing in this copy for an additional charge. Contact UMI directly to order.

UMI

A Bell & Howell Information Company
300 North Zeeb Road, Ann Arbor MI 48106-1346 USA
313/761-4700 800/521-0600

Resonant Magnetization Tunneling in High-Spin Molecules

by

Jonathan R. Friedman

A dissertation submitted to the Graduate Faculty in Physics in partial fulfillment of the requirements for the degree of Doctor of Philosophy, the City University of New York.

1996

This manuscript has been read and accepted for the Graduate Faculty in Physics in satisfaction of the dissertation requirement for the degree of Doctor of Philosophy.

September 24, 1996
Date

Myriam P. Sarachik
Dist. Prof. Myriam Sarachik
Chair of Examining Committee

September 24, 1996
Date

Joseph B. Krieger
Prof. Joseph Krieger
Executive Officer

Supervisory Committee

Prof. Eugene Chudnovsky
Dr. David DiVincenzo
Prof. Marilyn Gunner
Prof. Frederick Smith

THE CITY UNIVERSITY OF NEW YORK

Abstract

Resonant Magnetization Tunneling in High-Spin Molecules

by

Jonathan R. Friedman

Thesis Advisor: Dist. Prof. Myriam P. Sarachik

I present experimental data indicating that $Mn_{12}O_{12}(CH_3COO)_{16}(H_2O)_4$, a system of high-spin molecules, exhibits thermally assisted field-tuned resonant tunneling. I also develop a theoretical framework to explain much of the data. The evidence for tunneling is that, in oriented samples of this material, one finds steps in the hysteresis loops at regular intervals of magnetic field, dips in the superparamagnetic blocking temperature and concomitant increases in the magnetic relaxation rate at the same fields. This data is explained in terms of a simple model that makes quantitative predictions that are in reasonable agreement with the experimental data. In Chapter I, I review some of the theory of macroscopic quantum tunneling of magnetization and provide some background information about this molecular magnet . Chapter II covers experimental techniques: sample preparation, measuring devices and data-taking procedures. In Chapter III, I present the experimental data obtained from samples of Mn_{12}, showing the aforementioned steps in the hysteresis loops and related phenomena. A section of that chapter

will be devoted to a detailed study of the effect of a transverse magnetic field on the magnetic relaxation. The theory of tunneling in a large spin is developed in Chapter IV, where a simple Hamiltonian is shown to predict some very interesting effects and a phenomenological model of spin relaxation is analyzed. Chapter V consists of discussion and interpretation of the experimental data and comparison of the data with the theory developed in Chapter IV. The chapter ends with some detailed discussion of the data that so far eludes explanation. In Chapter V, I conclude by discussing possible future experiments and other systems that show magnetization steps.

DEDICATION

To the memory of my mother

Acknowledgments

There are many people who deserve my gratitude. Their contributions and support cannot be exaggerated.

Prof. Myriam Sarachik defines what it means to be a thesis mentor. Her insights and probing questions have served to hone my thoughts and clarify the essential issues just when I was getting bogged down in details. She has given me a great deal of freedom to pursue the research directions I thought were important. She has made me wiser in matters scientific, professional and personal. I am quite fortunate to consider her a friend. In comparison, it seems a trifle to also acknowledge her assistance in editing this dissertation.

I have been fortunate to effectively have had two thesis mentors. Prof. Eugene Chudnovsky is a rare theorist, capable of communicating easily with experimentalists , using clear physical pictures. I have learned a great deal from his tutorials and from many, many conversations. He is responsible for suggesting Mn_{12} as a material to study. Without him, this would be a very different manuscript: the data would be much less fully understood and chapter IV would probably not exist at all. I am grateful for his interest in my work, my career and my life.

I owe a great debt to Prof. Javier Tejada of the University of Barcelona. He was kind enough to bestow upon me a small portion of his knowledge of magnetism and to train me in magnetic measurement techniques. I also had the opportunity to work with his student Joan Manel Hernandez and postdoc Xixiang Zhang. It was a pleasure to work with them and learn from them. I hope they got as much from the collaboration as I did.

Ron Ziolo was the chemist of the collaboration. As well as making the samples, he was very helpful in helping me understand some of the underlying chemistry of Mn_{12} and assisted me in wading through some jargon. Jennifer Maciejewski was a summer student working with him who assisted in making some samples and deserves my thanks as well.

Outside of my immediate collaborators on this project, there are many other people who deserve acknowledgment and my gratitude. Snezana Bogdanovich is another member of Prof. Sarachik's research group with whom I have had the pleasure of working and consulting. She has made some very useful suggestions concerning the research and asked some probing questions. Her interest in my work, even when she was only serving as a sounding board, has always been appreciated. She has been extremely supportive to me at times when the research was not going very smoothly. I truly value her friendship.

Peihua Dai and Youzhu Zhang, former postdocs in the Sarachik group, trained me in the day-to-day life of a low-temperature physicist. From Peihua I learned that there is almost always a creative solution to every problem. He also taught me how to work cautiously but efficiently. Youzhu taught me the importance of patience in scientific work, a virtue I appreciate more and more as I acquire it.

Dimitri Simonian and Sergey Kravchenko, currently in the Sarachik group, have always expressed interest in my work. I have enjoyed talking to them about it.

Dariusz Przybylski and Lucianne Walkowicz assisted me in the preparation of samples for measurements. Lucianne along with Yuri Artemov also deserve thanks for helping me with some data analysis.

Mr. Joseph Altmann, the machine shop foreman, has always been extremely helpful to me, assisting me in the design of equipment, and instructing me in machining techniques and methods of technical drawing. Machinists Joseph Duke and Linden Langhorne are to be thanked for their very professional work. They never complained when I asked for a job to be modified.

I also wish to thank some of the people at Quantum Design, the company that designed and built the magnetometer used for the measurements presented herein. Chris Gardner installed the machine and made a special visit to investigate a temperature-control problem. I have had many useful conversations with him about cryogenic design and SQUID noise reduction. Ben Thorsen, now of the spinoff company Quantum Magnetics, gave me some very useful advice on how to reduce noise problems when I was trying (unsuccessfully) to build a homemade magnetometer. Ron Sager and Stefano Spagna gave me some useful tips on cryogenics on various occasions. Dr. Spagna also was generous enough to give me a tour of Quantum Design, show me new equipment and share with me some very interesting data on a material very similar to that studied for this work. Quantum Design also allowed me to reproduce some figures from their equipment manuals for use in this document.

Prof. Herman Cummins and his student Wolfgang Losert graciously permitted me to use their microscopes and imaging equipment to examine the orientation of the samples. Prof. Frederick Smith also allowed me to use his microscope, with its Polaroid camera.

Sheila Aubin of the UCSD Chemistry Department kindly discussed with me her similar work on other Mn_{12} compounds and sent me some relevant papers.

Dr. Alexander Burin has shared with me many of his theoretical ideas on magnetic relaxation. I have found our conversations to be very stimulating and informative.

Prof. Joseph Birman and I have had some interesting discussions about some theoretical questions. I very much appreciate his input and interest.

Prof. Simon Foner of the Massachusetts Institute of Technology has performed some pulsed-field measurements on some of our samples and has shared the results with me. He has also made some useful comments on some of our early preprints.

There are some people who have had less direct, but not less important, roles in this work. Dr. Ralph Siegel has always been available when I would get stuck in some calculation or when I needed an outside perspective. As someone only casually familiar with my area of study, he demanded clear physical explanations that often served to clarify my own ideas. I have gained a lot of insight through our conversations.

Jerry Altzman has allowed me to pick his brain about mathematical questions and has assisted me in some computer programming. Dr. Michael Cavicchia has given me a lot of support and advice, much of which is fairly intangible.

I also wish to thank the members of my thesis committee, who have all shown a great deal of interest in my work and my career. Other than those mentioned above, they include Dr. David DiVincenzo, Prof. Frederick Smith and Prof. Marilyn Gunner. I thank them for their support and for the task of reading this manuscript, a task I hope was not too grueling. Prof. Gunner deserves special thanks for the many times she permitted me to use her laboratory equipment.

None of this work would have been possible without financial support. I am grateful to the U.S. Air Force Office of Scientific Research, which funded this research project under grant number F49620-92-J-0190.

Lastly, I wish to express my gratitude to Teresa Buswell, who has provided me with extensive emotional support, bolstering me when I needed it and tolerating my need to work late hours.

Table of Contents

List of Tables

List of Figures

I. Introduction

The concept of quantum tunneling is almost as old as quantum mechanics itself. The ability of a particle to traverse a classically forbidden region has become ubiquitous in physics: an alpha particle decaying out of a nucleus, electron-hopping conduction in insulators, Cooper pairs tunneling through a Josephson Junction, etc. In the late 1970's and early 1980's, Caldeira and Leggett[1,2] developed the formal theory of macroscopic quantum tunneling, which predicted that under suitable circumstances "macroscopic" objects, consisting of many (thousands of) microscopic entities strongly coupled together, could exhibit uniquely quantum-mechanical properties. The first clear experimental evidence for macroscopic quantum tunneling was provided by Clarke, et al.[3], who showed that in a Josephson Junction the phase of the superconducting order parameter across the junction can tunnel from a "superconducting" zero-voltage state to a "normal" finite-voltage state.

The possibility of quantum tunneling of magnetization was first suggested by Bean and Livingston in their 1959 paper on superparamagnetism.[4] The concept has been revisited periodically,[5-11] and has recently become a subject of great interest. Guided by the work of Caldeira and Leggett,[1,2] important theoretical progress was made in the late 1980's.[12-14]

Experimental evidence for tunneling has been reported by Awschalom and coworkers,[15] who have observed a resonance in the susceptibility of horse-spleen ferritin at very low temperatures; they attribute this to quantum coherent tunneling of the magnetization vector between two degenerate orientations in a double well potential. These results have received much attention, and have elicited considerable debate.[16]

A great deal of effort has been devoted to obtaining experimental evidence of quantum tunneling of magnetization from measurements of the magnetic relaxation. In many materials[17-21] the magnetic viscosity levels off to a constant, temperature-independent value below some crossover temperature, contrary to what one expects by classical (thermal) processes. This has been attributed to quantum-mechanical reversal of the magnetization. The occurrence of this phenomenon in a wide variety of systems strongly supports this interpretation, although relaxation measurements do not often lend themselves to rigorous comparison with theory.[22] With the notable exception of single-crystal orthoferrite $TbFeO_3$, where exponential magnetic relaxation indicates a single energy barrier throughout the material,[23] the magnetic relaxation observed in most materials represents a statistical average over a large number of events broadly distributed in energy and time scale due to random factors such as particle size, thus making quantitative comparison with theory difficult.

It is thus very desirable for relaxation measurements (and imperative for experiments on resonant absorption) to obtain samples containing magnetic clusters that are closely monodispersed. In this work I present

results on such a material, $Mn_{12}O_{12}(CH_3COO)_{16}(H_2O)_4$, often referred to as Mn_{12} acetate, or simply Mn_{12}. Unlike most ensembles of magnetic clusters, the magnetic subunits of such a molecular crystal have unique, chemically determined properties: a macroscopic sample of Mn_{12} is comprised of a large (Avogadro's) number of identical (or nearly identical) entities with the same magnetic properties and identical characteristic energies. Another important feature of this system is that while the spin of each cluster, S=10, is large for a molecular system, it is small relative to most superparamagnetic systems. This small spin value together with the system's large magnetocrystalline anisotropy yields an appreciable energy separation between spin levels, allowing the observation of a novel physical effect: resonant spin tunneling between matching levels on opposite sides of a potential barrier.

In this dissertation, I will present experimental data indicating that Mn_{12} exhibits thermally assisted field-tuned resonant tunneling. I will also develop a theoretical framework to explain much of the data. The evidence for tunneling, in brief, is that in oriented samples of Mn_{12} one finds steps in the hysteresis loops at regular intervals of magnetic field, dips in the superparamagnetic blocking temperature and concomitant increases in the magnetic relaxation rate at the same fields. This data can be explained in terms of a simple model that makes quantitative predictions that are in reasonable agreement with the experimental data. Much of what is presented here has been published[24-26] or is in various stages of preparation for publication.[27,28] In addition, some very recent work[29] by independent researchers has confirmed some of the results presented in those papers and in this dissertation.

In the remainder of this chapter, I will review some of the theory of macroscopic quantum tunneling of magnetization and then provide some background information about Mn_{12}, summarizing what was heretofore known about this molecular-magnetic system . Chapter II will be devoted to experimental techniques: sample preparation, measuring devices and data-taking procedures. In Chapter III, I will present the experimental data obtained from samples of Mn_{12}, showing the aforementioned steps in the hysteresis loops and related phenomena. A section of that chapter will be devoted to a detailed study of the effect of a transverse magnetic field on the magnetic relaxation. The theory of tunneling in a large spin is developed in Chapter IV, where a simple Hamiltonian is shown to predict some very interesting effects and a phenomenological model of spin relaxation is analyzed. Chapter V consists of discussion and interpretation of the experimental data and comparison of the data with the theory developed in Chapter IV. An alternative interpretation of the data is mentioned and the chapter ends with some detailed discussion of the data that so far eludes explanation. I will conclude this dissertation in Chapter VI, where I discuss possible future experiments and end with comments on other systems that show magnetization steps.

A. Review of Quantum Tunneling of Magnetization

The semiclassical concept of tunneling usually involves the notion of a particle that escapes from a metastable potential well without having

sufficient energy to overcome the potential barrier: instead of climbing over the barrier, it "tunnels" through it. One imagines that such a particle moves from one place to another without having been anywhere in between. The tunneling of the magnetization vector in a small magnetically ordered particle differs somewhat from this picture in that there is no particle moving in real Cartesian space. Magnetization tunneling occurs in angular space with the magnetization vector rotating from one potential minimum to another.

In this section I shall review the theoretical and experimental work on magnetization tunneling developed over the last decade or so. Although a slight simplification, the field will be divided into two categories. The first, tunneling in single-domain particles, will be treated in a fair amount of detail, since it is the most relevant to the work presented in subsequent sections. The second, tunneling of domain walls and quantum nucleation, will be discussed very briefly at the end of this section.

Tunneling in single-domain particles was first described by Chudnovsky[30] and later developed theoretically by Chudnovsky, Gunther, Enz and Schilling, van Hemmen and Suto, Loss, DiVincenzo, Garg and Kim, Stamp, Barbara and others, and has been reviewed.[31-33] Following the treatment presented by Chudnovsky and Gunther[12] (but with slightly different notation), we shall consider a single-domain particle of sufficiently small size (smaller than the domain-wall width) that it can be treated as a single large spin. Further, we assume that the exchange interactions between the spins within the particle are so strong that the internal degrees of freedom (magnons) can be neglected. The presence of anisotropy gives the

magnetization vector a preferred direction, the easy axis. The Hamiltonian for the magnetization can be written as

$$\mathcal{H} = -DS_z^2 + D'S_y^2 - g\mu_B BS_z, \tag{1.1}$$

where D and D' are the anisotropy constants originating from either the crystal lattice or the shape of the particle, **S** is the spin vector and B the magnetic induction, applied along the z axis. In this model, the easy axis is the z axis, the hard axis is the y axis and the x-z plane is called the easy plane. It is in or near to this plane that the magnetization vector will rotate (or tunnel). Now, in the absence of a magnetic field, the magnetization has two equivalent energy minima, corresponding to being aligned parallel or antiparallel to the z axis. In order to switch from one minimum to another, the system must overcome a barrier of energy $U = DS^2$. The height of the barrier can be reduced by the applied field. The potential energy in the easy plane is shown schematically in Fig. 1.1, where the asymmetry is produced by an external field. At high temperatures, the magnetization is easily thermally activated over the barrier and remains in one well for a time much shorter than typical measurement times. Thus, it behaves like a paramagnet and, being a large-spin object, is dubbed a "superparamagnet."

The rate for making a transition from one well to the other is described by an Arrhenius law, $\Gamma = \omega_0 \exp(-U/kT)$, where ω_0 is called the attempt frequency and represents the frequency of small oscillations in the metastable well. When the temperature is reduced below a certain temperature (the so-called blocking temperature), there is not sufficient thermal energy to induce transitions over the barrier and the system is said

to be "blocked," or trapped in one well or the other. Transitions from one well to another can still be observed, but their rate is slow compared to the measurement time. It is in this low-temperature regime that one might expect to find evidence for tunneling.

The tunneling at zero temperature can be calculated by the WKB method using instanton techniques. While we shall not go into the details of these techniques here, a few words seem appropriate. In the WKB method the semiclassical transition rate is proportional to $\exp(i\, S_{cl})$, where S_{cl} is the classical (minimal) action for the motion in question. When a barrier is present, no classical action can be found and the use of instanton techniques

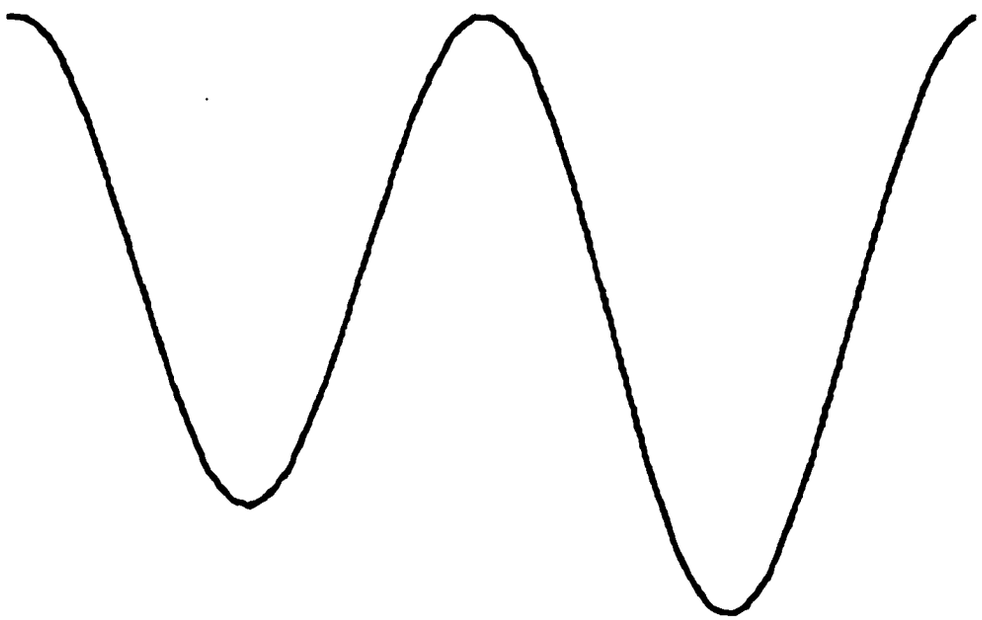

Fig. 1.1 Double-well potential relevant to spin tunneling. One well corresponds to spin up, the other to spin down. The asymmetry is due to an applied field.

is warranted. Briefly, the technique involves making time imaginary by the transformation $\tau=it$ and solving for the minimal imaginary-time action, S_{im}. This is equivalent to finding the minimal action for the inverted potential, where the barrier is now a well. The transition rate is then proportional to $\exp(-S_{im})$.

For the Hamiltonian given in Eq 1.1 with a small field-tuned barrier, Chudnovsky and Gunther found the tunneling rate to be

$$\Gamma \propto \exp[-\tfrac{8}{3}(\tfrac{D}{D'})^{1/2}(1-B/B_c)^{3/2}S], \qquad (1.2)$$

where B_c is the critical field at which the barrier disappears. Note that the tunneling rate goes to zero as D' goes to zero. This is expected since in that limit the Hamiltonian commutes with S_z and the eigenstates of S_z are then stationary.

One way to promote tunneling is by applying a transverse magnetic field, for example, to break the rotational symmetry of the system. This case has been treated in some detail by van Hemmen and Süto. Using WKB techniques, they calculated the tunneling rate for the following Hamiltonian (again in slightly different notation).

$$\mathcal{H} = -DS_z^2 - g\mu_B B_\perp S_x$$

For this case, they find the ground-state tunnel splitting to be

$$\Gamma \propto \left(\frac{eg\mu_B B_\perp}{4DS} \right)^{2S} \tag{1.3}$$

Tunneling is also possible from the excited states. I shall discuss this possibility in more detail in Chapter IV.

One can expect a crossover between this zero-temperature behavior and simple thermal activation. This should occur when the Arrhenius exponent and WKB exponent are equal. For the case of Eq. 1.1, for example, Chudnovsky and Gunther estimate that the crossover from quantum to classical behavior should occur at

$$T_c = \frac{3S\sqrt{DD'}}{8k_,} \sqrt{1 - B / B_c}\,. \tag{1.4}$$

Not surprisingly, the crossover temperature is a monotonic function of the anisotropy.

Quantum tunneling of magnetization is often referred to as an example of macroscopic quantum phenomena, like superconductivity and superfluidity. This is because the object that is tunneling is really a collection of many objects. A single-domain particle can be comprised of more than 1000 spins (and a domain wall several orders of magnitude more). What allows these many objects to act as one? And why does the collective coordinate behave quantum mechanically and not classically? The first of these questions we have already touched upon. The exchange interaction couples the spins in a single-domain particle together so strongly that they

are forced to rotate coherently. The alternative mechanism, the propagation of a domain wall across the particle, is opposed by the cost in exchange energy necessary to form the wall and thus is prohibited when the size of the particle becomes smaller than the domain-wall width.

The other question is more subtle. It can be rephrased as "Why doesn't every macroscopic object held together by strong forces exhibit quantum mechanical properties?" The answer to this question is that dissipation, or interactions with the environment, generally destroys quantum-mechanical coherence in macroscopic objects. In order to observe macroscopic manifestations of quantum-mechanical effects, dissipation must be low. The theory of Caldeira and Leggett [1,2] demonstrates that if one can treat the environment as a set of independent harmonic oscillators linearly coupled to the macroscopic object, then the effect of dissipation is to add a term to the WKB exponent, decreasing the tunneling rate. This effect will not destroy tunneling if the sources of dissipation are infrared-weak. For, they showed, it is the low frequency environmental factors that contribute most to dissipation. Phonons are in fact infrared-weak since, according to the Debye model, the spectral density for acoustic phonons of frequency ω is proportional to ω^3. Garg and Kim [34,35] have shown in detail that phonons have little dissipative effect on the tunneling of magnetization. Very general arguments [31] indicate that electrons in metallic particles can be a significant source of dissipation and so tunneling is generally sought in insulating materials.

We now very briefly review domain-wall tunneling,[31] which has been well reviewed by Stamp, Chudnovsky and Barbara. Here the macroscopic

coordinate is the position, suitably defined, of the domain wall. When a field is applied, the domain wall will move in a plane perpendicular to the field until it becomes pinned on a defect. A certain energy is required to unpin the wall; this energy is the analog of the potential barrier. As with tunneling in single-domain particles, the barrier can be traversed either by thermal activation or tunneling. One expects the tunneling process to dominate in the low-temperature regime. Dissipation for domain walls is not as simple as for particles [31]. Domain walls are solitons and so the assumption of linear coupling to the environment is not justified. Nevertheless, sophisticated techniques for dealing with non-linear couplings to the environment have been developed and show that most forms of dissipation are negligible. In particular, magnons become unimportant in the low-temperature, low-wall-velocity regime [31].

Experimental evidence for quantum tunneling of magnetization has been found in many materials at low temperatures. Many of these studies have been reviewed[15,36-38]. Typical samples consist not of a single barrier, but, rather, of a broad distribution of energy barriers so that only statistical quantities of the whole distribution can be studied. In general, systems with many energy barriers will relax logarithmically with time. The relaxation rate can then be characterized by the so-called magnetic viscosity, $S = dM/d(\ln t)$. For thermal activation, one expects the viscosity to increase linearly with temperature. However, in a variety of systems it is found to cross over to a temperature-independent regime at low temperatures. This temperature-independent viscosity is cited as evidence for quantum tunneling.

Some experiments have attempted to look at systems that have a narrow distribution of barriers. One such experiment by Awschalom, et al. [15] has studied horse-spleen ferritin, an iron storage protein with an inorganic antiferromagnetic iron core. Ac susceptibility measurements at temperatures below 200 mK show a resonance at about 1 MHz that has been interpreted as the signature of coherent tunneling between the two ground state orientations. Other attempts to study systems with well-defined barriers include the measurement of a single Ni or Co particle mounted directly onto a SQUID [37], and studies of high-spin molecules [37,39,40]. One such molecule, Mn_{12}, is the subject of this thesis.

B. Background on Mn_{12}

Mn_{12} acetate has been the focus of a great deal of experimental[37,39-47] and theoretical[48-50] activity since it was first synthesized by Lis[51] in 1980. He found that the compound contains four Mn^{4+} (S = 3/2) ions in a central tetrahedron surrounded by eight Mn^{3+} (S = 2) ions in a non-coplanar ring. The Mn ions are coupled by superexchange through oxygen bridges. Surrounding this central magnetic core are 16 acetate ions and 4 water molecules per molecular cluster. These molecules crystallize into a tetragonal lattice with the c axis having the smallest lattice parameter. Magnetic interactions between molecules are thought to be small both because the nonmagnetic ligands keep Mn ions of different clusters far apart (> 7Å)[51] and because the Curie-Weiss temperature for this system has been measured to be small: several different measurements put it in the range -50 mK to 70 mK.[39,41,42,46]

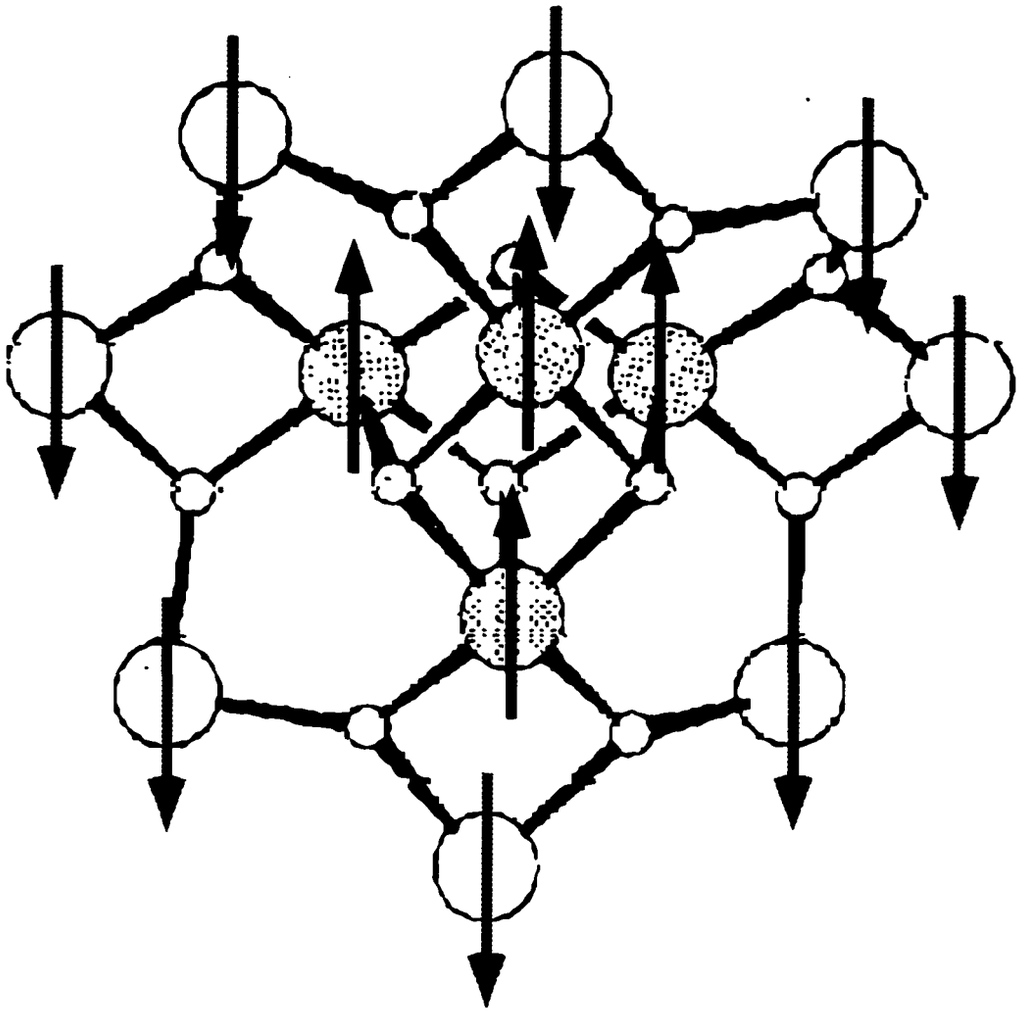

Fig. 1.2 Structure of magnetic core of Mn_{12} molecule. Only the Mn^{4+} (large shaded circles), Mn^{3+} (large open circles) and oxygen (small circles) ions are shown. The arrows indicate a possible configuration of the spins that results in a total spin of 10 for the molecule. (Adapted from Ref. [45]).

Interest in Mn_{12} was renewed in 1991 when the compound was discovered[43] to have an unusually high spin ground state of S=10. This was determined by AC susceptibility measurements in zero DC field and

confirmed by measurements of the DC saturation magnetization. The spin value suggests a simple picture of the spin order within a molecule, with all of the spins of one valence pointing up and the remainder pointing down.[43,44,48] ESR experiments also indicated that Mn_{12} has a large negative magnetocrystalline anisotropy[43,44]. This fact manifests itself in bulk measurements of the magnetization, which shows a peak in the imaginary part of the AC susceptibility[42-44,46] and hysteresis at low temperatures.[40,41,45,47] Unlike bulk magnets, where hysteresis is associated with the motion of domain walls, the hysteresis in Mn_{12} has been associated with the intrinsic bistability of the individual magnetic clusters.[45] Specific heat mesaurements show that no phase transition accompanies the onset of hysteresis[42,46], confirming that the hysteretic behavior is associated with superparamagnetism, not long-range order. AC susceptibility data as well as DC magnetic relaxation data have indicated a single characteristic relaxation time[37,39,41,42,45-47] that obeys an Arrhenius law down to 2.1 K, $1/\tau = (\omega_0/2\pi)\ \exp(-U/kT)$. This would indicate that this system is an ideal superparamagnet: a collection of identical magnetic entities with the same orientation and energy barrier.

From fits of the relaxation time to the Arrhenius law, the barrier height has been found[37,39,41,42,45-47] to be ~61-67 K and the attempt frequency is estimated to be ~10^7 Hz, which is unusually small for superparamagnetic systems. A rough estimate of the size of the energy barrier can be derived from the measured[46,47] anisotropy field for the system, which is about 10 T. This gives a barrier height of ~65 K. The size of the barrier is also estimated from ESR data, which can determine the zero-field splitting parameter D. To leading order, the barrier is simply DS^2. There are two published high-field

ESR studies[43,44] of Mn_{12}, both by the same research group. One gives D = 0.5 cm^{-1} and the other D = 0.6 cm^{-1}, resulting in barrier heights of 72 K and 86 K, respectively. The discrepancy between the two studies is never addressed. In fact, the ESR data reported were obtained using powdered samples. If these samples were orientationally disordered, then no ESR signal should have been found at all since for each crystallite orientation there is a different resonance field. As we shall see in the next chapter, the Mn_{12} crystallites in a powder can be oriented by a large magnetic field. This may explain why any signal was found at all. If the crystallites did not perfectly align with the applied field, the resonances would be shifted to a higher field. This might explain why the values for D are different and inconsistent with the magnitude of the energy barrier determined from the Arrhenius law. Hartmann-Boutron, et al.[50] have suggested a theoretical explanation for the discrepancy, suggesting that there may be a term fourth-order in spin in the Hamiltonian of the system so that the energy barrier would be $DS^2 + A'S^4$. The additional term, however, destroys the possibility for the effects that are described in this thesis.

A number of recent experiments have provided possible evidence for termpareature-independent quantum tunneling at low temperatures in Mn_{12}. Using small single crystals, Barbara *et al.*[37] and Paulsen *et al.*[39,41] found deviations below 2.0 K from Arrhenius-law behavior toward a temperature-independent relaxation rate. Much of their conclusions are based on relaxation experiments that sometimes last several days and, nevertheless, probe only a small fraction of the total decay of the moment. Paulsen *et al.*[39,41] also reported interesting avalanche effects in the hysteresis of this material. Interestingly, these avalanches always occur

near a magnetic field where my collaborators and I report finding a step in the hysteresis loop and accelerated relaxation.

Evidence for thermally assisted resonant tunneling in Mn_{12} has also been put forth. Barbara *et al.*[37] found a maximum in the relaxation time $\tau(H)$ near 2 kOe and a rapid decrease of $\tau(H)$ with decreasing magnetic field; they suggested that the increased tunneling rate at zero field may be due to "the coincidence of the level schemes of the two wells with $S=\pm10$". Very recently, Novak and Sessoli[42] found a similar maximum in the relaxation time at 2 kOe followed by a sharp minimum at approximately 3 kOe. They suggested that this behavior could be due to thermally assisted tunneling between excited states in a double well potential. It should be noted that 3 kOe is not one of the fields at which resonant tunneling is found in the present work.

In the coming pages, I will present what I believe to be compelling evidence that Mn_{12} does in fact exhibit manifestations of resonant tunneling. While not all of the data can be explained, the picture does work remarkably well for the most part. I hope the reader will agree.

II. Experimental Techniques

The experimental techniques employed in this study are fairly straightforward. One important technique is the preparation of oriented powders. Below I will describe this procedure. Then I will go into some of the details concerning the operation of the Quantum Design MPMS-5 magnetometer, which was employed for all of the measurements presented. In particular, I will concentrate on the use of the magnetometer's sample rotator. Lastly, I will sketch out the basic measurement procedure.

A. Sample Preparation

All of the data that are presented herein come from various samples of crystalline Mn_{12}. Powdered samples were obtained from Ron Ziolo at Xerox Corporation, who prepared the material according to the published procedure.[51] Single crystals of Mn_{12} were provided by Javier Tejada at the University of Barcelona. These crystals were prepared by a chemist working in Tejada's group, Elias Molins. Because the samples tended to chemically decompose over time (on the order of months), all samples not in use were stored in an ordinary refrigerator to slow the degradation.

The identity of the powdered sample was verified by Ziolo, who compared an X-ray powder pattern of the material to the published single-crystal

pattern.[51] The spacing along the c-axis lattice parameter was found to be slightly smaller (by about 2%) than the published results. This may be due to the fact that there are fewer molecules of solvation (waters and acetates trapped in the spaces between molecules) present in the crystals. The crystallites were on the order of 10 μm x 1 μm x 1 μm. Some batches provided by Ziolo contained crystallites that were about an order of magnitude smaller in each dimension. This made orienting the crystallites in these preparations particularly difficult (see below).

An X-ray pattern of one of the single crystals was performed by Molins to confirm its identity and verify that it was a single crystal. Other crystals were not checked in this way. However, magnetization measurements on the others could not be distinguished from those on the verified single crystal. It is possible that some of the samples believed to be single crystals are actually twin crystals, with one crystal differing from another by inversion symmetry. Since magnetization is a pseudovector, however, magnetic measurements on single crystals and such twin crystals will yield identical results.

Most of the measurements presented in this dissertation were performed on oriented powders. Only the measurements of relaxation rate in the presence of a transverse field were taken on single crystals. Oriented powder samples were prepared by the following (or similar) procedure. Approximately 10 mg of powdered sample was mixed into Stycast 1266, a non-magnetic epoxy. The epoxy/sample mixture was poured into an ordinary clear plastic soda straw that had been plugged on one end with Devcon 5-minute epoxy. Samples prepared in this way were usually about 0.5 cm in length, not including the plug, which was removed later. While the epoxy was still liquid the straw was

mounted onto a sample rod and placed in a 55-kOe magnetic field, the largest obtainable with our apparatus, at room temperature. The epoxy was allowed to cure in the field (~8 hours). Once the epoxy had cured, the sample was removed from the magnetometer, the straw stripped away and the plug snapped off the bottom of the sample with the help of a vice and a pair of pliers (the pliers were covered with paper towels to prevent contamination of the sample). No extraordinary precautions other than using clean instruments were needed in preparing or handling the sample since its magnetic signal was so large as to obviate anything but the most egregious contamination. Handling of the sample with fingers or a clean pair of tweezers made of non-magnetic stainless steel was usual practice.

The above procedure was performed in order to orient the crystallites so that their c-axes (the easy magnetization axis) aligned with the direction of the applied magnetic field. The crystallites torqued to orient with the applied field because their susceptibility is anisotropic. Most likely this anisotropy arises from the elongated shape of the crystals and the concomitant fact that the demagnetizing factor depends on the relative orientation of the sample with respect to the field direction. The orientation of the crystallites was verified by cutting a submillimeter-thick slice along the axis of one of the samples and examining the slice under a microscope with magnification as high as 1000X. Fig. 2.1 is a picture at 400x magnification of one such sample. The preferential alignment of the crystallites is visually evident.

The orientation of the crystallites could also be detected indirectly through magnetic measurements. A sample of oriented crystallites exhibited steps in the hysteresis loops, as shown in Figure 2.2. (These steps will be discussed in further detail in Chapter III.) Samples with randomly oriented crystallites (for which the epoxy was allowed to set in Earth's field) exhibited no steps, except one near zero field. In fact, the clarity of the steps can be used

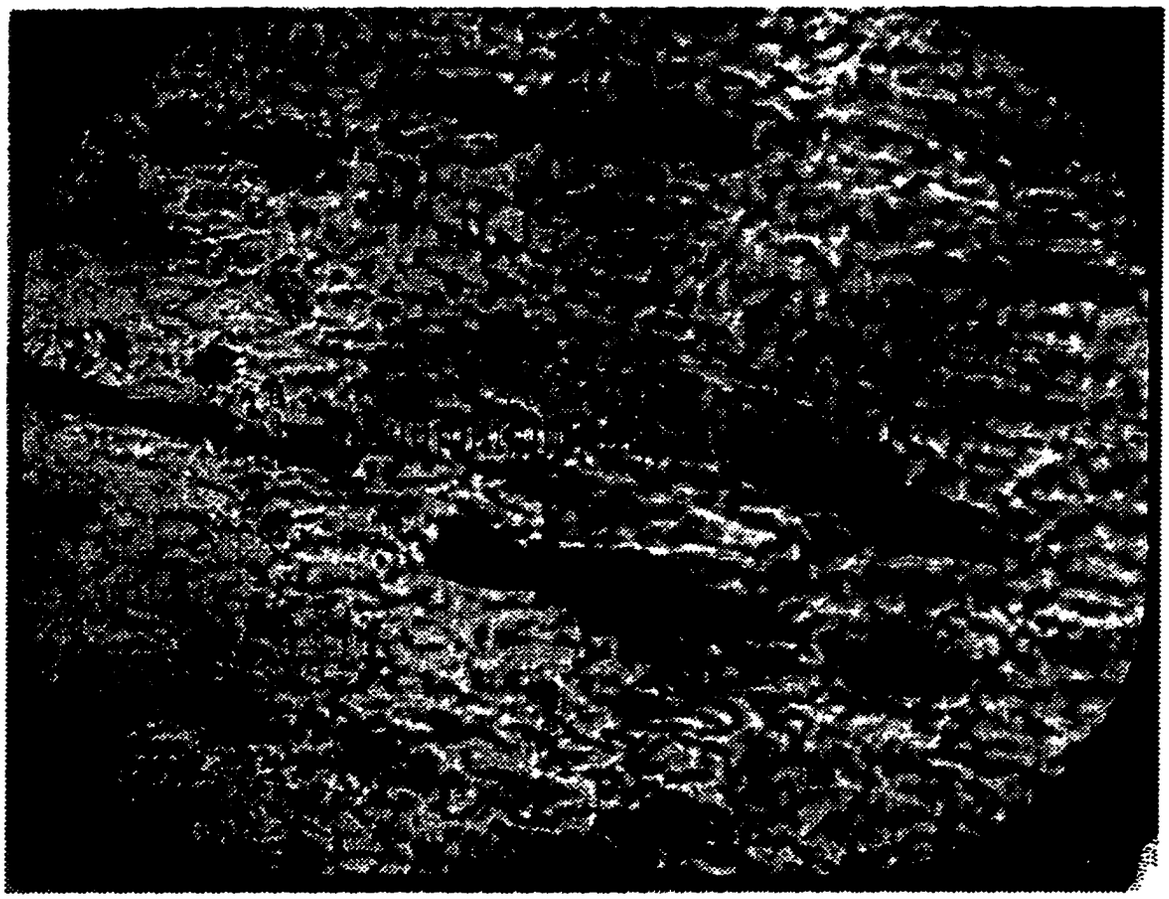

Fig. 2.1 Orientation of the crystallites. A sample of Mn_{12} powder was oriented and set in Stycast 1266 according to the procedure described in the text. A slice of the sample was viewed at 400x magnification under an optical microscope equipped with a Polaroid camera, which captured this image. The long dark structures are the crystallites, which can be seen to be well oriented along a common axis.

to gauge the quality of alignment. Figure 2.2 shows hysteresis loops for a sample oriented and frozen in three different matrices: Stycast, paraffin and toluene. Toluene, with its low viscosity and freezing point of -95 C, allows for much better alignment of the crystallites, as evidenced by the sharp steps and plateaus in the figure. Because the alignment is so much better for the samples frozen in toluene, it might seem preferable to work with them. However, such samples have a distinct disadvantage: whenever the sample is removed from the magnetometer to the ambient environment, the toluene melts and the crystallites lose their orientational order. While it is not very difficult to reorient the crystallites, one is always left with concerns about the precise reproducibility of results.

Samples in a paraffin matrix were also made by orienting the crystallites in paraffin at 340 K. Such samples are very well oriented and avoid the melting problem of samples frozen in toluene. However, these samples had one serious shortcoming: the paraffin matrix is so soft that the crystallites can change their orientation in an applied field even at low temperatures. This is a serious problem when one attempts to apply a magnetic field at some angle relative to the c axis. The crystallites in these samples follow the direction of the field and so one always measures the effect of the field along the c axis, making it impossible to study the effect of a field at an arbitrary angle with respect to the crystal's easy axis.

Single crystals that were measured were also mounted in Stycast 1266. This was done not to orient them, but rather to protect them: they are extremely fragile and break easily.

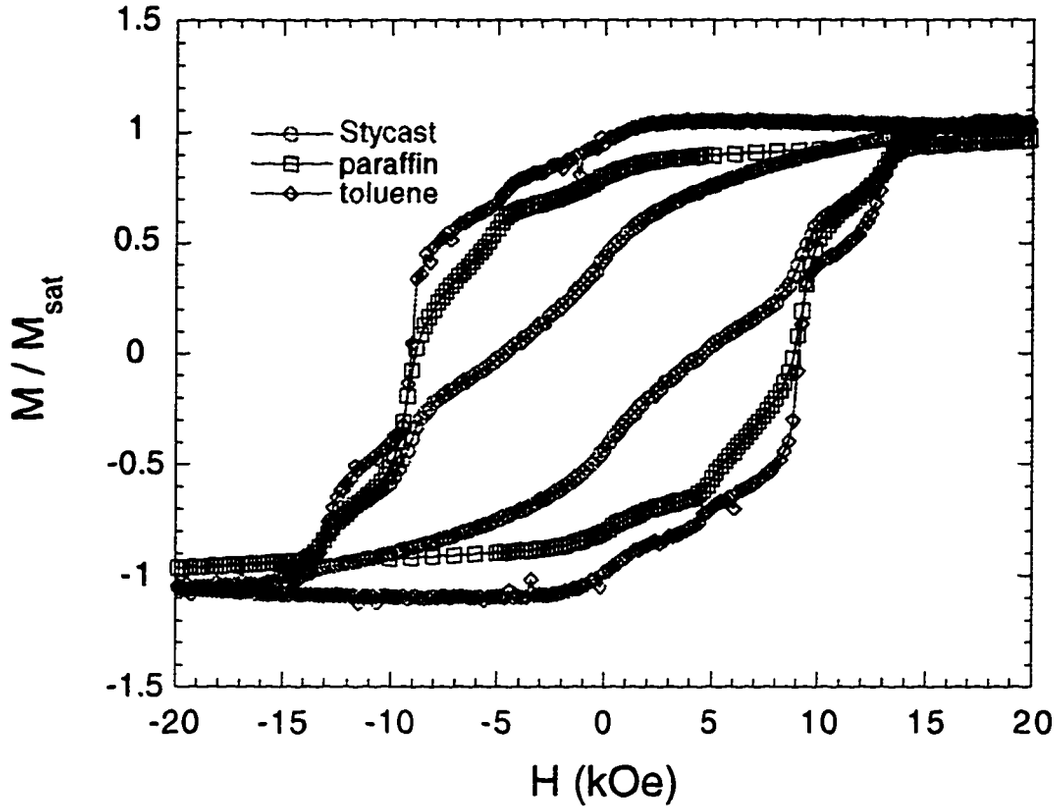

Fig. 2.2 Hysteresis loops of Mn12 powder oriented in different matrices, all taken at 2.4 K. The area inside the loops is larger for the sample in toluene, which has the best alignment.

B. Using the Quantum Design Magnetometer

All of the measurements presented in this study were performed with a Quantum Design MPMS-5 magnetometer. This is a SQUID-based system equipped with a 55-kOe superconducting magnet; sample temperatures can be set as low as 1.7 K and as high as 400 K. The system is equipped with two rf SQUIDs and associated pickup coils, one for measuring the sample moment parallel to the field direction and the other for measuring the perpendicular

moment. A separate sample rotator can be inserted into the system that will allow the sample to be rotated about a horizontal axis. The apparatus is immersed in a superinsulated dewar of liquid helium, which is supported on vibrational dampers and surrounded by a mu-metal and iron shield to expel noise and the Earth's field from the system.

In the remainder of this section, I will describe the basic principles behind making measurements with this system and delineate some of the non-trivial techniques employed in actual data taking.

Principles of SQUID Magnetometry

While one need know little about SQUIDs in order to use them as measurement devices, a few words on the underlying principles of their operation may be in order. For a more thorough review of their operation, the reader is referred elsewhere.[52] A SQUID is a superconducting loop with either one (the rf SQUID) or two (the DC SQUID) Josephson junctions in it. While the rf SQUID is employed in the present measurements, the DC SQUID is conceptually easier to understand. Consider the circuit in Figure 2.3: If one assumes that the two junctions are equivalent (have the same critical current I_c) and the flux through the loop is zero, then the phase shift of the superconducting order parameter across both junctions is the same. Suppose now that the SQUID is biased by a constant current larger than its critical current (equal to $2I_c$). The SQUID is now in the "voltage state" and the magnitude of the measured voltage is determined by how much larger the current is than the critical current. Now, if a small external flux of less than half a flux quantum, $\Phi < \Phi_0/2$, is applied to the loop, a current J will flow

around the loop to screen out the flux. The current passing through one junction will now be increased while in the other it will be decreased. The first junction will now switch into the voltage state when $I_1 + J = Ic$. In other words, a smaller applied current is needed to switch the SQUID into a voltage state. Therefore the SQUID's critical current is reduced by the flux. Since the SQUID is biased at a constant current and the critical current is reduced, the measured voltage is larger. The voltage across the SQUID then gives a measure of the flux through it. Now, if the flux through the SQUID becomes larger than half a flux quantum, a flux quantum will enter the SQUID loop and the current J will reverse direction. This non-linear behavior is prevented in practical SQUID devices by using feedback to always keep the flux through the loop near zero.

The key point of the above discussion is that a SQUID acts as a flux to voltage converter. An applied flux results in a measured voltage. SQUIDs can measure moments as small as 1000 spins and can be constructed to work near the quantum limit of sensitivity.[53]

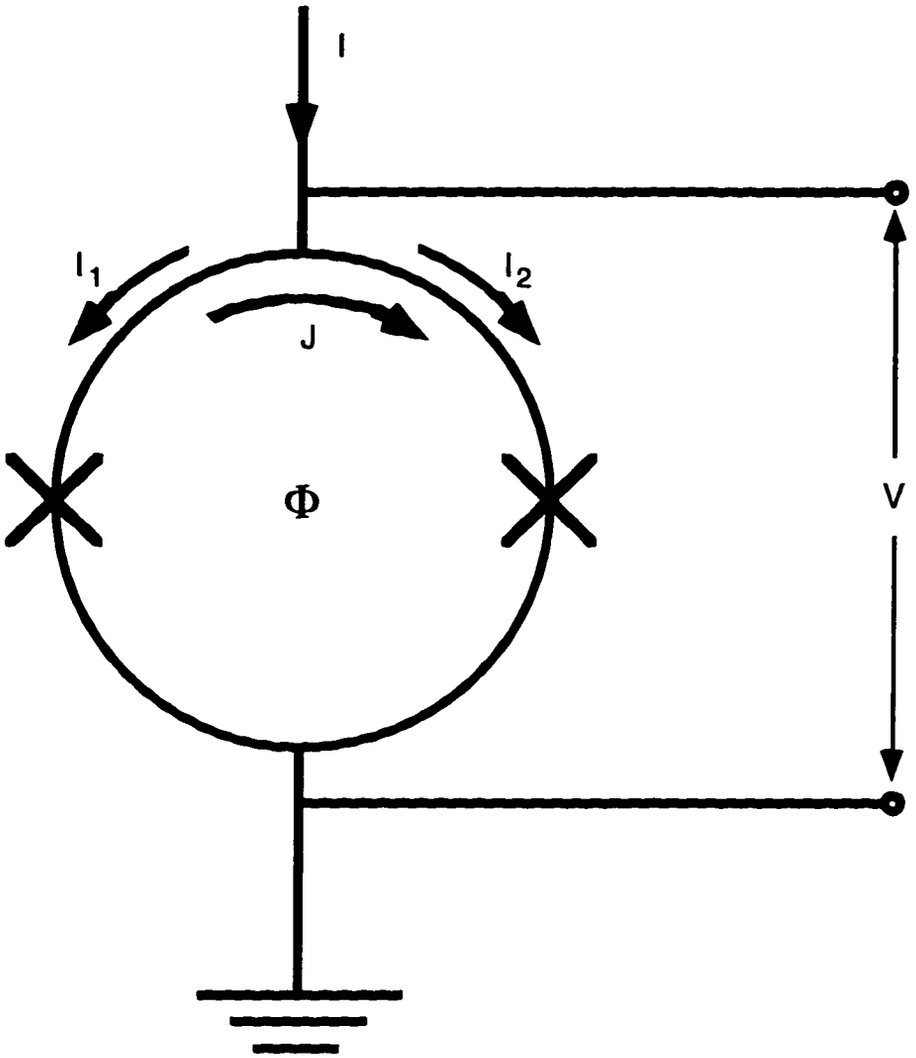

Fig. 2.3 Schematic diagram of a DC SQUID. An external source applies a bias current, which splits into two branches I1 and I2. An applied flux produces an additional current J around the ring. The measured voltage is a periodic function of the appled flux.

In practice the SQUID is far too sensitive to be exposed directly to the flux to be measured. Instead, it is usually housed in a superconducting shield and the signal is inductively coupled to the SQUID via superconducting leads attached

to superconducting pickup coils in the sample space. The design of the pickup coils bears some mention. These coils are usually wound in either "first gradiometer" or "second gradiometer" configurations. For the MPMS system the latter is used. A first gradiometer coil set consists of two coils wound in opposite directions, as show in Figure 2.4(a). A magnetized sample located in the center of one coil will cause a current to flow around that coil (because of the Meissner effect, not induction), while the current produced in the second coil will be relatively smaller since the sample is further away from it. On the other hand, if a uniform magnetic field is applied to the coils, the same current will be produced in each and, since they are oppositely wound, the total current produced will be zero. Therefore, the coils act to null out the signal from a uniform background field but not from a sample. To first approximation, the coils measure the field gradient, hence the name. A set of second-gradiometer coils can be obtained by placing two oppositely wound first-gradiometer coils end to end, as in Figure 2.4(b). These coils will now null out both a uniform magnetic field and a field gradient. The use of such gradient coils is imperative to reduce background noise in sensitive flux measurements.

When taking measurements with gradiometer coils, one generally moves the sample slowly through the coils. (This procedure is difficult at millikelvin temperatures, where the sample motion can produce unwanted heating.) Moving the sample has the advantage that any stray background signals that are not removed by the coil configuration do not move with the sample and so can easily be distinguished. As the sample moves through the coil set, it produces a different current (and hence output signal) depending on its position. This is illustrated in Fig 2.4(c) for the second derivative coil set depicted in Figure 2.4(b). The signal is maximal and positive when the sample

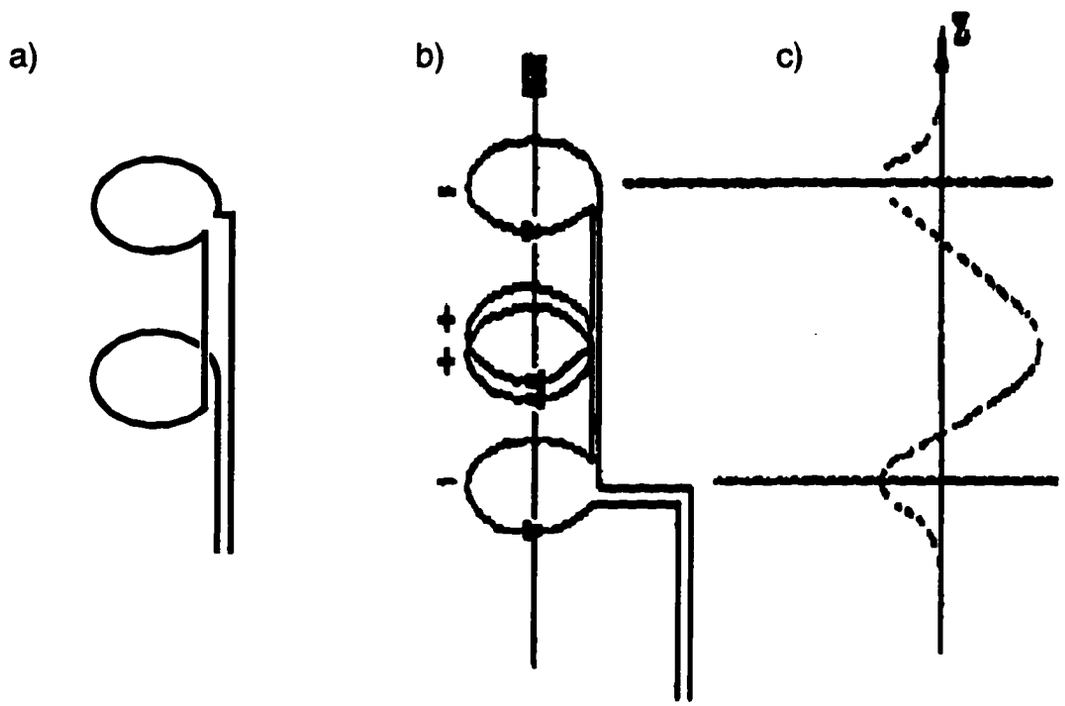

Fig. 2.4 Gradiometer coils. a) First-order gradiometer composed of an astatic pair of coils; b) Second-order gradiometer, essentially an astatic pair of first-order gradiometer coils; and c) the signal (horizontal axis) produced by a sample as it is moved vertically through the second-order gradiometer illustrated in (b). Parts (b) and (c) are reproduced, with permission, from the Quantum Design MPMS User Manual.

is in the center of the middle coil while it is most negative when the sample is in the center of one of the other coils. The magnitude of the peaks is proportional to the magnetic moment of the sample. A simple fitting procedure can extract the moment from the curve of signal versus position.

Sample rotator

While the MPMS system is basically straightforward to operate, one component requires a fair amount of sophistication. This is the sample rotator, which allows a sample to be rotated about a horizontal axis with a nominal 0.1-degree resolution.

The mechanical operation of the rotator is simple and is described in detail in the Quantum Design manual. A brief overview follows. The rotator is depicted in Fig. 2.5. Two concentric stainless-steel tubes lead from the rotator to outside the cryostat. The outer one is for support, the inner is attached to a stepper motor that rotates it. When the inner tube rotates, it turns a screw on the top of the rotator. A special washer fit to the screw is driven to move vertically by the motion of the screw. The washer pulls on a thin phosphor bronze wire that wraps around a small pulley in the center of the rotator. (The other end of the wire is attached to a spring at the bottom of the rotator; the spring serves to keep the wire under tension.) As the wire is pulled, the pulley rotates, as does the small sample platform attached to it.

The rotator was calibrated by Quantum Design before purchase. However, this calibration was done at room temperature and was found to be slightly inaccurate at low-temperatures, probably because of thermal contraction. A new calibration of the rotator was performed to correct for this error. A single crystal of Mn_{12} was attached to the rotator such that its easy axis (the c axis) lay in the rotation plane. The system was cooled to 5 K, a

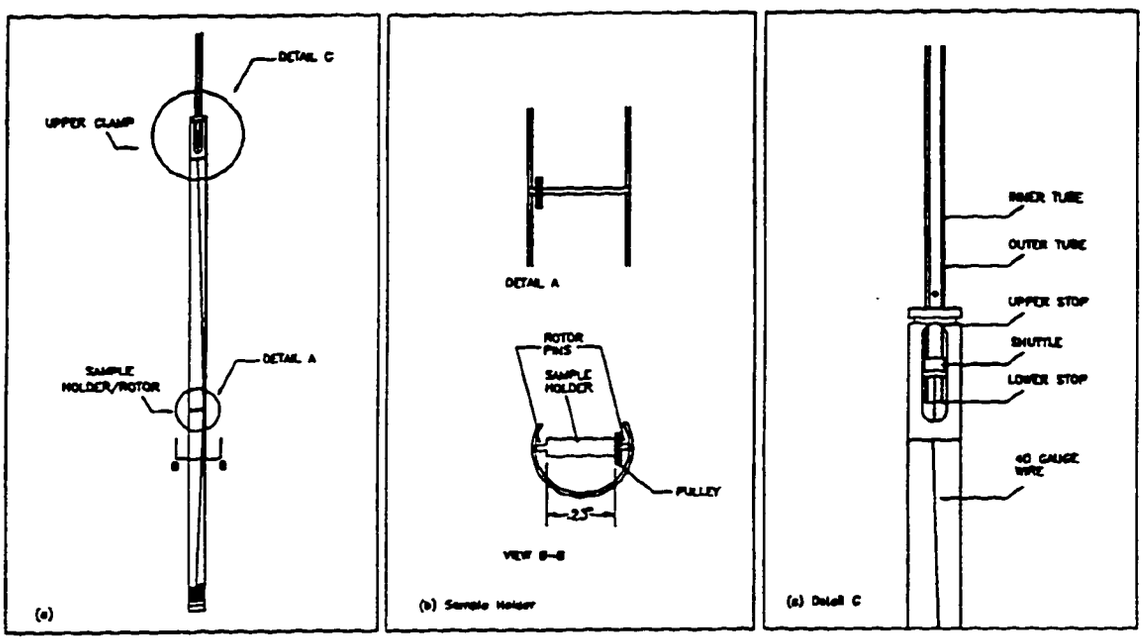

Fig. 2.5 The Quantum Design Horizontal Sample Rotator. A sample is mounted on the platform in the center of the rotator. Rotation is achieved by pulling on the wire that wraps around the pulley, as shown in (b). This figure was reproduced, with permission, from the Quantum Design Horizontal Sample Rotator User Manual.

temperature at which Mn12 is superparamagnetic (shows no hysteresis). The rotator assembly was turned about a vertical axis to maximize the signal coming from the transverse pick-up coils. Measurements of both the

longitudinal (with respect to the field axis) and transverse components of the sample moment were taken as a function of angle at 1-degree increments in a field of 100 G. The resulting data is presented in Fig. 2.6. For a system with large uniaxial anisotropy, like Mn_{12}, one expects the signal for both components to have a period of 180 degrees and for the two signals to be 45 degrees out of phase. The data were fitted to sine functions with an additional linear term and offset, the former to account for the fact that the sample also changes position as it is rotated and the latter to account for the fact that when the field is applied perpendicular to the easy axis, there is still a small signal. The fits indicate that the data actually show a periodicity of 174.5°. The software calibration factor was adjusted to correct this.

There are a few interesting things to note about the data in Fig. 2.6. First, the transverse signal is clearly unreliable in certain regions where the longitudinal signal is large relative to the transverse signal, i.e. where the angle of the easy axis relative to the field axis is small. There is no simple way to correct this problem since it depends on the details of how the pickup coils are wound. The problem was simply avoided by disregarding transverse moment data in this low-angle regime. One should also note that while the overall fit to a sine function is fine, there are some systematic deviations that can be as large as a few degrees. Possible sources for this are nonlinearity in the rotator mechanism or in the detection system.

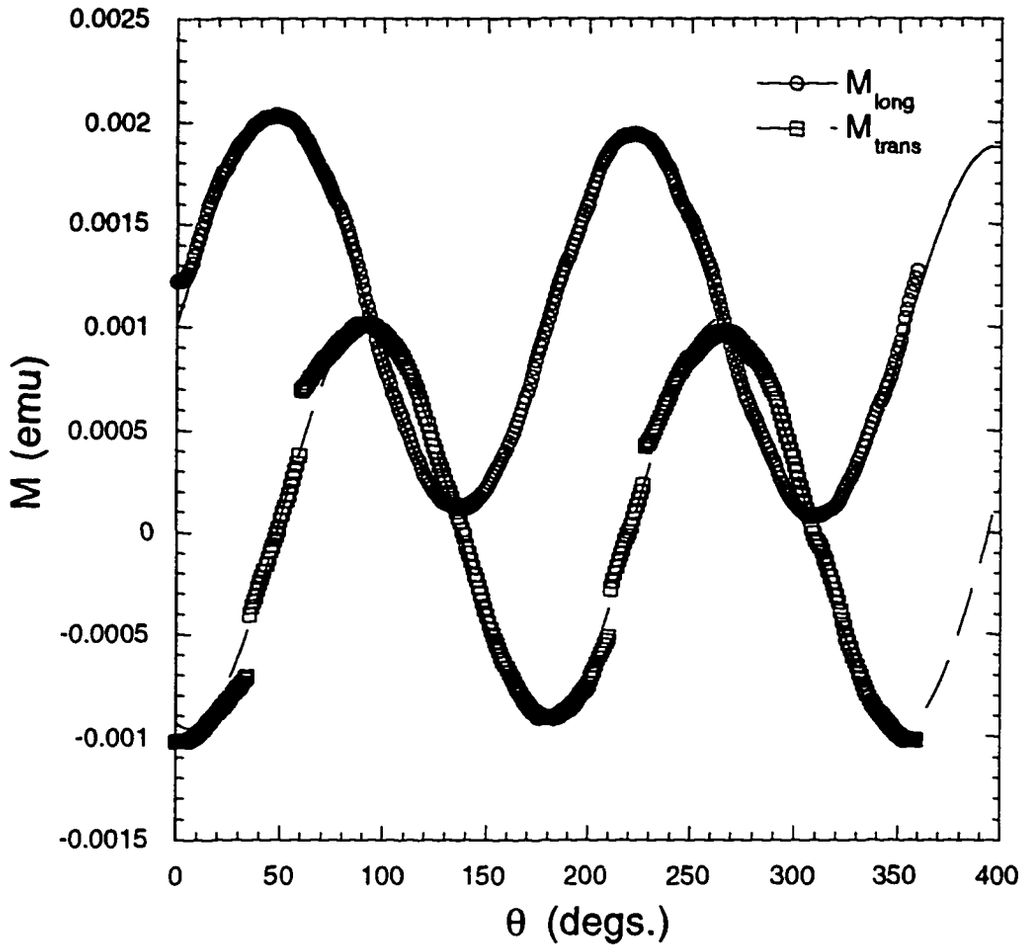

Fig. 2.6 Calibration of the rotator. The data show the angular dependence of the longitudinal and transverse signal for a single crystal of Mn12 in a field of 100 G at 5.0 K. Fits to sine functions show that the periodicity is 174.5°, indicating an error in the calibration of the rotator. The data also indicate that the transverse moment is not accurately detected when the longtudinal moment is large. Some nonlinearities in the rotator are also evident.

The wire in the rotator mechanism sometimes slips and there is also some backlash when the motor reverses direction. Both of these problems can

cause the zero-angle position to change after the orientation of the sample has been changed several times. To avoid this, the zero point was reestablished prior to each experiment. Appendix A contains the software program (written in Quantum Design's EDC language) that accomplishes this task. Briefly, the sample is rotated several degrees before "zero." Then zero degrees is approached, first by 1-degree increments and then by 0.1-degree increments, until the sample is within 0.1 degrees of the "zero." To do this, the transverse moment of the sample is monitored. Zero angle is determined to be the point at which the transverse moment is zero. (There is another point at which the transverse moment is zero: when the sample is at 90 degrees with respect to the field. It is hard to mistake the 90-degree orientation from the 0-degree orientation.)

Appendix B contains another program written for angular measurements. This program is used for performing magnetization measurements as a function of longitudinal field with a fixed transverse field. In other words, H $\sin(\theta)$ was held fixed while H $\cos(\theta)$ was varied. This required changing the value of the total field and orientation of the sample for each data point. Unfortunately, Quantum Design's EDC programming language does not support trigonometric functions or square roots. So, the program in Appendix B is a BASIC program that calculates the field and angle necessary for each point and then writes the EDC program.

C. Basic Measurement Procedures

The measurements performed for this work were standard, with the possible exception of the angular studies. I will briefly summarize the basic procedures for each type of experiment.

Hysteresis

Hysteresis loops were generally taken between -30 kOe and 30 kOe. The field was swept between these extremes (and back) at a continuous rate while measurements of the magnetic moment were taken. These measurements were usually performed in "Hysteresis Mode," where the persistent switch on the magnet was kept on (open) so that the field was never "trapped" in the magnet. This allowed measurements to be taken faster. Because the sample signals were usually very large, the additional noise from using this mode of operation was negligible. All the hysteresis data presented herein were taken this way with a field sweep rate of ~670 Oe/minute, unless otherwise noted.

Temperature dependence - ZFC and FC

Temperature dependence data fall into two basic categories: field cooled and zero-field cooled. In the former the sample is cooled to the lowest available temperature in a field and then the temperature is slowly raised while the moment of the sample is measured. In the latter procedure, the sample is cooled in zero field (in practice a field of at most a few Oersted), a field is

switched on and measurements are taken as the temperature is raised. The fields used in these experiments are always small compared to the anisotropy field of the material studied (~100 kOe for Mn_{12}). The time between successive data points is approximately 100 seconds, determined by the speed at which the magnetometer can change and stabilize the temperature.

The (higher temperature) regime in which the two sets of data coincide is known as the superparamagnetic regime.[4] At lower temperatures, if the curves diverge, hysteretic field dependence and relaxation phenomena are expected. The temperature at which the zero-field-cooled curve has a maximum is known as the blocking temperature and is interpreted as the temperature at which the system can be thermally activated over the mean energy barrier on the time scale of the experiment. The blocking temperature is then simply proportional to some average energy barrier of the system.

Relaxation

Relaxation phenomena can be studied directly by examining the decay of the magnetization when the field is changed. The procedure is as follows. The sample is cooled to the desired temperature in some field (usually zero for the present study) and then the field is switched to another value. As the moment of the sample decays to its new equilibrium value, its value is monitored as a function of time.

Angle-dependent measurements

All of the above measurement procedures can be performed with an added adjustable parameter: the angle θ between the field and the sample's easy axis. Measurements were made of hysteresis loops in which a fixed transverse field is applied to the sample while the field along the easy axis is varied, as described above. Zero-field-cooled temperature-dependence measurements were performed. Also, detailed measurements were made of the magnetic relaxation as a function both longitudinal and transverse magnetic field components.

In all of these angular measurements, two components of the magnetization were recorded: the component along the field direction, M_L, and a component perpendicular to it, M_T. In general, one is interested in the components of the magnetization parallel to the easy axis of the sample, $M_{\parallel}$, and perpendicular to it, $M_{\perp}$. The latter pair can be easily obtained from the former by a "rotation:"

$$\begin{pmatrix} M_{\parallel} \\ M_{\perp} \end{pmatrix} = \begin{pmatrix} \cos\theta & \sin\theta \\ -\sin\theta & \cos\theta \end{pmatrix} \begin{pmatrix} M_L \\ M_T \end{pmatrix}.$$

III. Experimental Results

Mn_{12} has proven to have some very interesting properties. Aside from behaving as a set of identical microscopic magnets and displaying hysteresis at low temperatures, it also exhibits uniquely quantum mechanical phenomena: steps at regular intervals of magnetic field in the hysteresis loops, as well as dips in the blocking temperature and concomitant increases in the magnetic relaxation rate at the same fields. In this chapter I will present experimental data detailing these effects. The interpretation of the data will be presented in the following two chapters.

A. Hysteresis loops

Fig. 3.1 shows the magnetization as a function of magnetic field at temperatures between 1.7 K and 3.0 K. This data was obtained with the magnetic field applied along the easy axis of the sample. Fig. 3.1(a) was obtained using a sample of oriented Mn_{12} powder in a matrix of Stycast 1266, while Fig. 3.1(b) contains results from a sample prepared in a paraffin matrix. As expected for superparamagnetic systems, the area enclosed within the hysteresis loops is found to increase as the temperature is reduced. In both parts of this figure, one can clearly see steps in the magnetization. These steps only occur in certain parts of the loop. As one proceeds around the loop, steps occur as the magnetic field is increased from zero, no noticeable steps occur when the field is reduced back to zero, steps

occur once more as the field is raised in the opposite direction, and so on. In short, steps are seen when the field increases in either direction, and they are absent when the field is decreased to zero. Control samples that were not oriented during preparation showed smooth hysteresis loops with no steps (except for a "pinched" shape near zero field), a clear indication that the steps are associated with the orientational ordering.

It should be noted that the hysteresis observed in this system is a manifestation of the bistability of the Mn_{12} molecules. Hysteresis in ordinary bulk magnets arises from the motion of domain walls. In Mn_{12} and other superparamagnetic systems, the interactions between magnetic elements are small. Hence, there are no domains, *per se*. The hysteresis is instead attributed to the fact that each magnetic entity has an energy barrier to magnetization reversal and can therefore be trapped for long times in a metastable orientation. The slow (temperature-dependent) relaxation from this metastability is responsible for the hysteresis and the other effects exhibited by Mn_{12} and discussed below.

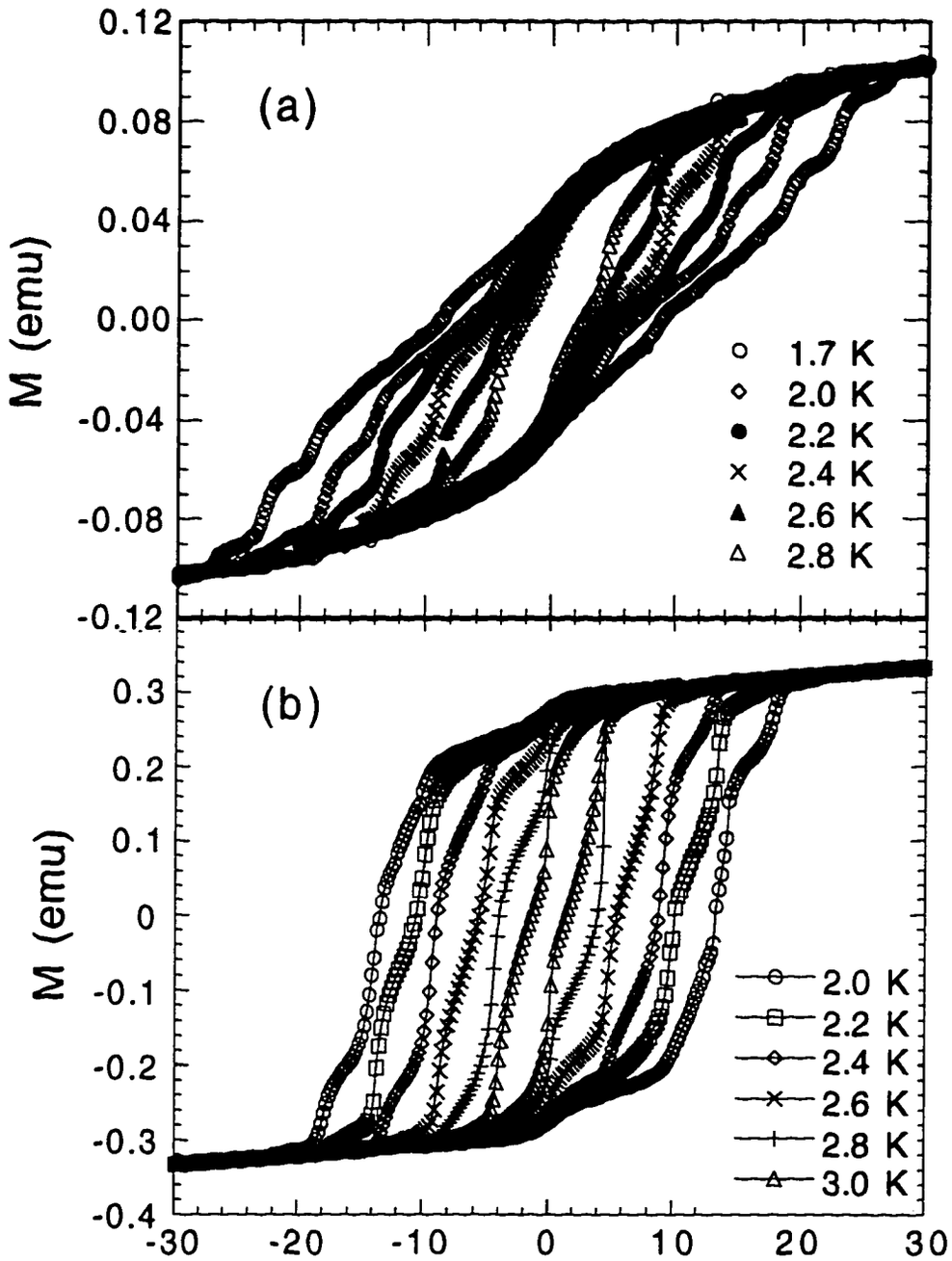

Fig. 3.1 Hysteresis loops of Mn12 in (a) a Stycast matrix and (b) a paraffin matrix. At all temperatures shown steps are observed in the hystresis loops as the field is increased (in either direction) from zero but not when it is decreased.

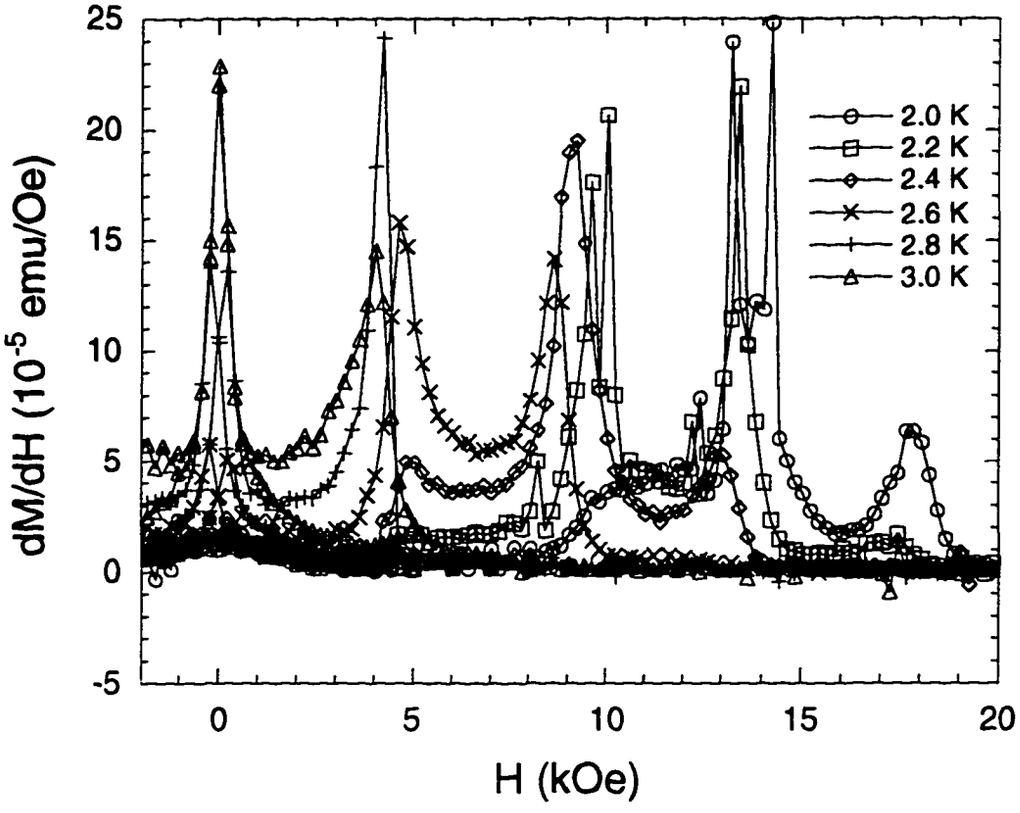

Fig. 3.2 Derivative of the Hysteresis loops in Fig. 3.1(a). The peaks indicate the fields at which the steps in the loops are steepest. The data indicate that the steps always occur near the same values of magnetic field.

Close examination of Figs. 3.1 reveals that, despite the apparent complexity, the steps occur at specific values of magnetic field. This is confirmed in Fig. 3.2, where the slope dM/dH of the curves shown in Fig. 3.1(b) is shown as a function of external magnetic field. Maxima (corresponding to the steepest portion of the steps) are found at particular values of the field that appear to be independent of temperature. A careful analysis shows that the external field H for each step does shift slightly with

temperature. While one might conjecture that this slight dependence is intrinsic, one finds a similar dependence on the rate at which the magnetic field is swept. The common thread in both cases is that the magnetization is a function of both variables. Fig. 3.3 shows the measured field for one step (near 4500 Oe) as a function of the measured value of the magnetic moment normalized to its saturation value; data for different temperatures and sweep rates are included. Clearly, all of the data falls on a straight line, indicating that the field at which the step occurs depends explicitly on the magnetization and only implicitly on the temperature and sweep rate.

This dependence can be easily explained by noting that each individual Mn_{12} molecule does not see the applied field, but sees rather this external field plus the mean dipolar field from all of its neighbors. In other words, it is the magnetic induction internal to the sample, $B = H + 4\pi M$, that is invariant for each step. In fact, the data in Fig. 3.3 can be used to determine the absolute value of the saturation magnetization for Mn_{12}. (Only the magnetic moment is measured directly, not the magnetization.) Extrapolating the data to $M=M_{sat}$, one finds that $M_{sat} = (B-H)/4\pi = (H(M=0) - H(M_{sat}))/4\pi = 58$ emu/cm^3. This is close to the saturation magnetization that one calculates for a spin 10 (magnetic moment = 1.85×10^{-19} emu) in a unit-cell volume[51] of 12.1 Å x 17.3 Å x 17.3 Å, which yields $M_{sat} = 51.2$ emu/cm^3. In Fig. 3.4, the calculated magnetic induction B is plotted as a function of the relative magnetization. For the steps at the lowest three field values, there is no obvious dependence on magnetization. For the higher steps, some negative slope remains. This may be due to some torquing of the crystallites at the higher fields. Further investigation of this effect may be worthwhile.

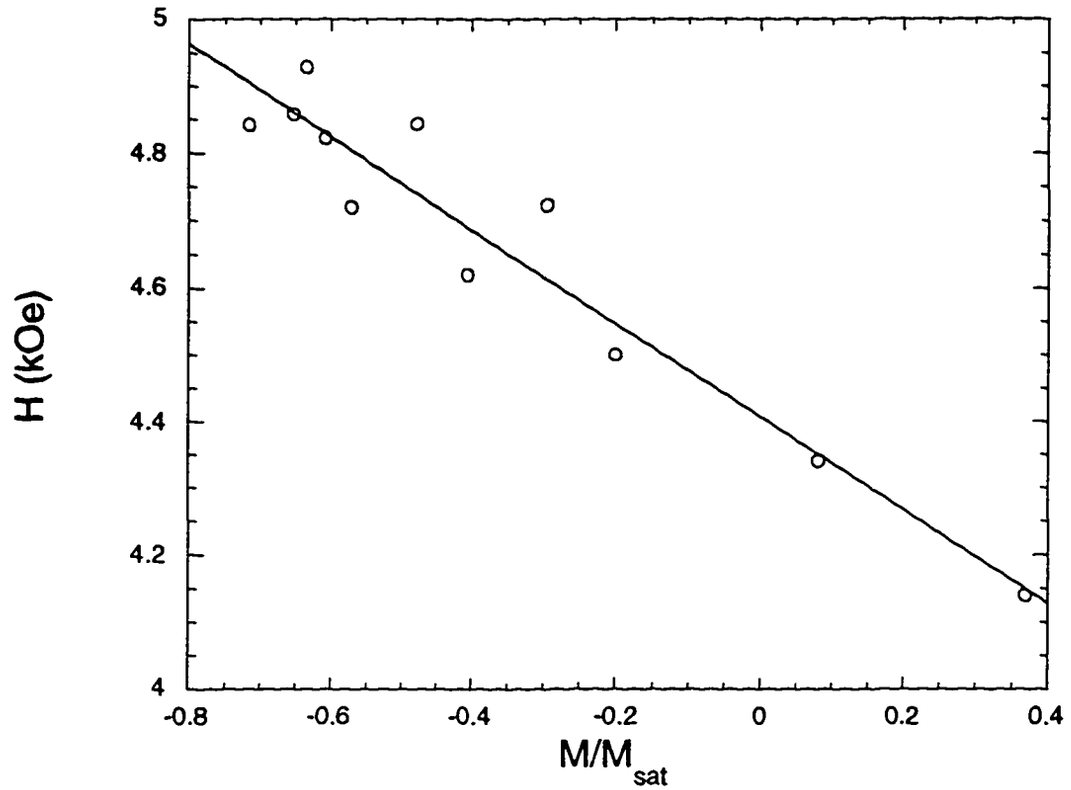

Fig. 3.3 Dependence of step field on magnetization. Here the field at which step #1 (the step near 4.5 kOe) occurs is plotted as a function of the relative magnetization. Data was obtained from hysteresis loops taken at various temperatures and field sweep rates using a sample in a toluene matrix. The data were fit to a straight line, from which the saturation magnetization was deduced as discussed in the text.

Fig. 3.5 shows the induction at which a step occurs plotted as a function of step number, where the steps have been labeled by integers starting with the one at zero field labeled #0. The straight line fit indicates there are steps at equal intervals of approximately 4.6±0.1 kG. The data in the figure indicate that seven steps, including #0, have been observed. At the

time of this writing, a total of 12 steps have been seen in pulsed-field measurements[54] at 1.53 K; additional steps are expected at lower temperatures. One can estimate the total number of steps expected from the data in the hysteresis loops by noting the temperature at which a step first appears. This temperature, T^*, should characterize the barrier height, which decreases with applied field as $(H - H_c)^2 \sim (n - n_c)^2$, since the step number n is proportional to H. This implies that $n - n_c \sim T^{*1/2}$. Fig. 3.6 shows the step number plotted as a function of this characteristic temperature $T^{*1/2}$. The linear fit extrapolates to $n_c = 20.6$ at zero temperature, indicating that there should be about 21-22 steps (counting n = 0).

Fig. 3.1 indicates interesting changes that occur with temperature: as temperature is lowered, new steps arise out of the saturation curve while others that are clearly observable at higher temperatures become less pronounced. These "frozen" steps can be recovered when the magnetic field is swept more slowly, as can be seen in Fig. 3.7, where first-magnetization data at 2.4 K is shown at a several different sweep rates. This figure also makes it clear that while steps occur at regular intervals of field, they have no definite height. The height of a step depends on the sweep rate and so has no intrinsic meaning. In fact, if one stops sweeping the loop at any point, the magnetization will relax toward its equilibrium value whether or not the field is tuned to one of the steps.

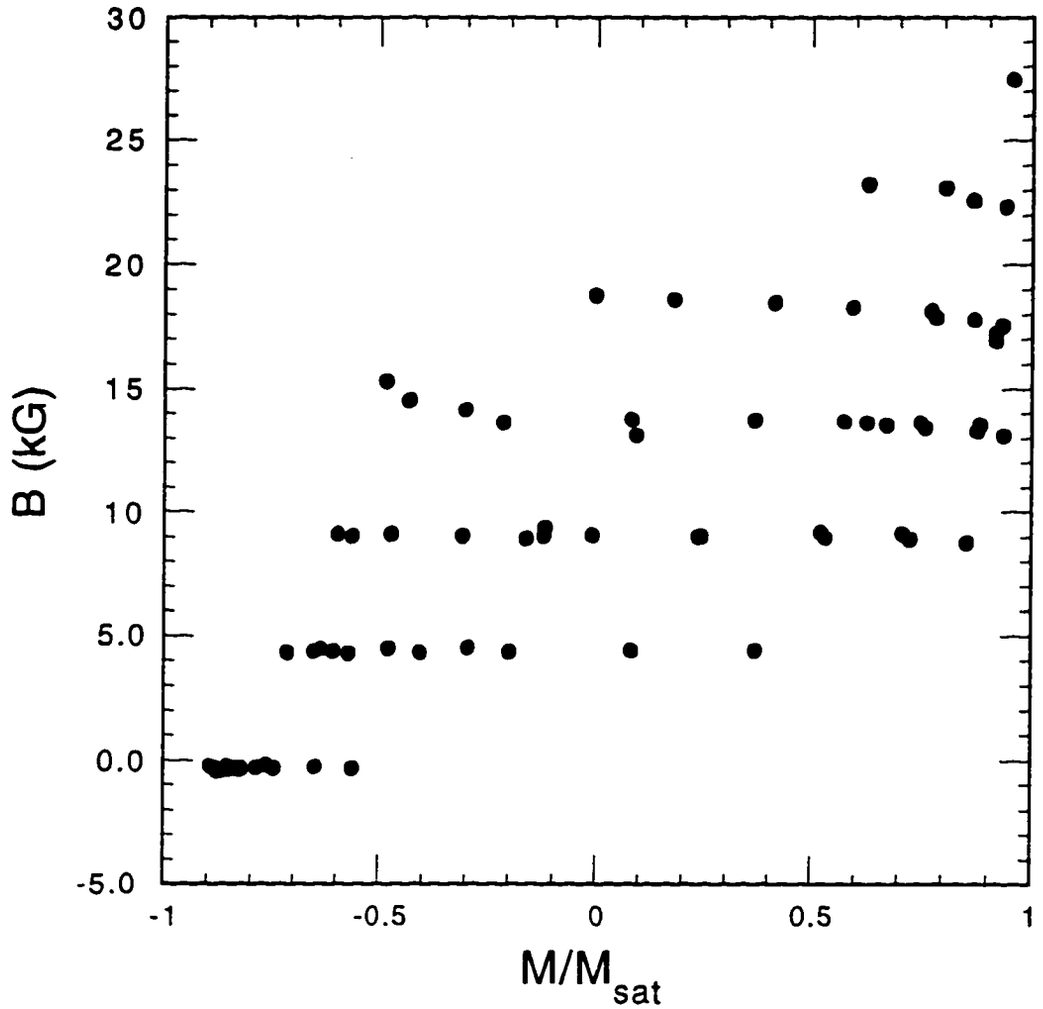

Fig. 3.4 Magnetic induction vs. magnetization. Data shown are for all observed steps for an oriented-powder sample in a toluene matrix. B was calculated using the saturation magnetization determined from Fig. 3.3. B appears to be independent of M for the low-field steps, while there is a negative slope for the higher-field steps.

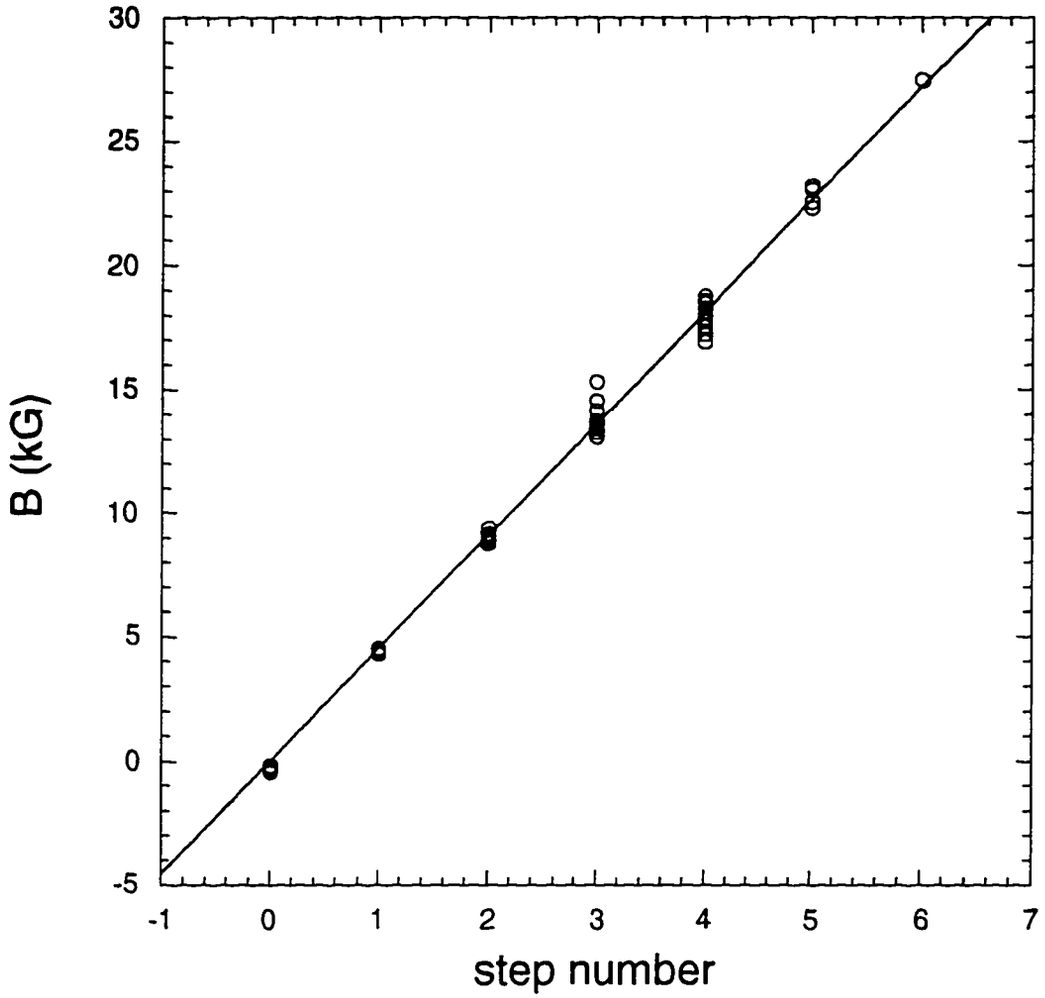

Fig. 3.5 The B field at which a step occurs as a function of step number. The same data displayed in Fig. 3.4 are plotted here. The steps are labelled by integers starting with the one near zero field (step #0). The linear fit indicates that a step occurs about every 4.6 ± 0.1 kG.

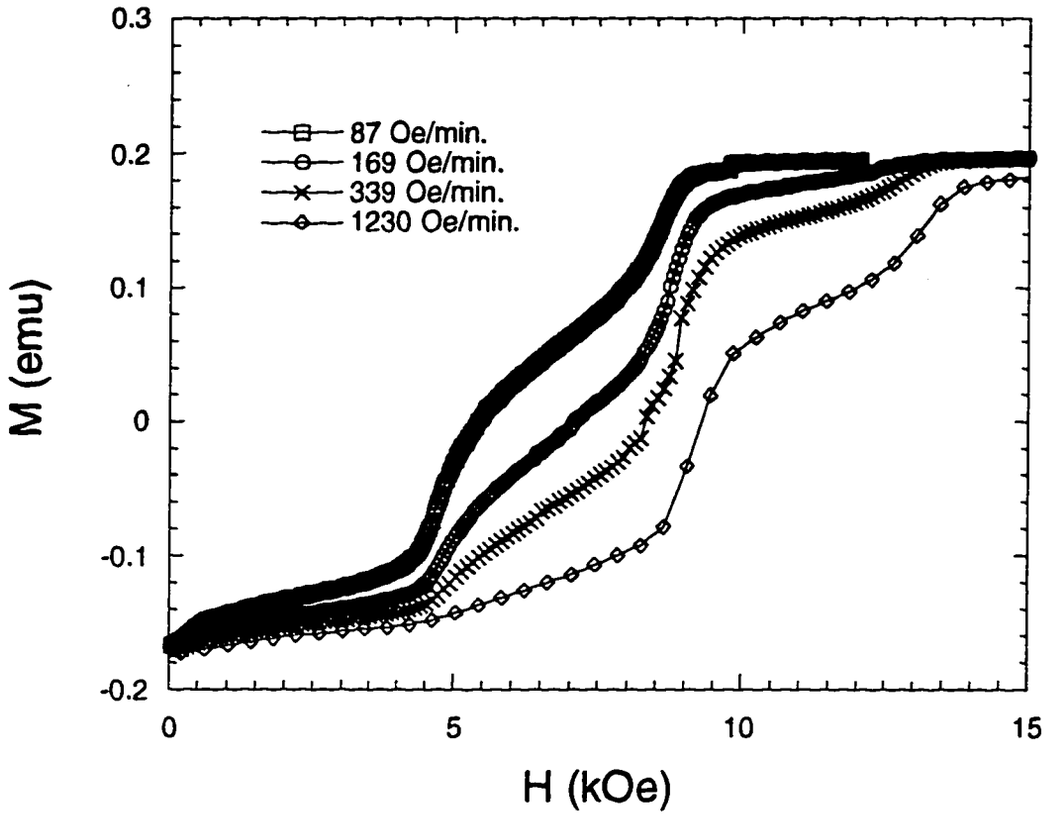

Fig. 3.6 Steps at different field sweep rates. Here the magnet moment is plotted as a function of field in the region of the hysteresis loop that shows the steps. All curves were taken at 2.4 K using a sample of oriented powder in a toluene matrix. The data show clearly that the "height" of a step depends on the rate at which the field is swept.

B. Temperature dependence

When magnetically characterizing a material, one often studies the temperature dependence of the magnetization as a means of estimating the mean barrier size, and the distribution of barrier sizes. In the case of Mn_{12},

one can also observe interesting effects in the temperature dependence at the same fields as one finds steps in the hysteresis loops.

First, consider Fig. 3.8, where the magnetization as a function of temperature for a sample oriented in toluene is plotted for a constant field of 100 Oe. The upper curve is data taken on a sample cooled in the field, while the lower curve is for the sample cooled in zero field. In both cases the magnetization was measured as temperature was increased. The fact that these curves diverge at low temperatures indicates that there are energy barriers to the reversal of the magnetization. The nonmonotonic behavior of the zero-field-cooled curve confirms this: the magnetization increases gradually as the spins "unfreeze" and the magnetization tends toward its equilibrium value. The magnetization decreases at higher temperatures, as expected for a quasi-paramagnetic or superparamagnetic system. The peak in the zero-field-cooled curve is at about 3.1 K, the so-called blocking temperature. Note that this is also the temperature where the two curves begin to diverge. This indicates that there is a narrow distribution of barriers. For the blocking temperature characterizes the mean barrier size, while the temperature at which the curves join corresponds to the largest measurable barrier. While we could estimate the mean barrier height from the blocking temperature in this figure, we will postpone this calculation until later, for reasons that will become evident.

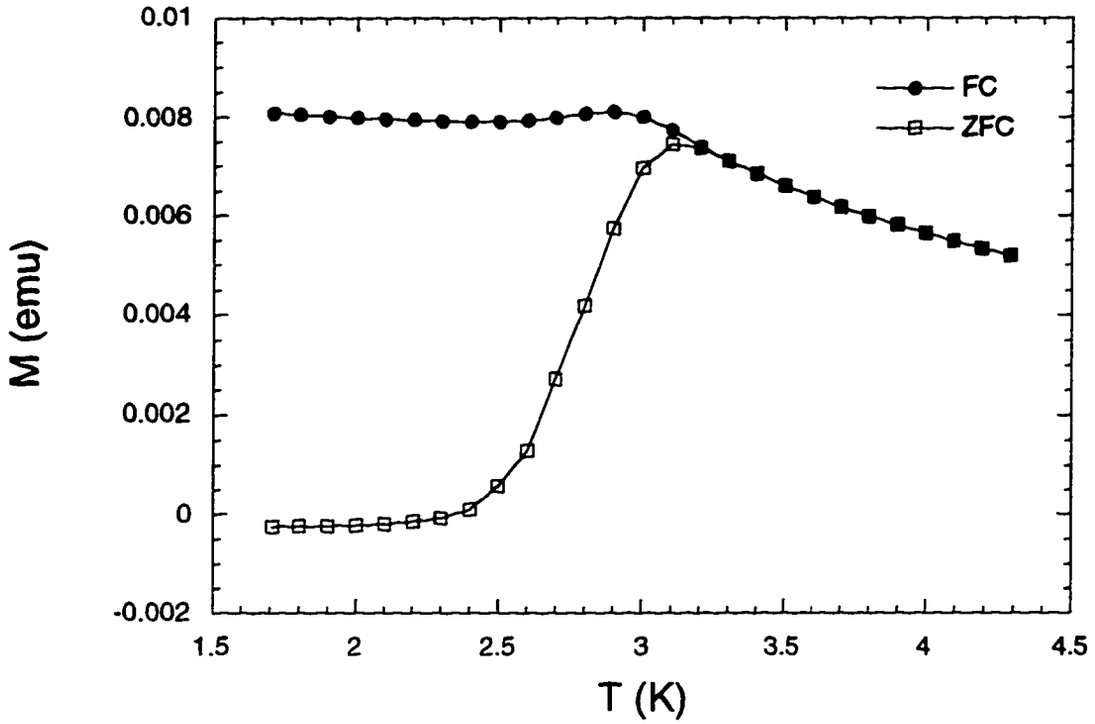

Fig. 3.8 Field-cooled and zero-field-cooled magnetization curves. The data is for a sample of oriented powder in a toluene matrix. The slight negative moment in the zero-field-cooled curve at low temperatures is due to the diamagnetism of the toluene. The fact that the two curves converge at the blocking temperature (peak in the zero-field-cooled curve) indicates a very narrow distribution of energy barriers.

For a zero-field-cooled sample, Figure 3.9 shows the magnetization measured in various magnetic fields as the temperature is increased. (For presentation purposes, curves taken at several other fields have been omitted.) At each field, the blocking temperature T_B, shows an overall decrease as the field is raised, as one expects for superparamagnetic particles. However, the curve obtained at 9.0 kOe exhibits an abrupt shift toward lower temperatures. Similar shifts are found at each of the fields where steps are seen in the hysteresis loops. In Fig. 3.10 the blocking temperature is plotted as a function of measuring field from 100 Oe to 19 kOe.

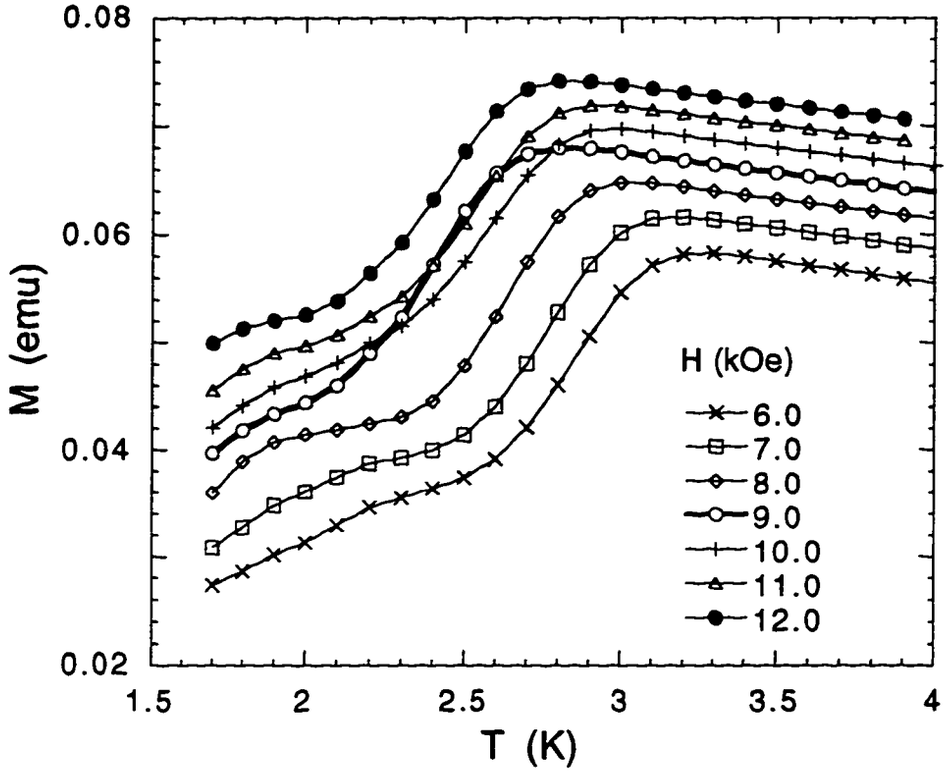

Fig. 3.9 Zero-field-cooled curves at various magnetic fields, as indicated. The magnetization is plotted as a function of increasing temperature for a sample of oriented powder in a Stycast matrix. The curve taken at 9.0 kOe is anomalous, apparently shifted toward lower temperatures relative to neighboring curves.

Superimposed on an overall decrease as a function of field, the blocking temperature T_B exhibits periodic dips, exhibiting minima at the same values of field as the steps in the hysteresis loops. Ignoring the dips, one obtains a zero-field blocking temperature of ~3.5 K. Using a measurement time of 100 seconds (the time between data points) and an Arrhenius prefactor, τ_0, of 2 x 10^{-7} seconds,[37,39,41,42,45-47] one can estimate the size of the energy barrier to be $U = kT_B \ln(t_{meas}/\tau_0) = 49\ cm^{-1} = 71$ K, in fair agreement with published results.[37,39,41-43,44,45-47]

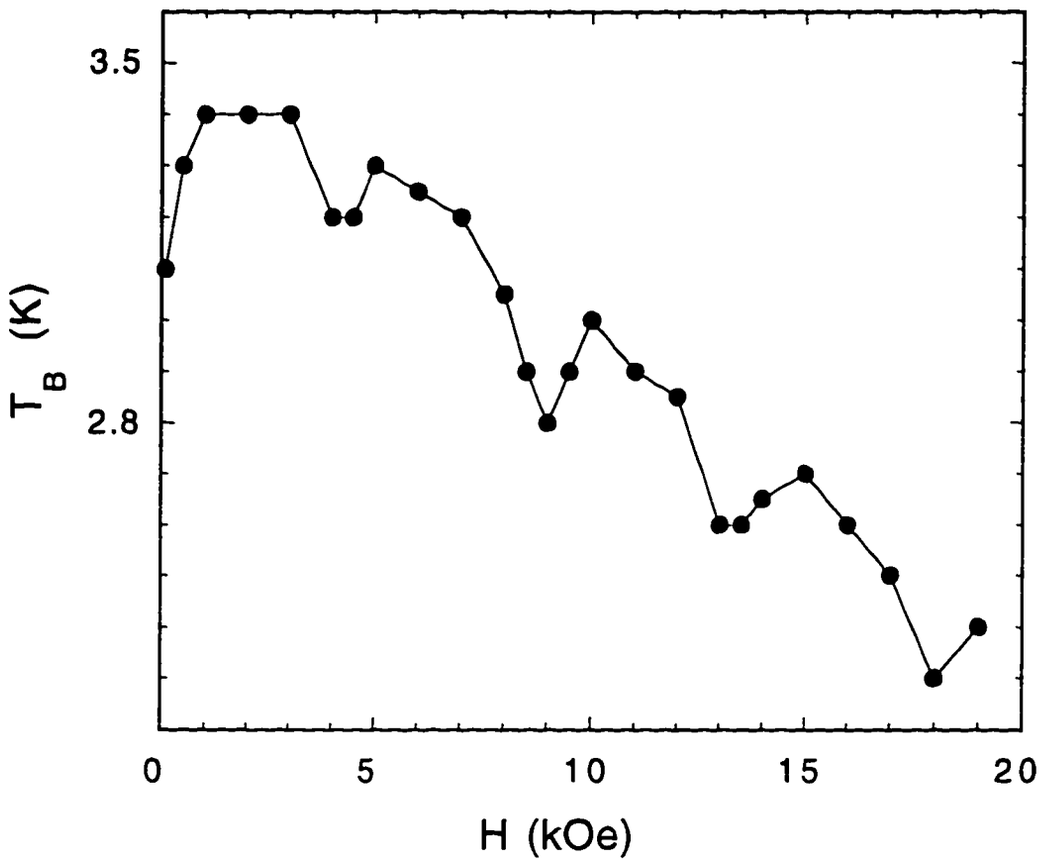

Fig. 3.10 Blocking temperature as a function of field. The blocking temperature was taken from the peaks of the curves in Fig. 3.9 and similar curves at other fields (not shown). The dips in the blocking temperature occur at the same fields as the steps in the hysteresis loops.

C. Relaxation Data

The periodic steps in the hysteresis loop, accompanied by dips in the blocking temperature at the same magnetic fields, as well as the crossing of the 9.0- and 10.0-kOe curves in Fig. 3.9, all imply that the relaxation rate is significantly faster whenever the magnetic induction is an integer multiple

of 4.6 kOe. As we shall see below, this conjecture is indeed confirmed. First, however, some discussion of the relaxation properties of Mn_{12} is warranted.

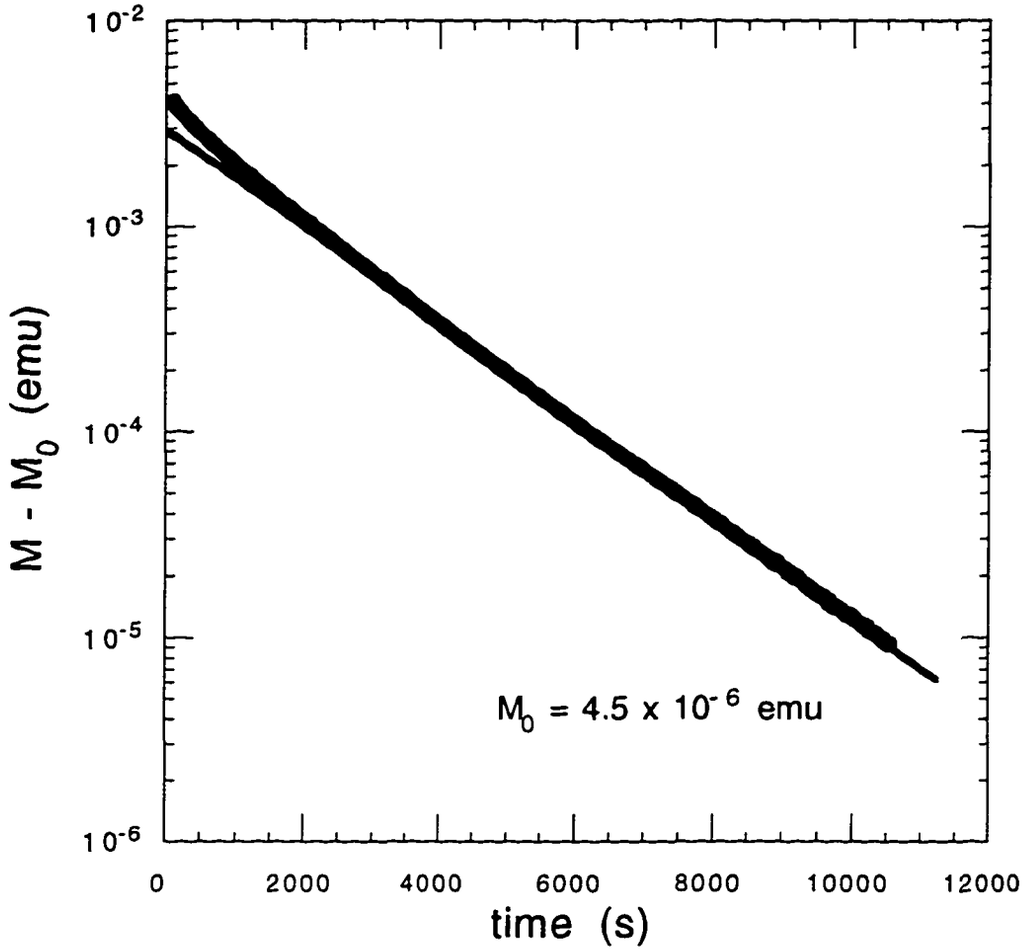

Fig. 3.11 Magnetic relaxation at 2.6 K. A single crystal of Mn12 was cooled in a field of 1 kOe (applied along the easy axis); the field was then switched to zero and the moment was measured over time. Plotted is the measured moment (after a small remnant moment was subtracted off) on a logarithmic scale as a function of time since the field was changed. Since the data do not fall on a straight line in the plot, the relaxation cannot be characterized by a single exponential.

For a system of non-interacting magnetic particles with identical energy barriers one expects to find that the magnetic moment decays exponentially with time toward its equilibrium value. However, for Mn_{12} one finds experimentally that the decay is not characterized by a single exponential. Fig. 3.11 shows relaxation data for a single crystal of Mn_{12} cooled to 2.6 K in a field of 1 kOe and then allowed to relax in near zero field. Plotted is the magnetization on a logarithmic scale as a function of time after the field has been turned off. (The small asymptotic value of the magnetic moment M_0, due to a remnant magnetic field of less than 1 Oe, has been subtracted off.) The fact that the data do not all fall on a straight line indicates that the relaxation is not purely exponential. Note that the long-time tail of the curve appears to be close to exponential, but that the earlier data (most of the decay of the moment) is faster. There are several possible explanations for this:

1) Dipole interactions are important for the relaxation process. As the magnetization decays, each Mn_{12} cluster has fewer neighbors that have not yet flipped and this (somehow) reduces the probability that the cluster will flip.

2) Self-heating. During the initial part of the relaxation process, each spin flip releases energy, raising the temperature of the system and resulting is a faster relaxation. As the relaxation progresses, less heat is produced and the system approaches the bath temperature, exhibiting a relatively slower relaxation rate.

3) There are impurities in the system that relax faster than Mn_{12}.

4) The effect is intrinsic to the Mn_{12} system. Instead of having a single well-defined energy barrier, Mn_{12} has a narrow distribution of barriers. Or there are slightly different species of Mn_{12} clusters that behave differently.

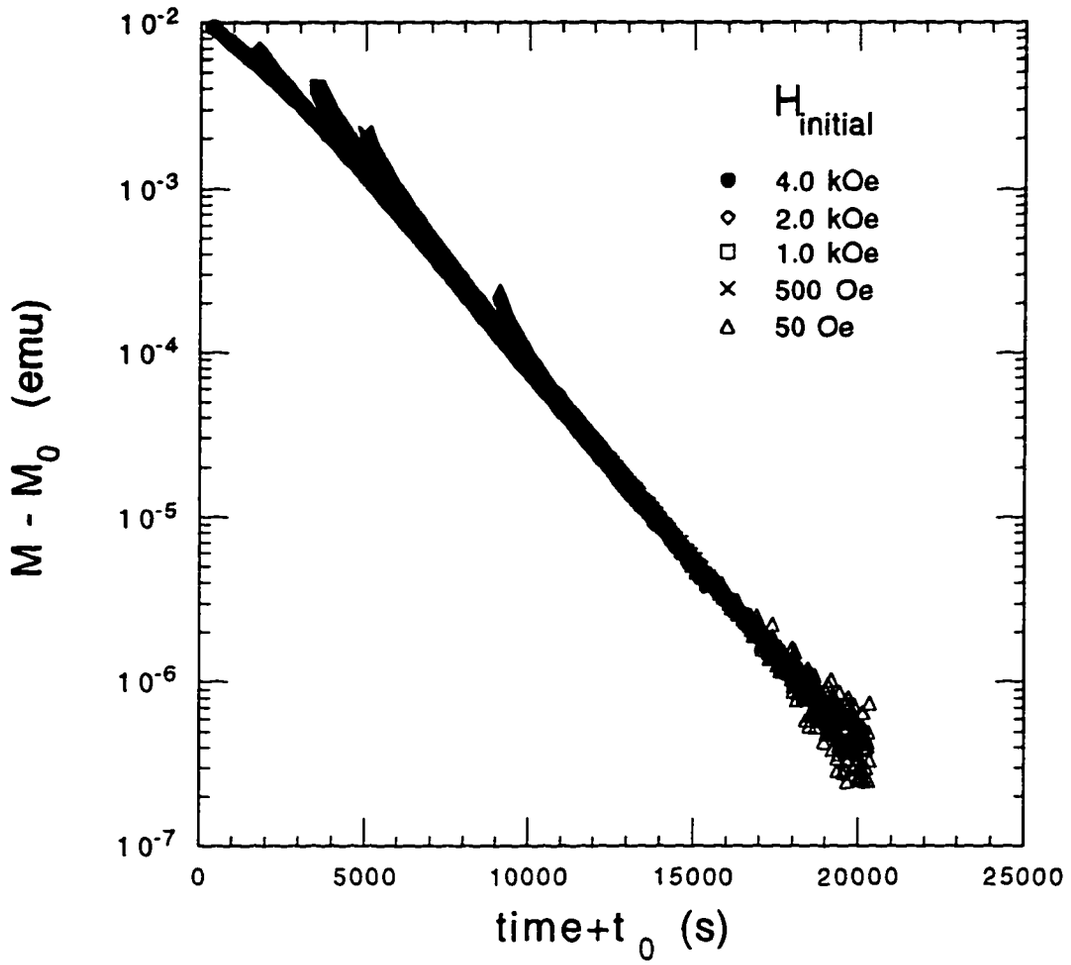

Fig. 3.12 Relaxation with various initial fields. Each relaxation curve shown was taken for a single crystal cooled to 2.6 K in the presence of the indicated field and then allowed to relax in zero field. As in Fig. 3.11, a small remnant moment, M_0, has been subtracted off from the measured value. The curves have also been shifted horizontally by t_0 so that they coincide. The success of such scaling indicates that the long-time relaxation rate is independent of the initial field.

The first two of these possibilities seem extremely unlikely, given the data in Fig. 3.12. Here several relaxation curves taken at 2.6 K have been superimposed. For each curve the sample is relaxing in near zero field, but the field in which it was cooled is different, i.e. its initial magnetization

varies from curve to curve. The curves have been shifted along the horizontal axis to make them superimpose in the long-time limit. That this can be done indicates that in this limit, the relaxation rate is independent of the initial conditions. It is interesting that the curves behave differently at short times, some relaxing faster, others slower. The initially slower rate for the curves with a large initial moment may be due to the fact that while the applied field is zero, the internal field B is not. Since, as we shall see below, the relaxation rate depends on field, the relaxation rate may be a function of magnetization. This effect, however, should be negligible when the moment is within a few percent of equilibrium, as for the curves that show an initial fast relaxation.

If dipole interactions or self heating were responsible for the initial faster relaxation, then those mechanisms should be suppressed when the initial magnetization is near equilibrium since the system starts relaxing in what should be tantamount to the long-time limit for these processes. Furthermore, since these curves are measured in zero applied field the energy released in a spin flip is zero and so there can be no self heating. Explanation #3 is also untenable: one reason is that it means the sample is almost entirely impurities. Another reason will be given shortly.

This leaves us with the tentative conclusion that the non-exponential decay is intrinsic to Mn_{12}. One possible reason for this is that the hyperfine field varies from cluster to cluster. The interaction with such fields can effect the height of the energy barrier (see Chapter IV). Another possibility is that the molecules of solvation trapped in the crystal are not distributed uniformly and therefore act as defects. The presence of such defects can cause local lattice distortions, slightly altering the energy barriers of nearby clusters.

The data shown in Figs. 3.11 and 3.12 can be roughly accounted for by a 5% dispersion in barrier heights.

Let us now consider the dependence of the relaxation rate on magnetic field. For a sample cooled to 2.4 K in zero field and measured in a field of 9.0 kOe or 9.5 kOe, Fig. 3.13 shows the difference between the magnetization and

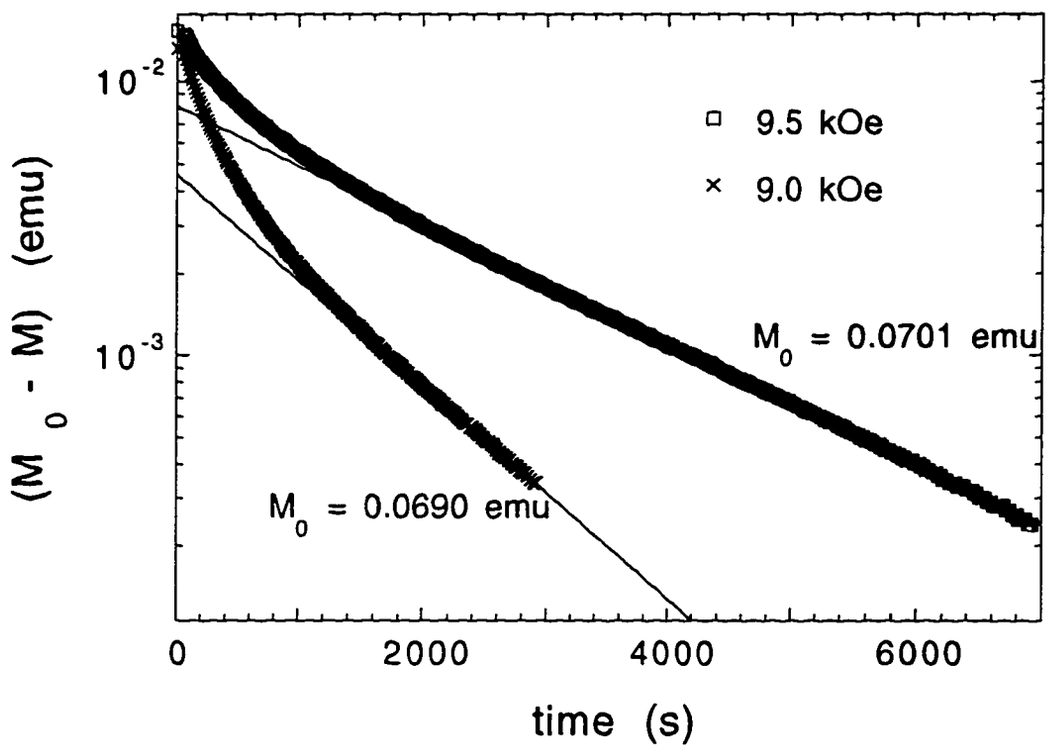

Fig. 3.13 Relaxation curves on and off resonance. Plotted is the difference between the magnetic moment and its asymptotic value on a logarithmic scale as a function of time for a sample of oriented powder in a Stycast matrix. The sample was cooled in zero field to 2.4 K and then the indicated field was applied. The data show that the relaxation is markedly faster for the curve taken with a field of 9.0 kOe, which is near where one of the steps occurs in the hysteresis loops. The straight-lines fits are to exponentials using data for t > 2000 s. The fits yield time constants of 1048 s and 2072 s for 9.0 kOe and 9.5 kOe, respectively.

its asymptotic value, M_0, plotted as a function of time on a semilogarithmic scale. While the asymptotic value of the magnetization is higher at the higher field, as expected, there is dramatically faster relaxation at 9.0 kOe (≈ 2 x 4.6 kOe) than at 9.5 kOe. Disregarding the faster-than-exponential decay during the initial ~2000 seconds, fits to an exponential form $M = M_0(1 - e^{-(t-t_0)/\tau})$ with M_0, t_0 and τ as free parameters yield time constants of 1048 s and 2072 s for 9.0 kOe and 9.5 kOe, respectively. Regardless of the exact functional form of the relaxation, the relaxation at both short and long times is distinctly faster at 9.0 kOe than it is at 9.5 kOe. This fact indicates that the non-exponential decay is intrinsic to Mn_{12} and not simply due to the presence of impurities.

The periodic increase in relaxation rate is confirmed through direct measurements of the relaxation at various fields and temperatures, shown in Fig. 3.14. Here the rate $\Gamma=1/\tau$ is plotted as a function of external field H at two temperatures. One can identify four maxima in the decay rate: at 0, and approximately H=4.6n kOe, with n=0, 1, 2, and 3.

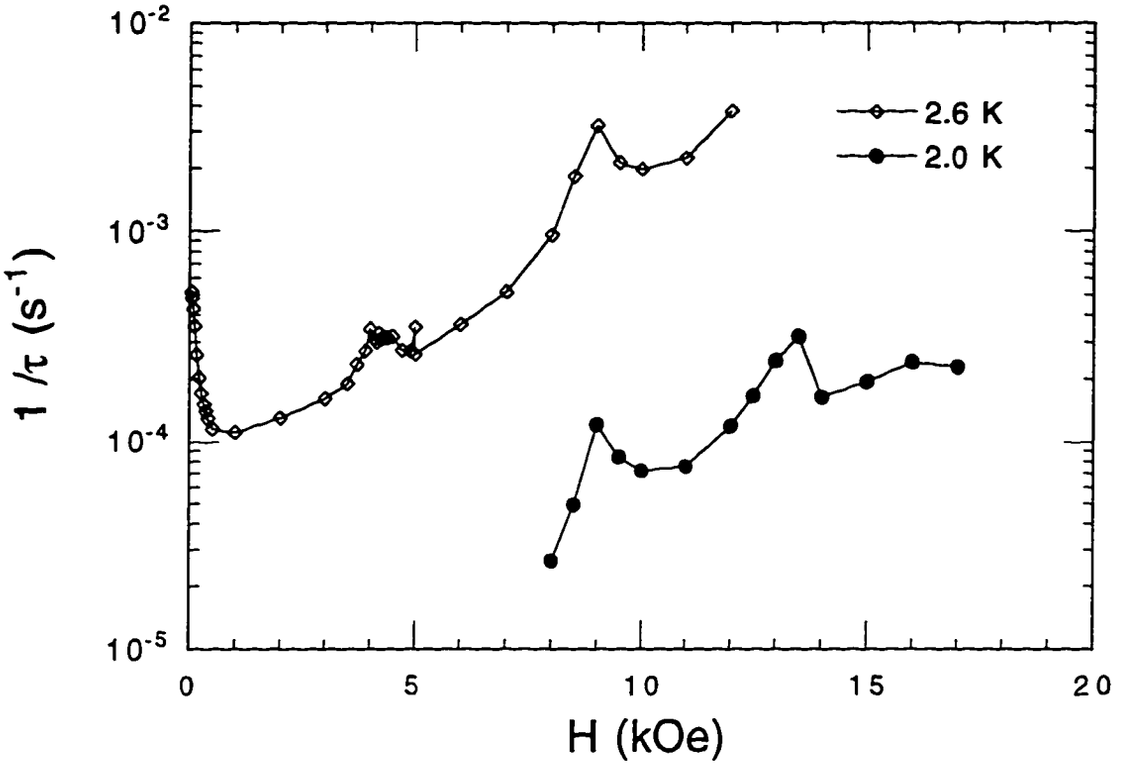

Fig. 3.14 Relaxation rate as a function of field for a powdered sample in a paraffin matrix. The rate was determined from fits to relaxation curves similar to those in Fig. 3.13. The peaks in the relaxation rate occur at the same fields as the steps in the hysteresis loops.

A careful study was done of the relaxation rate as a function of field near the zero-field resonance. The results for a oriented-powder sample in a paraffin matrix are presented in Fig. 3.15, where the relaxation rate is plotted as a function of field for three different temperatures. The data for each temperature fit very well to a Lorentzian function. This indicates that any inhomogeneous broadening of the resonance is negligible. The full width of the Lorentzian ranges from 234 Oe to 272 Oe and is not a monotonic function of temperature. The variation may be purely statistical in origin.

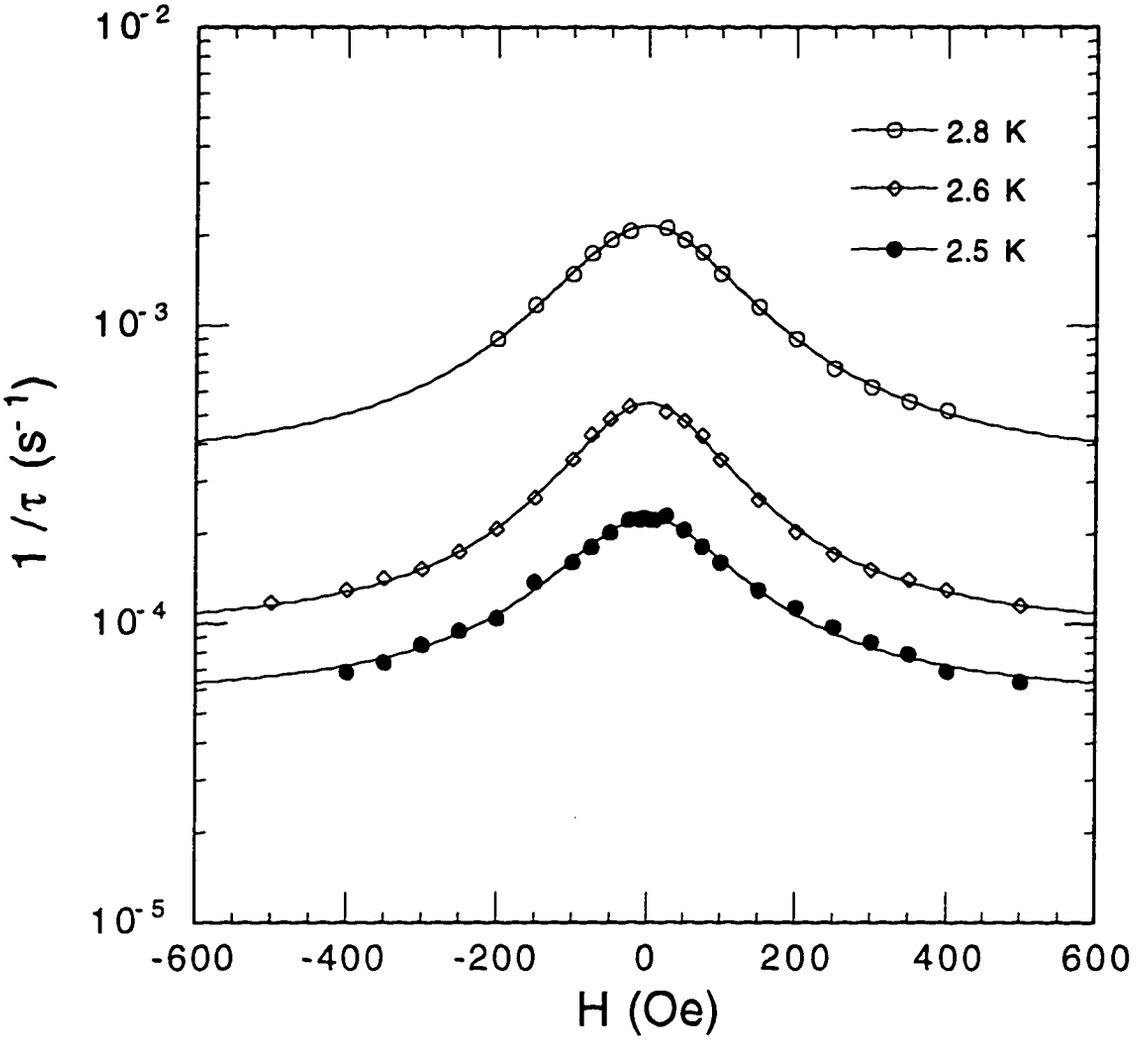

Fig. 3.15 Lineshape of resonance #0. The relaxation rate is plotted on a logarithmic scale as a function of field near zero field for a sample of oriented powder in a paraffin matrix. The data have been fit to Lorentzian functions plus a uniform background.

D. Angular studies

By varying the angle of the sample with respect to the direction of the magnetic field, one can study the effects of a transverse component to the

magnetic field on the phenomena discussed above. In brief, one finds that the steps always occur at the same values of longitudinal field, independent of the value of the transverse field. The transverse field lowers the effective energy barrier of the system. A detailed study shows that the barrier is reduced with transverse field in a way that is roughly consistent with classical expectations. Subtle deviations from the classical form may reflect the discrete quantum energy spectrum for the spin-10 system.

Fig. 3.16(a) shows the magnetization as a function of longitudinal field (essentially a quarter of the hysteresis loops) for various fixed values of transverse field at 2.0 K. As the transverse field is increased, one finds that the hysteresis is reduced and that steps that were "frozen out" become apparent again. This behavior is consistent with the fact that the transverse field reduces the energy barrier. It is also apparent that the longitudinal fields at which the steps occur does not change as a function of transverse field. This is more clearly demonstrated by the derivative of the magnetization, shown in Fig. 3.16(b), where the peaks always occur at the same longitudinal-field values. It should be noted that step #0 does not seem to occur at zero field. This is an artifact due to a slight miscalibration of the sample rotator. A small error in the angle of the sample is most significant when the sample is nearly perpendicular to the applied field since the error in the longitudinal field is $\delta H_{||} = - H \sin\theta \, \delta\theta$.

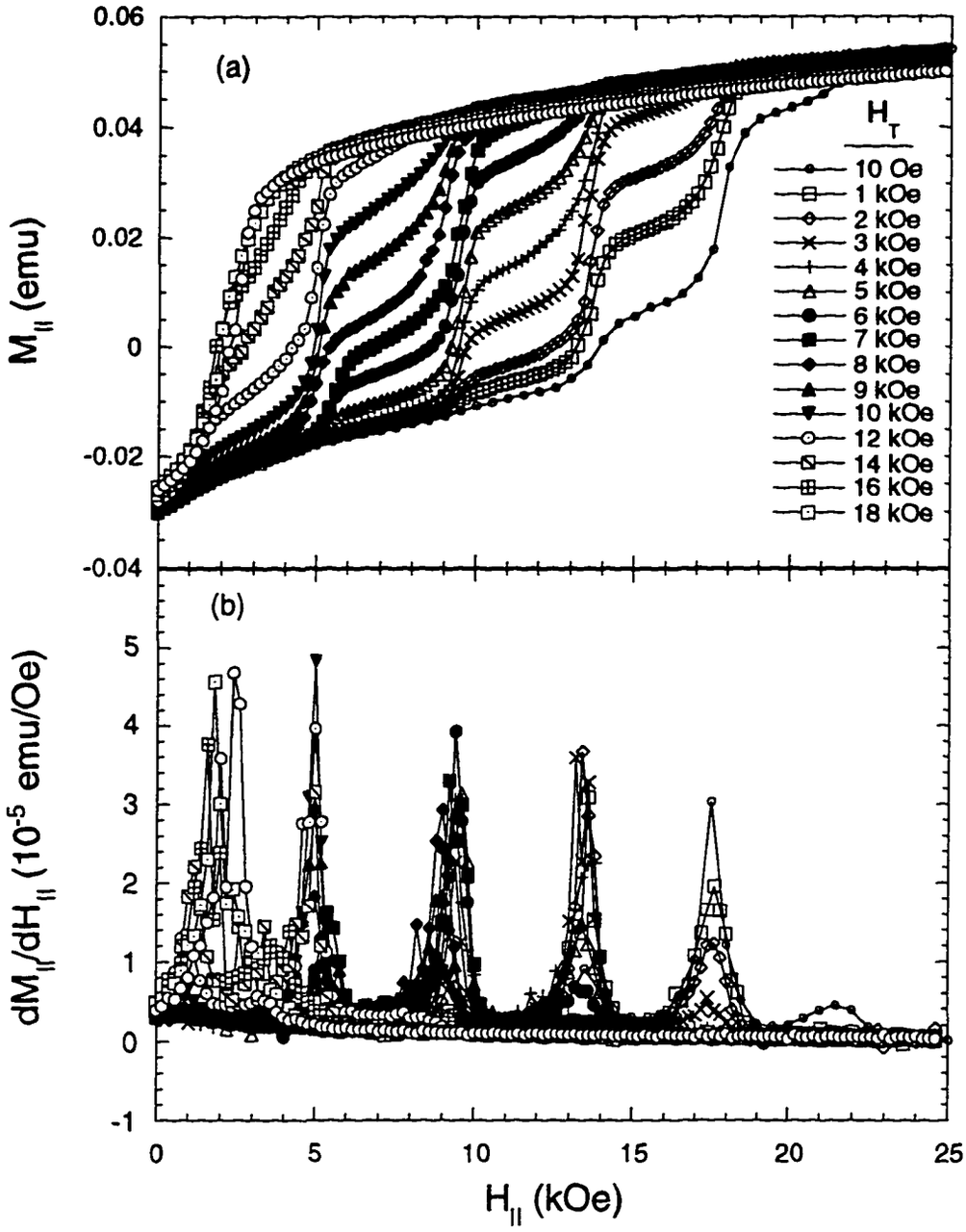

Fig. 3.16 Magnetization steps for various transverse fields. (a) Magnetization as a function of longitudinal field for several values of transverse field at 2.0 K. (b) The derivative of the curves in (a). The steps occur at the same values of longitudinal field for all values of transverse field.

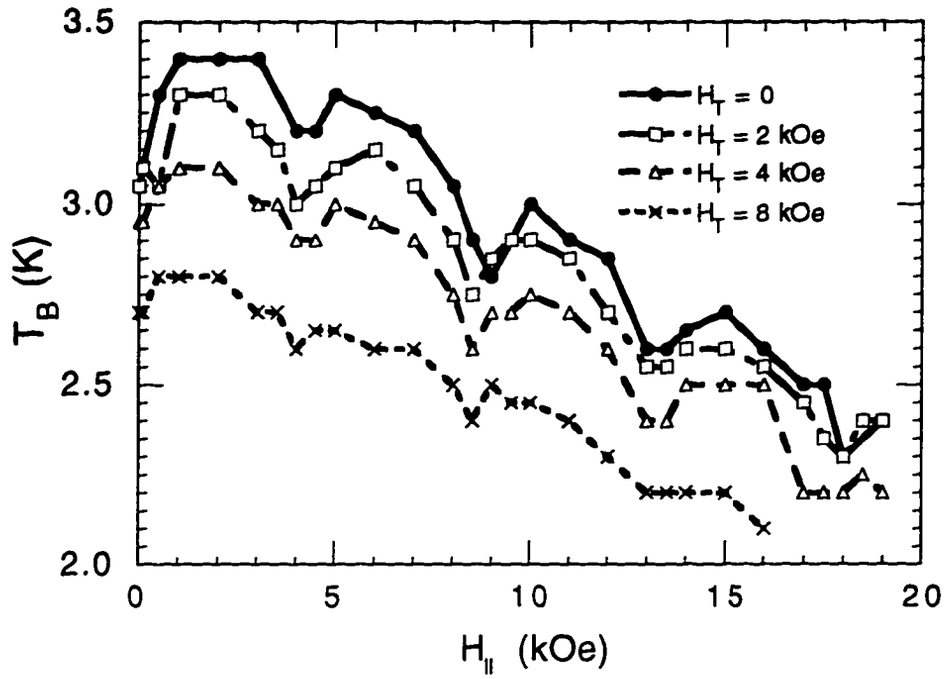

Fig. 3.17 Blocking temperature dependence on transverse field. The blocking temperature is plotted as a function of longitudinal field for four fixed values of transverse field. As the transverse field is increased, the entire curve shifts down, consistent with a decrese in the energy barrier. The dips remain at the same values of longitudinal field.

The temperature dependence of the magnetization confirms that the position of the steps is independent of transverse field. In Fig. 3.17 the blocking temperature T_B is plotted as a function of longitudinal field for several values of transverse field, as indicated. All of the data in this figure were obtained for a sample of oriented powder in a Stycast matrix. The figure shows that while the position of the resonances (dips) does not change as the transverse field in increased, the blocking temperature decreases monotonically for all values of longitudinal field. In other words, the transverse field has similar effects both on and off resonance. The

observations are consistent with the interpretation that the transverse field simply lowers the energy barrier of the system.

A detailed study of the relaxation rate as a function of both longitudinal and transverse field components was performed on a single crystal. Some of the results are shown in Fig. 3.18, where resonance #1 is mapped out at several transverse fields at a temperature of 2.7 K. The data were taken on a sample cooled in zero field. A field was then applied at an angle to the sample's easy axis so that the desired longitudinal and transverse field components were achieved. The relaxation rate was extracted by fitting the long-time tail of the relaxation curves to exponential functions. For consistency, the fit was applied to a subset of the data in which the moment is within 5 x 10^{-5} emu (~0.1% of saturation) of its equilibrium value. The resulting relaxation rates were fit to Lorentzian functions, shown by the curves in Fig. 3.18.

An initial inspection of the data reveals that the relaxation rate increases both on and off of resonance as the transverse field is increased, consistent with a reduction in the barrier height. One also finds that for a transverse field of 3 kOe, the relaxation rate does not increase as sharply as for other transverse field values. There is also a slight shift in the position of the peak as the transverse field is varied. This is most likely an experimental artifact, perhaps due to a nonlinearity in the rotator. The observed shift can be accounted for by an error in the angle of about 1°.

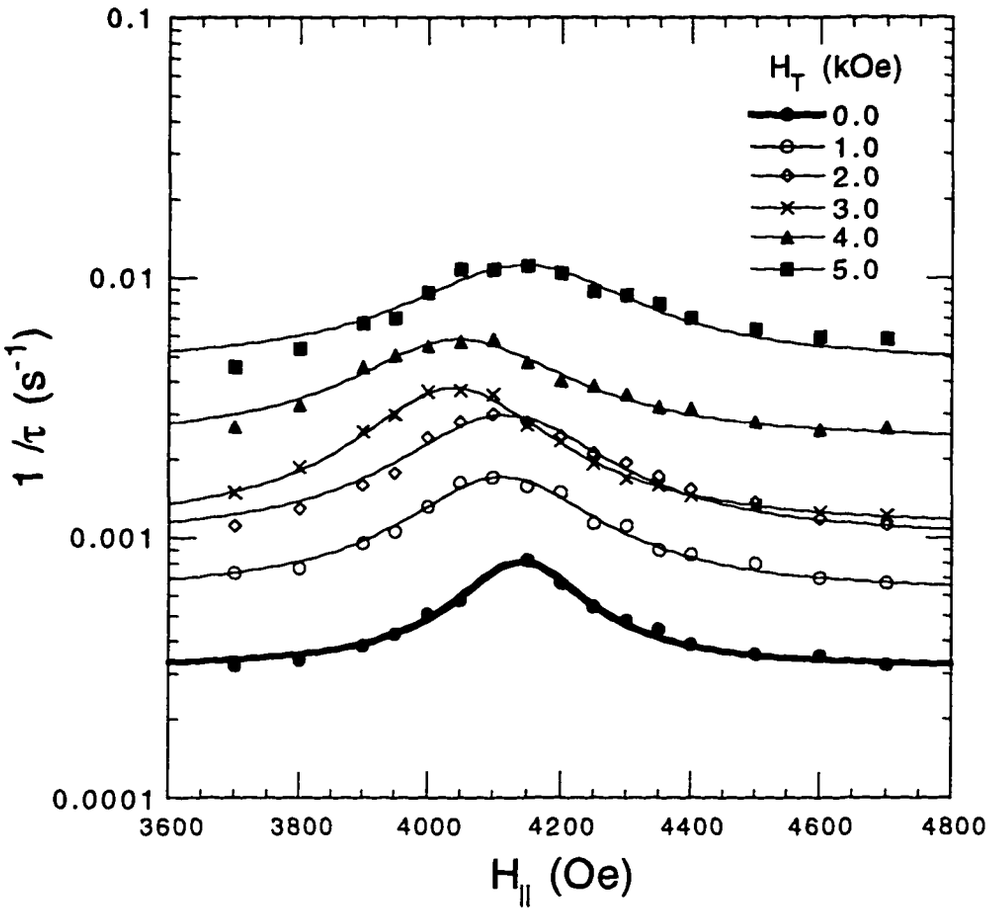

Fig. 3.18 Resonance #1 with various transverse fields. The relaxation rate is plotted as a function of longitudinal field for a single crystal sample cooled to 2.7 K and allowed to relax with given applied transverse and longidutinal fields. The fits are to Lorentzian functions with a constant background.

From the Lorentzian fits one can extract relaxation times both on resonance (peak of the curve) and off resonance. These are plotted as a function of transverse field on a semilogarithmic scale in Fig. 3.19. One sees that both on and off resonance, the relaxation rate "wiggles" as the transverse field is increased. (The non-monotonic behavior in the off-resonance curve may be suspect since it depends on one point and should be

studied more carefully.) The line labeled "classical" shows how the rate is expected to increase due to the classical lowering of the energy barrier by the transverse field. Interestingly, this line has no fitting parameters (its absolute value is, however, "pinned" to coincide with the zero-transverse-field, off-resonant rate). The relaxation rate is classically expected to obey the function

$$Log[\Gamma(H)] \propto U_0(1 - H/H_c)^2 / k_B T \approx U_0(1 - 2H/H_c)/k_B T,$$

the last step being valid for small H. Here $U_0 = DS^2$ is the magnitude of the classical energy barrier and $H_c = 2DS/g\mu_B$ is the field at which the barrier disappears (see Chapter IV). Substituting these definitions into the above expression, one finds that the anisotropy term D cancels out and the relative change in the relaxation rate is

$$Log[\Gamma(H)/\Gamma(0)] \approx g\mu_B HS / k_B T.$$

Using g=2, S=10 and T=2.7 K, results in the slope of the line shown in the figure. Note that both the on resonance and off resonance curves seem to have the same average slope. One is simply shifted vertically relative to the other. The systematic although slight deviation of the relaxation rate from the classical result may arise from the discrete level structure of this spin-10 system. This conjecture will be discussed further in the next two chapters.

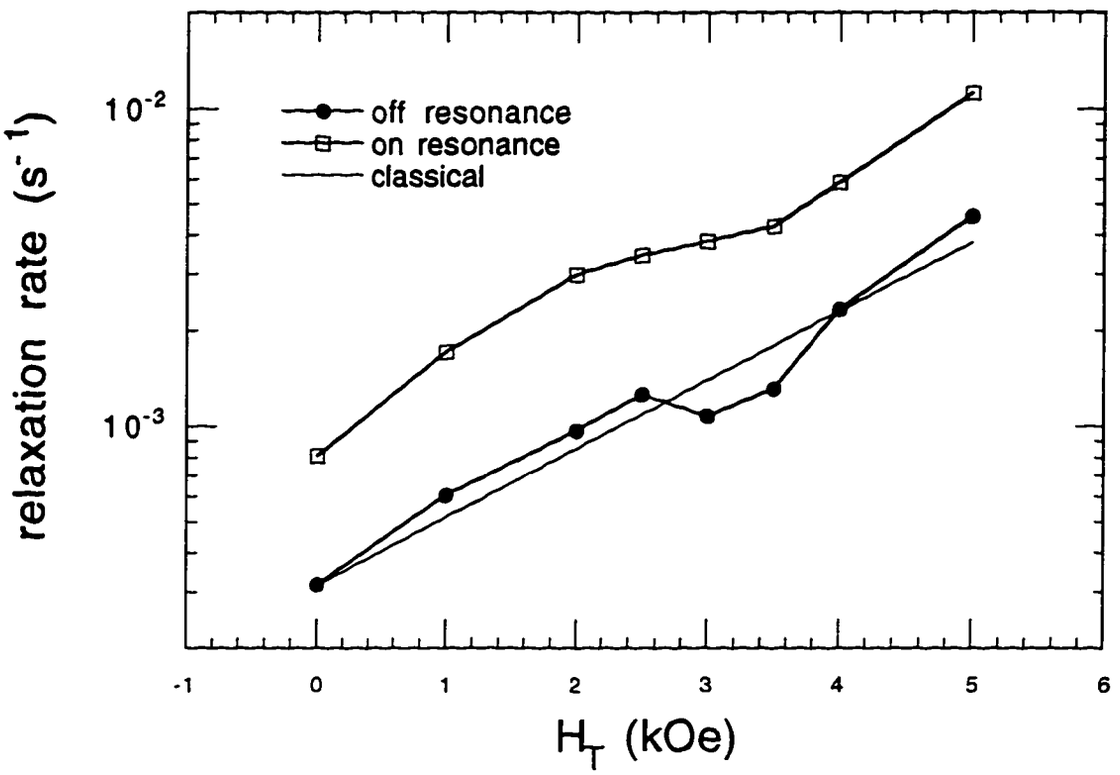

Fig. 3.19 Relaxation rate on and off resonance as a function of transverse field. The rates were determined from fits to the data in Fig. 3.18, with the rate on resonance corresponding to the peak in the data and the rate off resonance, the background. The stright line in this figure is the expected classical rate discussed in the text.

Let us summarize the results presented in this chapter. I have presented experimental findings for orientationally ordered samples of Mn_{12} acetate complex. The major results are as follows. (1) Steps are observed in the hysteresis loop with increasing field at equal intervals of 4.6 kG; no steps occur as the field is decreased. (2) The blocking temperature exhibits minima at the same magnetic fields. (3) The magnetic relaxation rate exhibits periodic maxima at these fields and these maxima have a Lorentzian lineshape. (3) New steps appear at higher fields as the

temperature is reduced while steps at lower fields become less apparent. (4) These "frozen" steps can be recovered by reducing the field sweep rate. (5) Angular studies demonstrate that these effects are periodic with longitudinal field, that is, the component of the field parallel to the easy axis of the sample. (6) A transverse field increases the relaxation rate in a way that roughly follows the expected classical behavior. In detail, however, the relaxation rate appears to exhibit small oscillations about the classical result.

IV. Theoretical Results

Mn_{12} can be thought of as a collection of independent spin-10 objects with large uniaxial magnetocrystalline anisotropy. In the presence of an applied magnetic field, the dynamics of such a spin can be described by the following simple Hamiltonian.

$$\mathcal{H} = -DS_z^2 - g\mu_B \mathbf{S}\cdot\mathbf{B}, \tag{4.1}$$

where D represents the anisotropy energy that breaks the zero-field Zeeman degeneracy and $\mathbf{B} = \mathbf{H} + 4\pi\mathbf{M}$ is the magnetic induction. (This is very similar to Eq. 1.1, except that the transverse anisotropy D' has been set to zero.) While this Hamiltonian seems extremely simple, it is remarkably rich and can be employed to explain many of the results presented in the previous chapter.

A. Review of current theory

First, let us review some things already known about this Hamiltonian. If the field is applied along the easy (z) axis, the eigenstates of this Hamiltonian are $|S,m\rangle$, where S is the total spin and m is the corresponding magnetic quantum number. The system can then be represented schematically as a double well potential, as shown in Fig. 4.1, where the 2S + 1 = 21 energy levels correspond to different projections of the spin along the easy axis. An

applied field is responsible for the asymmetry in the figure, making one well, say spin up, lower in energy than the other. In zero applied field the wells are symmetric and it is obvious that there is a two-fold degeneracy for each state (except m=0): m=10 and -10, m=9 and -9, etc. These degeneracies can be lifted by applying a symmetry-breaking field perpendicular to the easy axis. Garanin[55] has calculated this tunnel splitting for all these now quasidegenerate pairs. For future reference, it is useful to repeat a thumbnail sketch of his calculation here.

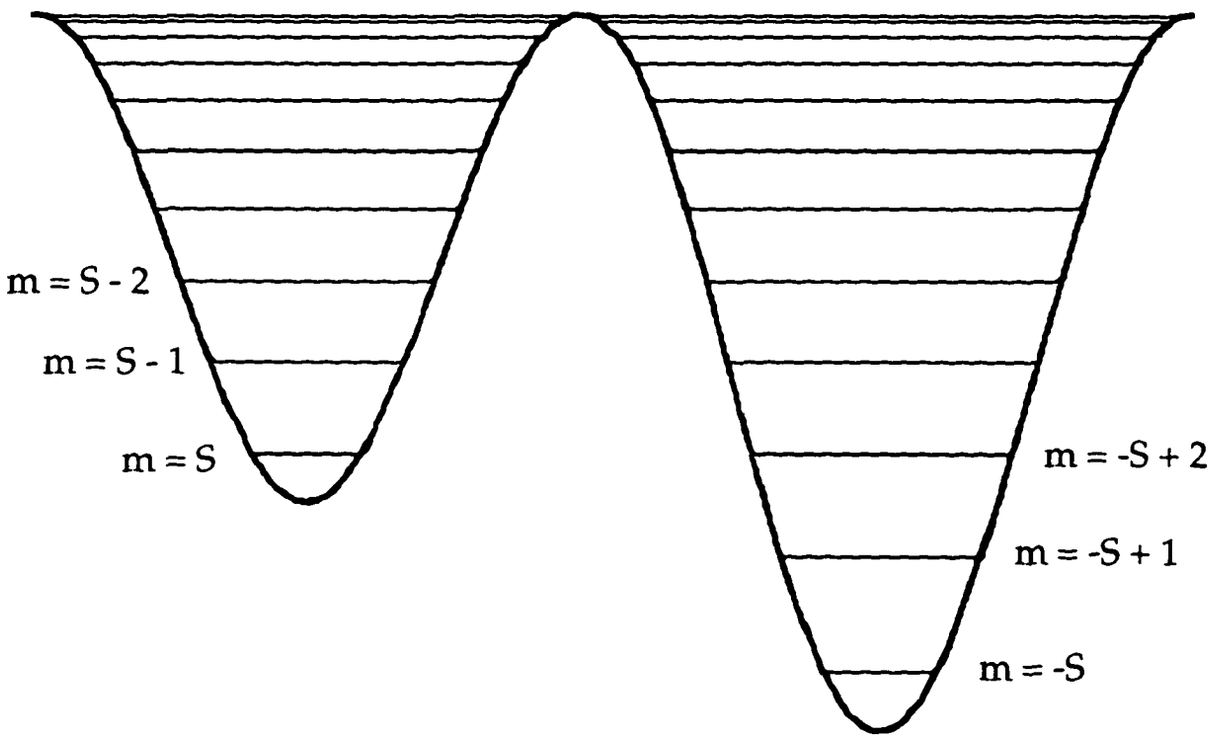

Fig. 4.1 Schematic double well potential for spin reversal. The energy barrier is due to the anisotropy and the asymmetry is produced by an applied longitudinal field. Energy levels correspond to different spin projections along the easy axis.

The transverse magnetic field can be treated as a perturbation:

$$H' = bS_x = \frac{b}{2}(S_+ + S_-), \tag{4.2}$$

where b = $g\mu_B B_{trans}$ and S_+ and S_- are the usual spin raising and lowering operators that allow transitions between states with m values that differ by 1. Given this fact and using standard degenerate perturbation theory, the lowest-order non-zero splitting of the degenerate pair of states m and -m is

$$\Delta E_m = 2\left\langle m\left|H'\right|m-1\right\rangle \frac{1}{E^0_{m-1} - E^0_m}\left\langle m-1\left|H'\right|m-2\right\rangle \frac{1}{E^0_{m-2} - E^0_m} \cdots$$
$$\cdots \frac{1}{E^0_{-m+1} - E^0_m}\left\langle -m+1\left|H'\right|-m\right\rangle$$

where $E_m{}^0 = -Dm^2$. Collecting similar factors and using the fact that $\left\langle l+1\left|S_+\right|l\right\rangle = \sqrt{(s-l)(s+l+1)}$, one obtains

$$\Delta E_m = \frac{2(b/2)^{2m}}{D^{2m-1}} \prod_{k=-m+1}^{m-1} \frac{1}{m^2 - k^2} \prod_{l=-m}^{m-1} \sqrt{(s-l)(s+l+1)}.$$

The products are easily evaluated to give

$$\Delta E_m = \frac{2D}{\left[(2m-1)!\right]^2} \frac{(s+m)!}{(s-m)!}\left(\frac{b}{2D}\right)^{2m}. \tag{4.3}$$

This formula indicates that the tunneling rate is a very strong function of m, with states near the top of the barrier (m << S) having much faster rates than states near the bottom (m ~ S). This is illustrated in Table I, which contains the tunneling rates calculated from Eq. (4.3) for all quasidegenerate pairs of states. A transverse field of 100 G was assumed for this calculation; all other parameters were taken from measured values for Mn_{12}. It is interesting to note that in the limit of large spin and m = S Eq. 4.3 reduces to the semiclassical result (up to a constant factor) calculated by van Hemmen and Süto[33] (Eq. 1.3).

TABLE I: Tunneling rates for different m values calculated from Eq. 4.3 with s=10, B_{trans}= 100 G and D=0.41 cm^{-1}.

m	Tunneling rate (Hz)
1	3.2×10^{8}
2	1.1×10^{5}
3	3.5×10^{0}
4	2.3×10^{-5}
5	4.7×10^{-11}
6	3.7×10^{-17}
7	1.2×10^{-23}
8	1.7×10^{-30}
9	1.1×10^{-37}
10	2.11×10^{-45}

One of the interesting open questions about Mn_{12} is the mechanism of thermal activation over the energy barrier. From a classical point of view, the thermal activation rate is described by an Arrhenius law, $\Gamma = \omega_0 e^{-\Delta E / k_B T}$, where ΔE is the height of the energy barrier and ω_0, called the attempt

frequency, represents the frequency of small oscillations in the metastable well (i.e. the left well in Fig. 4.1). Physically, this frequency is usually associated with the Larmor precession frequency of the spin in the anisotropy field and is generally on the order of the ferromagnetic resonance width: 10^{10} - 10^{12} Hz. The temperature dependence of the relaxation rate for Mn_{12} fits an Arrhenius law well. However, the attempt frequency ω_0 is around 10^7 Hz, several orders of magnitude smaller than expected.

Villain, et al.[48,50] have attempted to explain this anomaly through a generalized Orbach process. Their model entails the absorption of a series of acoustic phonons, each of which brings the system to the next highest energy state in the metastable well, as illustrated in Fig. 4.2. Once over the top of the barrier, the system emits a cascade of phonons as it decays to the ground state in the right well. Since the spectral density of acoustic phonons goes as ω^3, where ω is the frequency of the phonon, the rate-limiting step in this model is at the top of the barrier where the energy difference between levels is minimal and so the phonon needed is of smallest energy. The attempt frequency in this model is then the lifetime for the highest-lying state, m=0, to decay to m=1 (or , equivalently, -1). The result of their calculation is that at low temperatures the relaxation rate is

$$1/\tau = \frac{3}{2\pi}\frac{|V_{10}|^2}{\hbar^4 \rho c^5}\left[\frac{\Delta}{S^3}\right]^2 \frac{exp(\Delta/k_BT)}{1-exp(\Delta/k_BTS^2)}, \qquad (4.4)$$

where Δ is the energy barrier, ρ is the density and V_{10} is the spin-phonon matrix element between two highest-lying states. The essential result of this calculation, according to Villain, et al.[48,50], is the fact that the relaxation rate is

proportional to S^{-6} (appearing in the prefactor to the exponential). Mn_{12}, with S=10, they argue, will have an attempt frequency that is reduced by six orders of magnitude relative to that of a more common S=1 system.

While this model seems compelling, providing a microscopic physical picture to the Arrhenius law in a large-spin system, it does have a serious fault. As we will discuss in more detail below, whatever our model of the relaxation process is, it must correspond to classical physics in the macroscopic (high-spin) limit. However, Villain, et al.'s result, Eq. 4.4, implies that the relaxation will become infinitely slow as S become large.

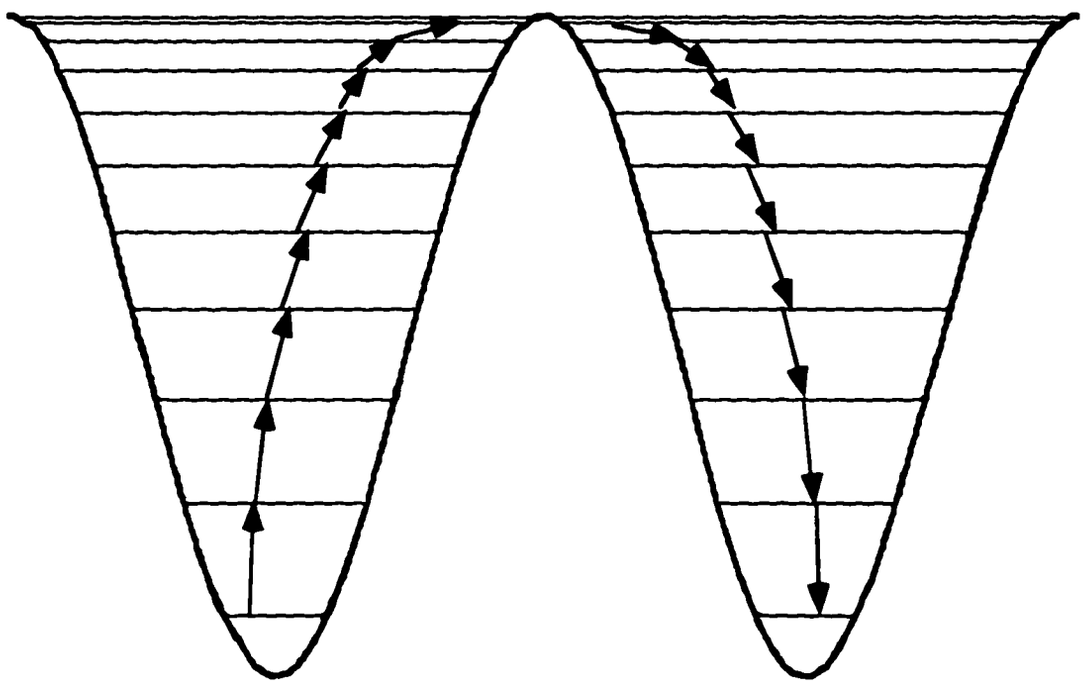

Fig. 4.2 Illustration of the model of Villain, *et al.* for spin reversal. The relaxation process proceeds by the absorption of a series of phonons until the top of the barrier is reached. The system then decays down the other side of the barrier by releasing a cascade of phonons.

Currently there are no other available microscopic models that adequately account for the dynamics of Mn_{12} and its anomalously slow attempt frequency. It is conceivable that suitable modifications to the model put forth by Villain, et al. may yield a theory with a realistic classical limit. More work in this subject is certainly warranted.

B. New Theoretical Results

Now that we have reviewed some of the theoretical models and results concerning the dynamics of a spin with uniaxial anisotropy, let us examine some others aspects of the Hamiltonian, Eq. 4.1. As noted above, this simple form has some remarkable consequences. Among other things, one finds: degeneracies occur at regular intervals of longitudinal field, multiple resonances occur simultaneously, a transverse magnetic field does not alter the values of longitudinal field at which the resonances occur, and the classical reduction of the energy barrier by a transverse field can be explained in terms of the tunnel splitting of excited states, as calculated by Garanin, Eq. 4.3.

First, let us show that there are resonances at regular intervals of the longitudinal component of the magnetic field. Consider the case where the field is parallel to the easy axis. Then Eq. 4.1 can be written as

$$\mathcal{H} = -DS_z^2 - g\mu_B BS_z.$$

Completing the square, one obtains

$$\mathcal{H} = -D(S_z + \frac{g\mu_B B}{2D})^2 + D(\frac{g\mu_B B}{2D})^2,$$

and the state $|m\rangle$ has energy

$$E_m = -D(m + \frac{n}{2})^2 + D\frac{n^2}{4},$$

where n = $g\mu_B B/D$. Now it is clear that the state $|-m+n\rangle$ has the same energy; i.e. this eigenenergy formula is invariant under the transformation $m \rightarrow -m+n$. Note, however, that this transformation is only meaningful if n is an integer since the state $|-m+n\rangle$ does not exist otherwise. So, one can conclude that states $|m\rangle$ and $|-m+n\rangle$ will have the same energy when the magnetic induction B satisfies

$$B_{m,-m+n} = -\frac{Dn}{g\mu_B}, \tag{4.5}$$

with n an integer. It is important to note that this result is independent of m, implying that all levels in the left well come into resonance with levels in the right well at the same values of magnetic field. Fig. 4.1, where the field has been set such that n=2, illustrates this multiple resonance.

It is useful to relabel the states to reflect the degeneracy more clearly. If one defines $m' = m - n/2$, then for a given value of n the degenerate states $|m\rangle$ and $|-m+n\rangle$ can be relabled as $|m'\rangle$ and $|-m'\rangle$. When operated upon by S_z, these states have eigenvalues of [m' + n / 2] (= m) and [-m' + n / 2] (= -m +

n), respectively. With this labeling, each degenerate pair comprises states with labels that differ only by a sign, making it clear that they are degenerate. The new label m' can be thought of as a counting number, indicating how far down the state is from the top of the barrier (see Fig. 4.1).

The resonance condition, Eq. 4.5, was calculated for the case in which the field is applied parallel to the easy axis. It is not *prima facie* clear that this condition would be unaltered if an additional component of the field is applied perpendicular to the easy axis. Such a field, treated as a perturbation (Eq. 4.2), will certainly alter the energy of the states. Using standard non-degenerate perturbation theory, one can calculate the second-order correction to the energy of each state in the case when the unperturbed system is tuned to resonance n. The result is

$$E_m^{(2)} = -\frac{b^2\,(s\,(s+1)+m\,(-m+n))}{2D\,(n^2-1-4m\,(-m+n))} = -\frac{b^2\,(s\,(s+1)-m'^2+(n/2)^2)}{2D\,(4m'^2-1)}, \tag{4.6}$$

which is manifestly invariant under the transformation $m' \rightarrow -m'$ ($m \rightarrow -m+n$). Hence, two states that are degenerate in the unperturbed case ($|m'\rangle$ and $|-m'\rangle$) both have the same correction to their energy and remain degenerate when the perturbation, Eq. 4.2, is turned on. Note that the denominator of Eq. 4.6 is zero when m' = ±1/2. As is usual in perturbation theory, this indicates that degenerate perturbation theory must be invoked. The proper treatment does not lead to a correction in the resonant condition for this pair but rather a calculation of the tunnel splitting *á la* Garanin (see below).

Since there is no correction to the resonant condition to second order in perturbation theory, it seems reasonable to ask if any correction exists at all. The next non-zero correction to the energy of the states is fourth order (all odd orders are trivially zero). The result is

$$E_{m'}^{(4)} = \frac{b^4}{32D^3}\left(-4m'^6 + 9m'^4 - 5m'^2 + 5/4n^2 - m'^2n^2/2 + 6m'^4n^2 - \right.$$
$$-7/16n^4 - 5/4m'^2n^2 - 2s - 22m'^2s + 24m'^4s + 7/2n^2s +$$
$$+10m'^2n^2s - 9s^2 - 42m'^2s^2 + 24m'^4s^2 + 7/2n^2s^2 + 10m'^2n^2s^2 -$$
$$\left.-14s^3 - 40m'^2s^3 - 7s^4 - 20m'^2s^4\right) / (m'^2 - 1)(4m'^2 - 1)$$

While this expression is quite messy, it is clear that all powers of m' are even. Hence, up to fourth order in perturbation theory, the correction to the resonance condition is exactly zero. Note that the denominator here becomes zero when m' = ±1/2,±1, requiring again the use of degenerate perturbation theory for these states.

Although calculations to higher-orders of perturbation theory have not been done, one can conjecture that for any given order, the presence of some not-yet-understood hidden symmetry will cause the resonance condition, Eq. 4.5, to be unaltered for all states that are not tunnel-split up to that order. In other words, it seems reasonable to say that a transverse magnetic field will not alter the value of the longitudinal field at which two levels cross up until the point that those levels have been split by tunneling. The symmetry responsible for the this odd result is not exact, as can be determined numerically, but is apparently broken by the tunneling.

We have already studied in detail the tunnel splitting for the case of zero longitudinal field, as calculated by Garanin. Since we now know that degeneracies arise at other values of longitudinal field, we can attempt to extend Garanin's calculation to these other resonances. Let us consider the system tuned by the longitudinal field to resonance n. Then the state $|m\rangle$ $(=|m'\rangle)$ is degenerate with $|-m+n\rangle$ $(=|-m'\rangle)$. So, the lowest order splitting for this pair is

$$\Delta E_m = 2\left\langle m\left|H'\right|m-1\right\rangle \frac{1}{E^0_{m-1}-E^0_m}\left\langle m-1\left|H'\right|m-2\right\rangle \frac{1}{E^0_{m-2}-E^0_m}\cdots$$
$$\cdots \frac{1}{E^0_{-m+n+1}-E^0_m}\left\langle -m+n+1\left|H'\right|-m+n\right\rangle ,$$

where now $E_m{}^0 = E_{-m+n}{}^0 = -Dm\,(m-n) = -D\,(m'^2 - n^2/4)$. After evaluating the matrix elements, one obtains

$$\Delta E_m = \frac{2\,(b/2)^{2m-n}}{D^{2m-n-1}} \prod_{k=-m+n+1}^{m-1} \frac{1}{(m-n/2)^2-(k-n/2)^2} \prod_{l=-m+n}^{m-1}\sqrt{(s-l)(s+l+1)}$$
$$= \frac{2\,(b/2)^{2m'}}{D^{2m'-1}} \prod_{k'=-m'+1}^{m'-1} \frac{1}{m'^2-k'^2} \prod_{l=-m'+n/2}^{m'+n/2-1}\sqrt{(s-l)(s+l+1)}$$

Finally, the result for arbitrary integer n (< 2s + 1) is

$$\Delta E_m = \frac{2D}{[\,2m-n-1)\,!^2}\sqrt{\frac{(s+m)\,!\,(s+m-n)\,!}{(s-m)\,!\,(s-m+n)\,!}}\left(\frac{b}{2D}\right)^{2m-n}$$
$$= \frac{2D}{[\,2m'-1)\,!^2}\sqrt{\frac{(s+m'+n/2)\,!\,(s+m'-n/2)\,!}{(s-m'-n/2)\,!\,(s-m'+n/2)\,!}}\left(\frac{b}{2D}\right)^{2m'} \quad (4.7)$$

One of the interesting things about Garanin's tunneling result, Eq. 4.3, is that in the semiclassical (large-spin) limit it can be used to obtain the classical reduction of the energy barrier by a transverse magnetic field. To see this, we consider a large spin with uniaxial anisotropy described by the Hamiltonian, Eq. 4.1, with the field, **B**, along the x direction:

$$\mathcal{H} = -DS_z^2 - g\mu_B BS_x.$$

Considered classically, the lowest energy orientation for the spin is an angle of $\theta = \sin^{-1}(g\mu_B B/2DS)$ or $\pi - \sin^{-1}(g\mu_B B/2DS)$ from the z axis. The lowest energy path to get from one minimum to another passes through a saddle point where $\theta = \pi$. The energy difference between these extrema defines the height of the energy barrier, U:

$$U = U_0\,(1 - B/B_c)^2 = U_0\,(1 - 2B/B_c + (B/B_c)^2), \quad (4.8)$$

where $U_0 = DS^2$ is the height of the barrier in zero field and $B_c = 2DS/g\mu_B$ is the critical field at which the barrier disappears. Now, the leading term in this expression is linear in B. This leads to an interesting paradox since the lowest-order correction to the energy of any state, Eq. 4.6, is quadratic in B.

In order to resolve this seeming contradiction we must carefully approach the question of what we mean by an energy barrier in the quantum picture. Naïvely, we can define it as the energy difference between the lowest-energy state (m=S) and the highest-energy state (m=0). But this definition leads us to the paradox, as the energies of these states vary as B^2. One arrives at a better definition of the energy barrier by recognizing that the transverse field produces tunneling in the levels and that the tunneling is orders of magnitude faster for the highest levels than for the lower ones (see Table I). We can then define the energy barrier as the energy difference between the lowest level and a level where the tunneling occurs "sufficiently fast." As we shall see, this definition of the energy barrier corresponds to the classical result in the large-spin limit. That is, the term linear in B is obtained.

In the limit of large spin (S >> m >> 1) Garanin's result, Eq. 4.3, can be simplified to

$$\Delta E_m = \frac{2Dm}{\pi}\left(\frac{bSe^2}{8Dm^2}\right)^{2m},$$

where we have used Stirling's approximation $x! \approx \sqrt{2\pi x}\, e^{-x} x^x$ and the identity $(1+1/x)^x \xrightarrow[x\to\infty]{} e$. The level m becomes the top of the barrier when the tunnel splitting is on the order of Dm, the distance between neighboring levels, i.e. when $\frac{\Delta E_m}{Dm} \approx O[1]$. The field at which this happens is then

$$b = \frac{8Dm^2}{Se^2}\left(\frac{\pi}{2}O[1]\right)^{1/2m} \xrightarrow[m>>1]{} \frac{8Dm^2}{Se^2} \tag{4.9}$$

since the term in the brackets rapidly approaches 1 as m gets large. This indicates that the precise criterion used for a level to be tunneling "sufficiently fast" is irrelevant, as should be the case in the classical limit.

Our definition of the barrier as the energy difference between the lowest state $|S\rangle$ and this critical tunneling state $|m\rangle$ gives

$$U = DS^2 - Dm^2 - \frac{b^2S^2}{8Dm^2},$$

where the last term is the second-order correction to the energy of state $|m\rangle$, Eq. 4.6, in the limit S >> m >> 1 (the correction to the energy of state $|S\rangle$ is negligible). Using the critical tunneling criterion, Eq. 4.9, we can eliminate m from this expression to obtain

$$U = DS^2\left(1 - \frac{2b}{2DS}\left(\frac{e^2}{8} + \frac{1}{e^2}\right)\right) = U_0\left(1 - \frac{2b}{b_c}(1.06)\right), \tag{4.10}$$

where $b_c \equiv g\mu_B B_c = 2DS$. This reproduces the leading term in the classical result, Eq. 4.8, except for the factor of 1.06, which should be exactly 1. The discrepancy can be attributed to the fact that Garanin's result, Eq. 4.3, is valid when $b << Dm^2$, and we are employing it for $b \approx Dm^2$, exactly where it begins to break down.

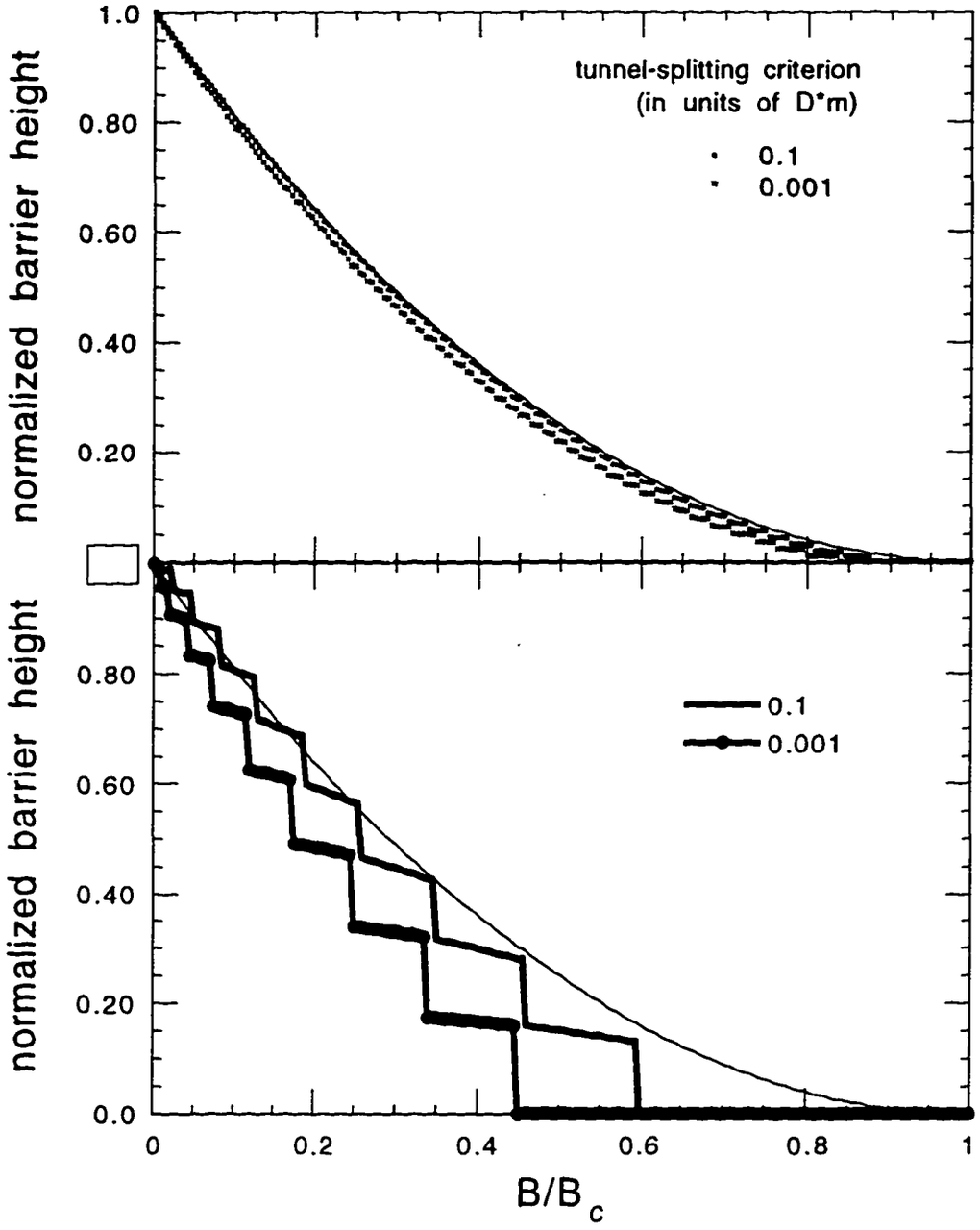

Fig. 4.3 Calculated barrier reduction by a transverse field for (a) spin 100 and (b) spin 10. The thin lines are the classical result while the points are the results of numerical diagonalization of the Hamiltonian, defining the top of the energy barrier to be the level for which the tunnel splitting is comparable to the spacing between levels, as described in the text.

This model of barrier reduction can also be simulated numerically by diagonalizing the Hamiltonian and again defining the top of the barrier to be the state where the tunnel splitting is on the order of the spacing between levels. The results of such a simulation for a spin of 100 are shown in Fig. 4.3(a), where the critical tunneling criterion was taken to be $\Delta E_m = 0.1 Dm^2$. The solid curve is the classical result; the agreement is quite good. Notice that changing the splitting criterion for the critical level by two orders of magnitude (from 0.1 to 0.001) only creates minor deviations that are most apparent near the critical field. (The Mathematica script used to produce these results in given in Appendix C.)

It is interesting to ask what happens to this picture when the magnitude of the spin is not very large so that the levels do not form a quasi-continuum. The analytical result derived above breaks down in this case, but the simulations are still valid. Fig. 4.3(b) shows the result for a spin of 10 (i.e. Mn_{12}). The barrier is now no longer reduced smoothly as a function of transverse field. Instead there are a series of jumps and plateaus. This is easy to interpret within the picture presented above: as the transverse field is raised, the "fast-tunneling" level abruptly changes from one level to the next lowest when the selected criterion is reached for the lower level. It should also be noted that here the result is more susceptible to the particular criterion one chooses for the critical tunnel splitting. Experimentally this criterion is selected by measurement time scales and temperature. Thus, one might expect measurements of the barrier height to depend on the precise experimental parameters. In this low-spin limit, the barrier ceases to have intrinsic significance and retains only empirical significance. For example, in the low-temperature, long-time-scale limit, tunneling from the ground state is the

dominant process. The system no longer needs to reach any excited levels and so effectively there is no barrier.

C. Temperature Dependence of Thermally Activated Tunneling in the Presence of a Transverse Magnetic Field.

In the preceding discussion, we have treated the barrier as a static object and have not addressed the question of how it is traversed. As mentioned toward the beginning of this chapter, there is no adequate theory to describe the kinematics of this process. The picture of Villain, et al.[48,50] has some physical sense but does yield the classical result in the high-spin limit.

I will not try to develop here a microscopic model to describe the dynamics of spin reversal. In the absence of such a proper treatment, I will present a phenomenological model that may have relevance to experimental results.

The model is qualitatively simple and much of the logic and notation are taken from Villain, et al.[48] Let us break up the relaxation process into three steps: the system is first thermally activated within the metastable well to some high-lying level, it then tunnels across the barrier, and finally it spontaneously decays to the ground state of the right well. This process is depicted in Fig. 4.4. On resonance, there are several of these processes occurring in parallel, one for each pair of excited state. For the moment, we will consider just one process, which includes four states: $|S\rangle$, $|m'\rangle$, $|-m'\rangle$ and

$|-S\rangle$. It is straightforward to write down differential equations for the populations p_i of these states:

$$\begin{aligned}
\frac{dp_S}{st} &= -\gamma_{m'} e^{-\varepsilon_{m,s}/T} p_S + \gamma_{m'} p_{m'} \\
\frac{dp_{m'}}{dt} &= \gamma_{m'} e^{-\varepsilon_{m,s}/T} p_S - \gamma_{m'} p_{m'} - \Gamma_{m'}\left(p_{m'} - p_{-m'}\right) \\
\frac{dp_{-m'}}{dt} &= \gamma_{-m'} e^{-\varepsilon_{-m',-s'}/T} p_{-s} - \gamma_{-m'} p_{-m'} + \Gamma_{m'}\left(p_{m'} - p_{-m'}\right) \\
\frac{dp_{-s}}{dt} &= -\gamma_{-m'} e^{-\varepsilon_{-m',-s'}/T} p_{-s} + \gamma_{-m'} p_{-m'}
\end{aligned} \tag{4.11}$$

where γ_m is the spontaneously (natural) lifetime of state $|m\rangle$, $\varepsilon_{m,s}$ is the energy difference between states $|m\rangle$ and $|S\rangle$ and Γ_m is the tunneling rate for the state $|m\rangle$. It should be noted that the this tunneling rate is related but not equal to the tunnel splitting calculated above, Eqs. 4.3 and 4.7. These calculations assume that the levels involved have infinitesimal width. In reality, the width of the levels homogeneously broadens the resonance. Garg[56] has calculated the effect of such broadening on the tunneling rate. His result (in somewhat different notation) is

$$\Gamma_{m'} = \Delta E_{m'}^2 \frac{\gamma_{m'}}{\varepsilon_{m',-m'}^2 + \gamma_{m'}^2/4}$$

and it is this result that will be used for all of the calculations performed in the remainder of this chapter. This form also allows us to calculate the tunneling rate as one tunes away from resonance. While this calculation is technically only valid when $\Delta E_{m'} << \gamma_{m'}$, it will be employed outside this limit since, as we

shall see, excited states with very large tunneling rates become largely irrelevant.

Eqs. 4.11 can be simplified by noting that at low temperatures (T << DS) the population of the excited states in both wells is small and so one can make the approximation, following Villain, et al., that $dp_{m'}/dt = dp_{-m'}/dt \approx 0$. After some algebra Eqs. 4.11 can be reduced to

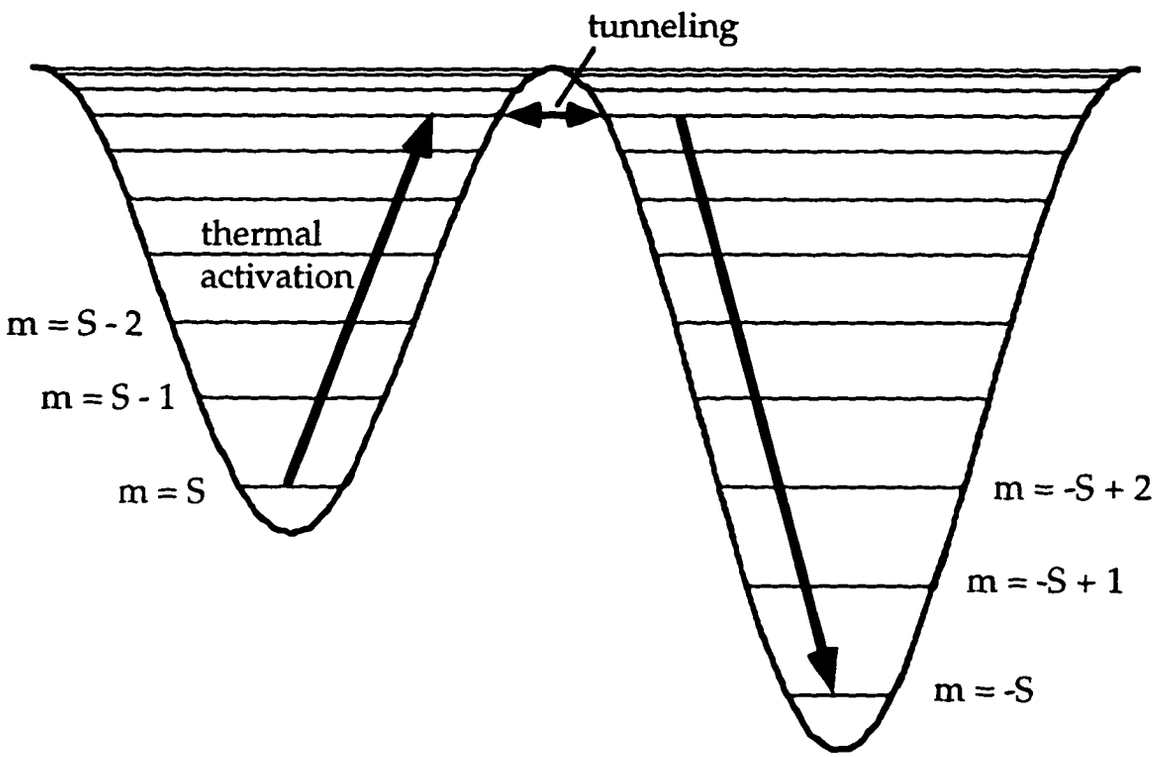

Fig. 4.4 Thermally assisted tunneling scheme. The system is thermally activated in the left well to an excited state for which the tunneling rate is significantly faster than the thermal repopulation rate. It then rapidly tunnels across and spontaneously decays to the ground state of the right well. The tunneling level depends on the transverse magnetic field.

$$\frac{d\left(p_s - p_{-s}\right)}{dt} = -\frac{\gamma_{m'}}{1+\dfrac{\gamma_{m'}}{2\Gamma_{m'}}} e^{-\varepsilon_{m',s}/T}\left(p_s - e^{-\varepsilon_{s,-s}/T} p_{-s}\right).$$

Noting that the magnetization M at low temperatures is approximately $(p_s - p_{-s}) / (p_s + p_{-s})$ and that the equilibrium magnetization is given by $M_{eq} = -\tanh(\varepsilon_{s,-s} / T)$, we can rewrite this expression as

$$\frac{dM}{dt} = -\frac{\gamma_{m'}}{2\left(1+\dfrac{\gamma_{m'}}{2\Gamma_{m'}}\right)} e^{-\varepsilon_{m',s}/T}\left(1+e^{-\varepsilon_{s,-s}/T}\right)\left(M - M_{eq}\right). \qquad (4.12)$$

This differential equation is now easily integrated to give an exponential decay of the magnetization. The relaxation rate is simply the factors in front of (M - M_{eq}) above, aside from the minus sign. In the limit of large tunneling, $\Gamma_{m'} >> \gamma_{m'}$, the relaxation rate reduces to that for simple thermal activation over a barrier of height $\varepsilon_{m',s}$, while in the opposite limit of small tunneling, the rate goes to zero linearly in $\Gamma_{m'}$ since now the tunneling is the rate-limiting step for the channel involving state $|m'\rangle$. Since Table I indicates that the tunneling rate is a very fast function of m, it becomes clear that one (or at most two) level(s) participates significantly in the relaxation for any given experimental situation. Levels lower in energy have too small a tunneling rate and are "closed" while levels above are completely "open" but require more thermal energy to reach.

As one turns up the transverse field, tunneling increases and one expects the critical level to drop to the next-lowest-lying level, as in our discussion of barrier reduction above. Given the formalism developed in this section, one can attempt to understand how this transition from one critical level to another occurs. The total relaxation rate is simply the sum of the rates from all of the channels since all of the channels are in parallel:

$$\Gamma_{total} = \left(1 + e^{-\varepsilon_{s,-s}/T}\right) \sum_{m' \geq 0} \frac{\gamma_{m'}}{2\left(1 + \frac{\gamma_{m'}}{2\Gamma_{m'}}\right)} e^{-\varepsilon_{m',s}/T} + \Delta E_s , \qquad (4.13)$$

where the last term represents the tunneling directly from the metastable ground state without thermal activation, which is only important at low temperatures or large values of transverse field. (Furthermore, the unphysical "tunneling rate" from the very top of the barrier (m = 0) is defined to be $\Gamma_0 = \infty$.) The lifetimes of the states $\gamma_{m'}$ are not known and cannot be estimated without a better knowledge of the relaxation dynamics. The measured attempt frequency is ~10^7 Hz and while this is much slower than typical spin-lattice relaxation rates, for simplicity and reasonable comparison with experiment we will take this value as the lifetime of every state.

For concreteness, the measured values for Mn_{12} are used for the calculations presented below. The calculations are for resonance #1, with S = 10, D = .41 cm^{-1} =4.6 kG and T = 2.5 K. (Appendix D contains the Mathematica script used for these calculations.) In Fig. 4.5, the calculated relaxation rate is plotted as a function of transverse field up to 10 kG. The upper curve is the relaxation rate at the peak of the resonance, while the lower curve is the rate

at a longitudinal field of 1 kG below the peak. The straight line is the classical result. The steps in the calculated curves indicate transitions to new critical tunneling levels, similar to the lowering of the barrier shown in Fig. 4.3(b). One interesting feature is that the relaxation rate on resonance increases on average faster than off resonance: the off-resonance curve seems to follow the classical curve fairly well, while the on-resonance curve is clearly steeper.

Another view of this level-switching process is given in Fig. 4.6. Here the relaxation rate is plotted as a function of longitudinal field for several fixed values of transverse field. The figure shows that as the transverse field is

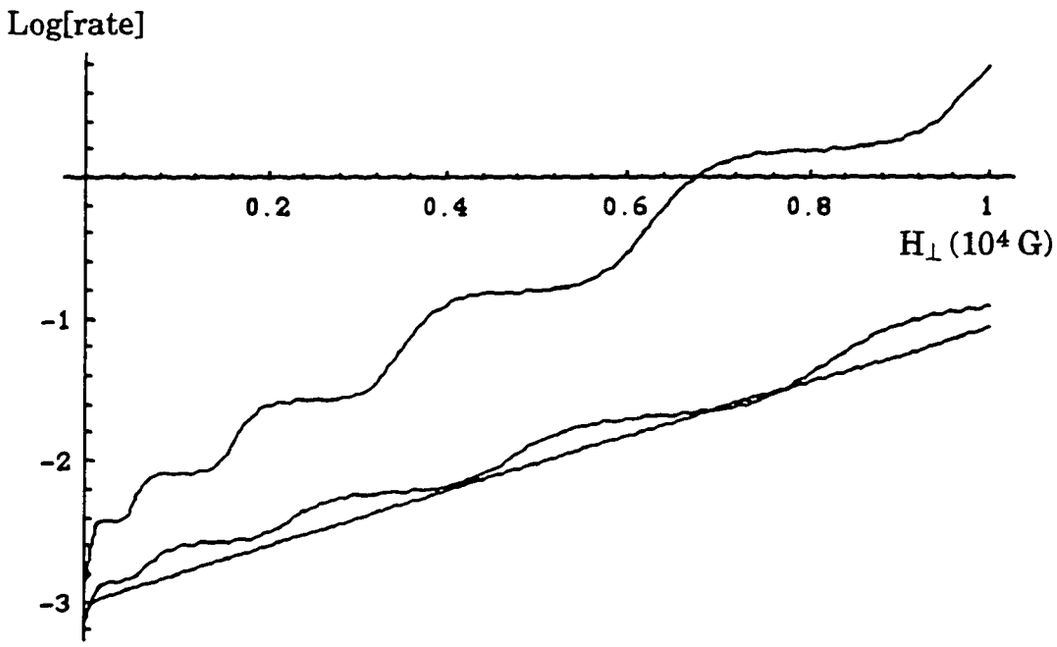

Figure 4.5 Calculated tunneling rate as a function of transverse field. The upper curve is the logarithm of the rate calculated using Eq. 4.13 and setting the longitudinal field to the peak in resonance #1. The lower curve is for the longitudinal field set 1 kG below the peak. The straight line is the expected classical behavior.

increased the width of the resonance grows (since the tunneling rate increases). The resonance becomes so broad at some point that it essentially forms a uniform background. That level has now become the top of the barrier. At the same time that the resonance is disappearing into the background a new resonance appears on top of the old. This is the next lowest level coming into play. It, too, broadens as the transverse field is increased until it becomes another, higher baseline. And so the process continues with a new level coming into play just as the preceding one broadens appreciably.

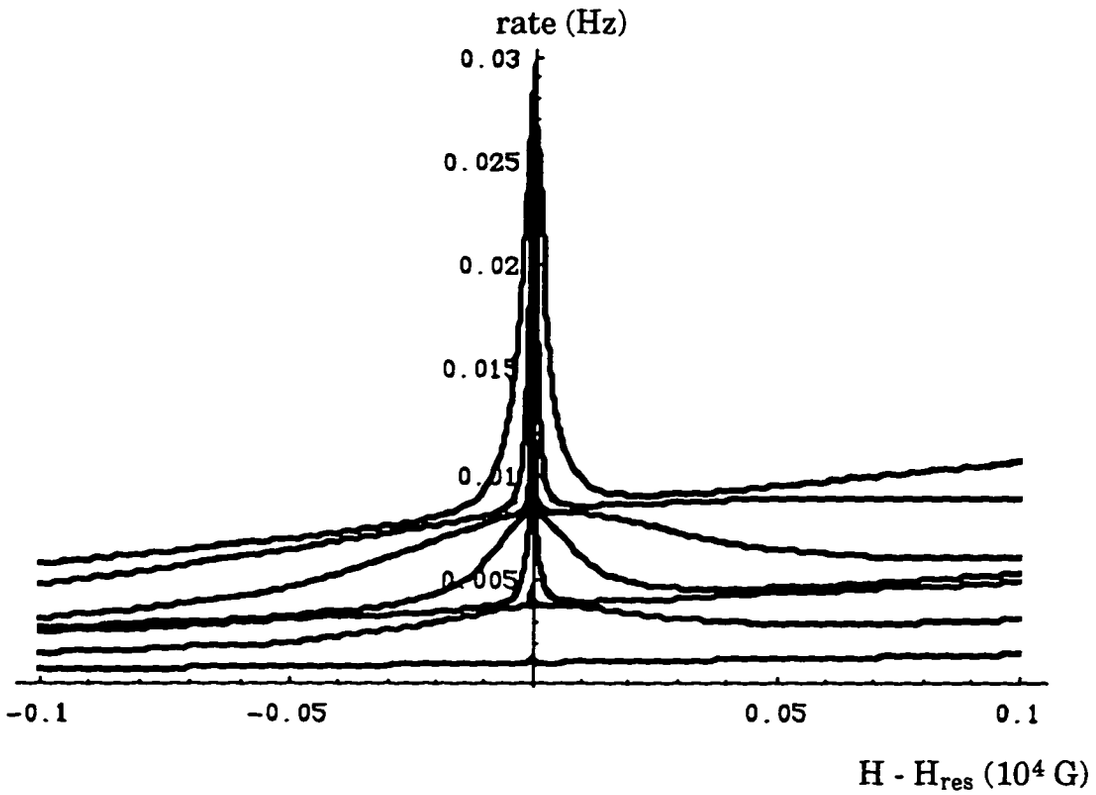

Figure 4.6 The effect of a transverse field on resonance #1. The calculated relaxation rate is plotted as a function of longitudinal field about the center of the resonance. Each successive curve corresponds to an increase in the transverse field of 500 G with the bottom curve for $H_{\perp} = 0$. As the transverse field increases, the resonance broadens until it becomes a uniform background upon which a new, sharp resonance forms.

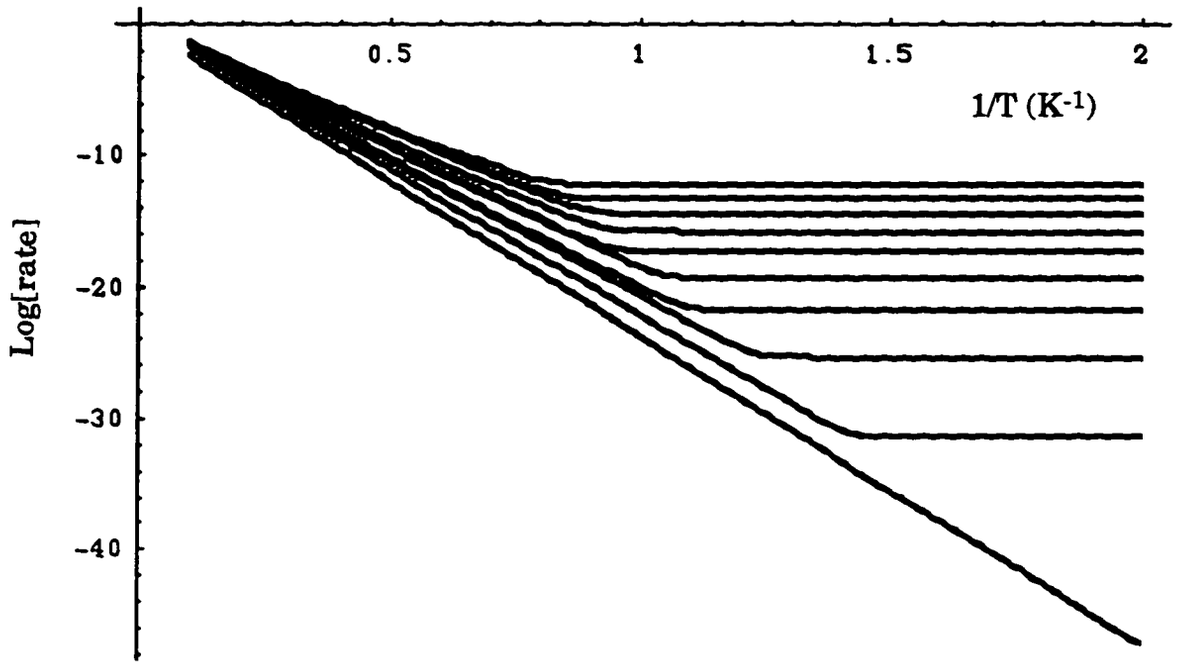

Figure 4.7 Temperature dependence of relaxation rate for various transverse fields. The logarithm of the calculated relaxation rate is plotted as a function of 1/T. The different curves correspond to 1-kG increments of the transverse field, with the lowest curve for $H_\perp = 0$. The transverse field promotes tunneling and so increases the temperature at which the relaxation becomes temperature independent.

Finally, one can study the temperature dependence of the relaxation. Fig. 4.7 shows the logarithm of the relaxation rate as a function of 1/T for several values of transverse field when the system is tuned to a resonance (#1, in this case). For zero transverse field there is no tunneling, the relaxation proceeds by pure thermal activation and a straight line results. As one increases the transverse field, the slope of the line changes a bit, indicating a change in the height of the barrier. More striking, however, is the appearance of a temperature-independent relaxation rate at low temperatures. This

plateau arises when the rate for thermal activation to any excited level becomes small compared to the rate for tunneling from the lowest level in the metastable well. The relaxation rate is then dominated by direct tunneling from one well to another without any thermal assistance. This is precisely the effect predicted by the semiclassical theories reviewed in Chapter I. As the transverse field is raised, the temperature at which the plateau appears - the "crossover temperature" - becomes larger. This is not surprising since the tunneling rate from the lowest level increases with transverse field.

Let us now summarize the theoretical results presented in this chapter. 1) The simple Hamiltonian Eq. 4.1 predicts that degeneracies between spin states form at regular intervals of longitudinal magnetic field. 2) Multiple resonances occur simultaneously, with all of the levels in one potential well matched up with levels in the other. 3) A transverse magnetic field does not alter the values of longitudinal field at which the resonances occur, but does produce tunnel splitting, removing the degeneracies according to Eq. 4.7. 4) The classical reduction of the energy barrier by a transverse field can be explained in terms of this tunnel splitting of excited states. For a system with not too large a spin (S~10) the barrier is expected to be reduced in a series of steps. 5) A simple kinematic model of the relaxation process in terms of thermal activation to tunneling levels predicts that the relaxation rate should show similar steps as a function of transverse field and that the width of the resonances should oscillate as the tunneling level changes.

V. Discussion of Results

In this chapter, I will show that much of the data presented in Chapter III can be quantitatively explained in terms of tunneling, using the theoretical apparatus developed in the last chapter. Tunneling is not the only interpretation available, however, and I will briefly present an alternative interpretation developed by Burin, et al.[57,58] I will devote a fair amount of this chapter to discussing the experimental data that cannot presently be fully explained with the theoretical apparatus developed in Chapter IV, namely the width of the resonances and the dependence of the relaxation rate on transverse magnetic field.

A. Tunneling Interpretation

Many of the major experimental results presented in Chapter III can be interpreted as manifestations of thermally assisted field-tuned resonant tunneling between spin states within a spin-10 manifold.

Let us recall Eq. 4.5:

$$B_{m,-m+n} = -\frac{Dn}{g\mu_B},$$

which predicts that resonances occur at even intervals of magnetic field. This is precisely what is observed in the steps shown in Fig. 3.1. Given that a step occurs every 4.6 kG, Eq. 4.5 yields $D/g = 0.21\ cm^{-1}$, consistent with the published values of $D \sim 0.5\ cm^{-1}$ and $g \sim 1.9$ obtained from high-field[43] and ESR experiments.[43,44] As a further check, one can estimate the anisotropy barrier at zero field to be $g(D/g)S^2 \sim (1.9)(0.21\ cm^{-1})\ (100) = 41\ cm^{-1} = 59$ K, consistent with the estimate of $49\ cm^{-1} = 71$ K obtained from the blocking temperature in Chapter III and 61-64 K obtained by others[37,39,41,42,45-47] from the temperature dependence of the relaxation rate. The theory developed in the previous chapter indicates that there should be $2S + 1 = 21$ steps (n = 0 to 20), the last corresponding to the elimination of the barrier. The discussion of Fig. 3.6 in Chapter III indicated that by extrapolating the data to zero temperature one can estimate the total number of steps to be ~21-22, in very good agreement, given the fact that this extrapolation is based on only the first 7 steps. Measurements at lower temperatures are needed to observe the higher-numbered steps and, as mentioned, pulsed-field measurements have shown evidence of at least 12 steps.[54] The last step, #20, should occur at a field of 4.6 kG x 20 = 92 kG. This is close to published estimates[46,47] of the anisotropy field of around 100 kG.

Knowing the total number of steps gives some physical insight into the mechanism responsible for the tunneling. Since the Hamiltonian, Eq. 4.1, commutes with S_z, this simple form does not allow any tunneling at all. Tunneling must derive from off-diagonal terms in the Hamiltonian. Magnetic tunneling is most often attributed to the presence of a transverse component in the magnetocrystalline anisotropy tensor. Such an anisotropy must appear as an even power of the spin operator: $H' \sim aS_x^{2n} + bS_y^{2p}$, where n and p are integers. Mn_{12} has tetragonal symmetry, so that the lowest order transverse term is $H' = k(S_x^4 + S_y^4)$, which can be rewritten as $H' = k/8(S_+^4 + S_-^4)$ + (terms

that produce no transitions), where S_+ and S_- are the usual spin raising and lowering operators.[49,50] This form only allows transitions that obey the selection rule $\Delta m=\pm 4q$ (integer q). This would, in turn, prohibit every other step: for whenever the system is tuned to an odd numbered step (e.g. n=1), the levels in resonance are always matched even/odd and odd/even (e.g. 10/-9, 9/ -8, 8/-7,...), yielding a forbidden, odd Δm for all matched levels.

On the other hand, the data indicate that all steps are observed and none are forbidden. A possible source of tunneling, one that does not prohibit any steps, could be a small transverse magnetic field, perhaps of dipole or hyperfine origin. A transverse field would give rise to a perturbative term of the form Eq. 4.2:

$$H' = bS_x = \frac{b}{2}(S_+ + S_-),$$

which allows all transitions $\Delta m=\pm 1q$, prohibiting no steps. The tunneling produced by such a term was discussed in the last chapter.

The data shown in Fig. 3.1 indicate that temperature plays an important role in the relaxation process. As mentioned earlier, steps in the hysteresis loop at the lower fields are quite pronounced at 2.8 - 3.0 K, and gradually fade as the temperature is lowered. This indicates that the tunneling is thermally assisted, and takes place from excited states near the top of the potential well. As the temperature is decreased, the levels near the top of the metastable well become depopulated and the transition rate decreases.

The model presented in the last section of Chapter IV suggests that the tunneling is dominated by one (or at most two) levels near the top of the well, and the time rate of decay is determined by the time required to repopulate these levels. Hence, on resonance the effective energy barrier is reduced: the system no longer needs to be thermally activated to the top of the barrier, but only to a fast-tunneling level at a somewhat lower energy, as illustrated in Fig. 4.4. The dips in the blocking temperature shown in Fig. 3.10 can be interpreted as drops in the effective energy barrier, consistent with this picture.

The model also predicts that the longitudinal fields at which steps occur are unchanged by the presence of a transverse field to at least fourth order in perturbation theory. This prediction is borne out remarkably well by the data presented in Fig. 3.16, which shows that the steps occur at regular intervals of longitudinal field, independent of the transverse field.

The proposed model of field-tuned, thermally assisted resonant tunneling out of a metastable spin state is consistent with the experimental observations: (1) Resonant tunneling causes the transition rate to increase at values of the magnetic field that yield energy level crossings in the two wells. (2) When the field is reduced from saturation, no steps are seen because the spins are already in the lower-energy potential well. When the field is reduced to near zero or reversed, the populated well becomes metastable allowing resonant transitions out of the populated states and the corresponding steps. (3) The higher-numbered steps have progressively faster magnetic relaxation times because the anisotropy barrier is lowered by the applied field. Therefore, lower temperatures are needed to observe them. (4) The recovery of frozen steps as the field sweep rate is reduced can be understood qualitatively. If the field is swept too fast, not enough time is spent in

the region of a step, and no appreciable relaxation occurs; the step is "frozen out". It will appear when the sweep rate is sufficiently slow that the time spent within the region of the step is comparable to its characteristic relaxation time. (5) The steps occur at regular intervals of the longitudinal field, independent of the value of the transverse field, as predicted theoretically.

While the tunneling model explains many of the observations, an alternative interpretation, employing the same Hamiltonian but a different physical mechanism, has been proposed to account for the same phenomena. Burin, Prokof'ev and Stamp[57,58] have proposed that the relaxation proceeds via flip-flop transitions induced by dipolar coupling between Mn_{12} clusters. As discussed above, the energy levels on the two sides of the barrier coincide when the field is tuned to resonance. These authors suggest that the decay of the magnetization in the right-hand well generates energy quanta which precisely match the energies needed to raise a neighboring spin to excited levels in the left-hand metastable well, thus promoting relaxation at resonant values of the external field. This process involves the exchange of virtual photons since it is mediated by dipolar interactions. In essence, the model says that on resonance as one spin climbs down the ladder in one well, it assists another in climbing up the ladder in the other well, hence the faster relaxation. It should be noted that the Curie -Weiss temperature, a measure of the dipolar interaction strength, is on the order of ±0.05 K for Mn_{12},[39,41,42,46] and one might thus expect interactions between spins to be negligible compared to spin-phonon couplings at measuring temperatures of 2 - 3 K. However, the spin-phonon relaxation times are uncharacteristically slow in this system, as evidenced by the anomalously small Arrhenius prefactor found experimentally, perhaps making it possible for dipolar interactions to be the dominant process. Measurements in similar materials in which the magnetic

clusters are further apart could provide a test of this model. In fact, steps have recently been observed[59] in the hysteresis loops of related materials that has the same magnetic core but different organic ligands. A detailed comparison of the behavior of those systems with the one studied here may be illuminating.

So far, this chapter has focused on the data that is understood and can be explained in terms of tunneling (or perhaps dipolar-mediated flip-flop processes). I will now turn to things that are not understood: the linewidth of the resonances and the transverse field dependence of the relaxation rate. A more complete understanding of these phenomena may shed light on the fundamental process of relaxation in this and other systems of high-spin molecules.

B. The Lineshape of the Resonances

The data in Fig. 3.15 shows quite clearly that the resonances are homogeneously broadened. That is, the data can be fit extremely well to a Lorentzian function. (Attempts to fit the data to a Gaussian yielded very poor results.) An obvious interpretation of this fact is that the data represent the natural lineshape of an excited state in the system. This interpretation is problematic: the width of the resonance seems too large. As discussed in Chapter III, the full width of the resonances is roughly $\Delta H \sim 250 \pm 20$ Oe. If we assign this width to the state $|m\rangle$ then the corresponding frequency width of the state is $\gamma = g\mu_B m\Delta H / \hbar \sim 4.4 \times 10^9\, m$ Hz. This is not an uncommon value for spin-lattice relaxation rates and, *prima facie*, it is consistent with the interpretation that this is the natural linewidth of some state. However, the

Arrhenius prefactor (attempt frequency) for this system of ~10^7 Hz is much smaller than this value. The prefactor is usually thought to be related to the Larmor frequency for the spin precessing in the crystal anisotropy field. For Mn_{12}, this field is on the order of 100 kG, which yields a precession frequency of $\omega_L \sim 3 \times 10^{11}$ Hz, orders of magnitude larger than both the attempt frequency and the measured linewidth. One possibility for the small attempt frequency is that the spin-phonon coupling is weak and so the spin precesses many times before it finds a phonon that will allow it to attempt to traverse the barrier. This interpretation leaves open the question of how to interpret the width of the resonance. For it can be used to explain the slow attempt frequency or the width but not both, at least at present.

One might argue that the width may have no real fundamental meaning, that it could be due to the hyperfine splitting of the tunneling excited state. An approximate hyperfine level structure has been calculated for this system by Hartmann-Boutron, et al.[50], who find that the splitting is equivalent to a field of ~300-500 G, which is the right order of magnitude for the observed width. However, the density of hyperfine levels follows a binomial distribution and hence should produce a Gaussian resonance.[60] Simply put, the hyperfine interaction is like a random field that varies from cluster to cluster and should therefore be statistically distributed. That the measured resonance fits a Lorentzian function so well indicates that the lineshape cannot be due to hyperfine splitting (although the hyperfine field may well produce the tunneling, making the resonances observable at all).

C. The Effect of the Transverse Magnetic Field

Another possible interpretation of the linewidth is that it represents the tunneling rate. This would explain why it agrees with neither the attempt frequency nor the Larmor precession frequency. At a minimum, the width of the resonance must be the natural lifetime of the state, but the tunnel splitting can widen the state beyond this. One would then expect that the application of a transverse field should widen the resonance. As the calculation illustrated in Fig. 4.6 indicates, the resonance is expected to widen with the application of a transverse field until it becomes a uniform background. At the same time, a new resonance forms on top of the old and the process continues. According to the calculation, one should see the linewidth go through several of these cycles as the transverse field is raised from zero to a few kOe. The actual data presented in Fig. 3.18 does not show anything approaching this effect. In fact, the width of the resonances roughly doubles as the transverse field is increased from zero to 5 kOe and this effect may be spurious since errors in the sample angle become magnified as the transverse field is increased. Certainly, there appears to be no point at which the resonance broadens significantly and a new, narrower one appears on top of it.

This is a serious problem and cannot be readily explained. An "easy" way out is to conclude that the phenomenological model that produced Fig. 4.6 is simply wrong. The model certainly has its deficiencies: most notably, it allows transitions directly between the lowest state in the left well to any excited state in that well, but requires an intermediate tunneling step to reach

the right well. This is certainly unphysical. If there are no selection rules governing transitions within a well, then direct transitions between any two states, independent of which well they are in, should be allowed. Imposing dipole selection rules ($\Delta m = 1$) would yield a model similar to that of Villain, et al.[48] As discussed in the previous chapter this model also has its shortcomings. Adding tunneling to that model yields a relaxation rate that depends on the transverse field much faster than the classical result. A satisfactory dynamical model must yield results that are consistent with classical physics. This requirement follows not only from fundamental considerations, but also because the data in Fig. 3.19 indicate that the relaxation rate depends on transverse field in a way that roughly follows the classical prediction.

Independently of the dynamical model we use to describe the relaxation, one still expects that the barrier should decrease stepwise as a function of transverse field. The calculation of this effect, presented in Fig. 4.3, is based on very general arguments that do not depend on the details of the relaxation process, but only on the discreteness of the energy spectrum of a finite-spin object and the tunneling produces by a transverse field. The data presented in Fig. 3.19 show that the relaxation rate oscillates subtly, but systematically, about the classical prediction. This behavior may be evidence of the discrete level structure. This effect needs to be verified at other temperatures to see that the observed oscillation repeats; data should also be taken at higher transverse fields to see if there are more oscillations.

The data in this figure should be compared with the results of the theoretical calculation, Fig. 4.7. The theory predicts that the relaxation rate on resonance should increase faster than the classical result. However, the data

in Fig. 3.19 shows that the relaxation rate both on and off resonance seems to have the same dependence on transverse field. The steps and plateaus in the theoretical plot are much clearer and sharper than the oscillation in the actual data. This may indicate that the expected sharp steps are somehow "smeared out." Again, one can conclude that our present understanding of the relaxation process is incomplete.

It remains to be seen whether the model of Burin, et al. can adequately explain the enigmatic results presented above. The correct picture, whether it involves tunneling or not, must adequately explain the width of the resonances and the dependence of the relaxation rate on transverse field. Perhaps all of the data discussed in this section can be understood with the addition of a single theoretical idea. One can speculate that a proper theory may need to invoke two processes: a slow one that is responsible for the small attempt frequency and a faster one that explains the width of the resonances.

VI. Concluding Remarks

The discussion at the the end of the last chapter made it clear that further theoretical work is needed to understand the relaxation process in Mn12. In this chapter, I will discuss future experiments that may be done to deepen our understanding of Mn12. These include magnetization measurements at lower temperatures, measurements with a microwave field and neutron scattering experiments. I will close by discussing the magnetization steps in other materials, including some materials similar to Mn12.

A. Ideas for Future Research

The data I have presented in Chapter III indicates that seven steps have been observed and that extrapolations to zero temperature indicate the total number of steps is near 21. As one lowers the temperature or increases the field sweep rate, the number of observable steps should increase. In fact, pulsed field measurements have already shown evidence of at least 12 steps. The disadvantage of using pulsed fields is that they can introduce significant heating into the sample. Measurements with slow field sweep rates and lower temperatures would be desirable. A careful study of steps at higher fields and lower temperatures could prove very useful. By observing more steps, one can

obtain a better estimate of the total number of steps. One could also look for any deviations from the linear dependence of the step number on magnetic field. Such deviations might indicate the presence of other terms in our model Hamiltonian that we have neglected.

High-field ESR measurements also need to be done. Not only would it be useful to obtain an accurate measure of D, but many other important pieces of information can be gleaned. By working at higher temperatures, where some of the excited states are substantially populated, one can try to map out the energy-level spectrum and compare it with that predicted by the theory in Chapter IV. Microwave experiments can also help shed light on the relaxation process. If the magnetization of the sample is measured in the presence of a microwave field, one might expect to see the relaxation rate increase when the frequency of the radiation matches the energy splitting of two levels. One can test to see if the relaxation is enhanced when one tunes to certain transitions but not others. This may shed light on what selection rules play a part in the relaxation process. One exciting possible microwave experiment is to try to induce a population inversion in the system by backpumping the system from the lower well to the higher well with microwave radiation. A conceptually similar experiment has recently been done in SQUIDs that show resonant tunneling.[61,62] In the case of Mn12, such an experiment is particularly challenging since it requires microwaves in the Terahertz range, which are extremely difficult to produce. On the other hand, if microwave experiments show promise, Mn12 may eventually become a useful source of Terahertz radiation or perhaps even a Terahertz laser.

Since the desired microwave frequencies are difficult to produce, a different method of reaching excited states may be warranted, namely neutrons. Neutron scattering can give information about the energy level spectrum, selection rules, tunneling rates and intra- and intercluster correlations. On the other hand, neutron fluxes are small and so one cannot hope to use them to appreciably alter the measured relaxation of the system.

Inelastic neutron scattering can probe the entire energy-level spectrum for Mn12. While the spectrum may be at the low end of typical neutron energies, sophisticated techniques may be employed to improve the signal. As discussed in Chapter IV, a magnetic field applied perpendicular to the easy magnetization axis of the sample can promote tunneling between the two wells. This would allow the observation of "dipole-forbidden" transitions and hence a direct measurement of the inter-well-transition matrix elements.

Elastic neutron scattering can be employed to determine the ground state configuration of the spins within the molecule, for which there are only some conjectures.[43,44,48,50] For example, as mentioned in Chapter I, one possible configuration is that the central Mn^{4+} ions point up and the outer Mn^{3+} ions point down. The measured structure factor can be compared to those calculated from proposed models to determine which, if any, are correct.

Elastic scattering can also be used to study the interactions between clusters by allowing a direct probe of the spin-spin correlation function. Scattering from a sample that has been cooled to low temperatures (~1.5 K) in zero field can determine the correlations between molecules. If there are no correlations, then the spins should freeze randomly either up or down and the measured

short-range correlation function should be consistent with zero. Measurements at dilution temperatures may be performed to see if there is an onset to an ordered state at these temperatures.

B. Steps in other Systems and Related Materials

I shall close this thesis by making some comments about the uniqueness of the results presented herein. Whether or not the experimental results are manifestations of resonant tunneling, the data are the first observation of magnetization steps at an *ordered* set of fields within a hysteresis loop. Steps have been seen within hysteresis loops many times (Barkhausen noise, for example) but occur at random fields, although sometimes the effects are reproducible for a given sample during a particular experimental run. Magnetization steps at regular field intervals have been seen in some systems, but not in hysteretic regimes and so these steps are not related to relaxation phenomena. In what follows I will briefly review some of the relevant work on these systems and how they contrast with Mn_{12}.

Steps that occur with both increasing and decreasing field have been seen in dilute magnetic semiconductors with antiferromagnetically coupled spin pairs[63,64] and $[Fe(OMe)_2(O_2CCH_2Cl)]_{10}$, a paramagnetic molecular ring of Fe^{3+} ions that order antiferromagnetically.[65] These steps are found in a regime where the magnetization is reversible and mark the points when the field induces the total spin to change between discrete values. In contrast, for Mn_{12} there are no stable, stationary magnetization values other than equilibrium, and the system will

always relax toward its equilibrium value; however, it does so most rapidly at specific values of magnetic field that correspond to level crossings. Furthermore, treating the observed steps in Mn12 as due to total-spin transitions yields an unphysically low exchange constant of less than 1 K for Mn_{12}.

More similar to the present work are steps that have been observed in dilute paramagnetic systems, where the steps mark transitions between states within the same spin manifold.[66-68] The essential difference between all of these systems and Mn_{12} is that they all have a positive anisotropy parameter D and so have no magnetic metastability, no hysteresis and no possibility of tunneling. In other words, the level spectrum in these systems is inverted from that shown in Fig. 4.1. The zero-field ground state is the m=0 state and there are two branches of excited states, but no metastable wells. As the field is applied, the ground state level switches to a different value, say, m=1 and a step is observed in the magnetization. Just like in Mn12, the steps in these systems occur whenever the field is an integer multiple of D. However, the physics is quite different since it has nothing to do with the crossing of levels in neighboring wells.

Steps in the magnetization of hysteretic systems are not uncommon. For example, $SmCo_{3.5}Cu_{1.5}$ has shown sharp step in the hysteresis loops at low temperatures.[69] In this system, the steps occur at irregular fields that depend on the details of the measurement, such as the field sweep rate or temperature, and have been attributed to avalanches triggered by domain-wall depinning events. Steps have also been seen in some site-diluted antiferromagnets.[70] These steps also occur at irregular fields and are attributed to the motion of domain walls.

Very recently, other researchers[59] studying compounds related to Mn12 have also discovered steps in the hysteresis loops. These materials have the same magnetic core as the Mn12 acetate studied here, but different organic ligands. The substitution results in a different spin ground state[44,47] (S = 9 for Mn12 Benzoate and S = 19/2 for a reduced form of the benzoate), different anisotropies (Mn12 Benzoate has a blocking temperature of about 2.7 K) and different crystal structures (Mn12 Benzoate is triclinic). Despite these differences, both systems have now been found to have steps in the hysteresis loops. As of this writing, these results have not been published and, so, a thorough comparison of the steps found in these materials with those found in the acetate cannot be made. It would indeed be very interesting to see if the different crystal structure or lattice spacings have significant effects.

C. Summary

In this dissertation, I have presented experimental evidence for resonant magnetization tunneling in a system of high-spin molecules. The evidence, in essence, is that at regular intervals of magnetic field, the magnetic relaxation rate of the system increases markedly, producing steps in the hysteresis loops and dips in the blocking temperature. The theoretical apparatus developed in Chapter IV explains these observations in terms of level crossings in a double-well potential. The tunneling appears to be due to a symmetry-breaking transverse field internal to the system (hyperfine or dipolar in origin). However, the application of an external transverse field intended to augment the tunneling produces some results that do not agree with expectations. I

hope that future work will resolve some of the discrepancies and provide insight into the nature of the magnetic relaxation in this and other high-spin molecular systems.

Appendix A

The following program was used to "zero" the sample rotator so that the sample's easy axis was aligned with the magnetic field. The values of the magnetic moment used in the inequality conditions depend on the sample. This program was written in Quantum Design's EDC language.

```
setmag(1000,0,1)
wait(mag)

repeat
        write(706,"rtd -994")
        measure(trans)
        ctransemu(mt)
until (mt < -.0001)

repeat
        write(706,"rtd 99")
        measure(trans)
        ctransemu(mt)
until (mt > -.00001)

repeat
        write(706,"rtd 10")
        measure(trans)
```

```
        ctransemu(mt)
until (mt > -.0000005)
```

Appendix B

To perform hysteresis loops with a constant transverse magnetic field component, the field and the samples angle with respect to the field needed to be varied simultaneously. The following BASIC program calculates the field and angle needed for each measurement point and writes an EDC program that takes the data. Following the BASIC program is some of its typical output.

```
OPEN "10KHYST.EDC" FOR OUTPUT AS #1
theta0 = 0
Ht = 10000
Hlmax = 25000
Hmax = (Hlmax ^ 2 + Ht ^ 2) ^ .5
PRINT #1, "MaxField ="; Hmax
PRINT #1, "FTOCRAT = 1534.916"
PRINT #1, "MagnRes = -.21"

PRINT #1, "SetMag(0,1,1)"
PRINT #1, "Wait(mag)"
PRINT #1, "Pause (4)"

PRINT #1, "WRITE(706,"; CHR$(34); "SMP 1"; CHR$(34); ")"
PRINT #1, "WRITE(706,"; CHR$(34); "SMR 1"; CHR$(34); ")"
```

```
    PRINT #1, "Voltmeter = "; CHR$(34); "RVC 2"; CHR$(34)
    PRINT #1, "MagnRes = MagnRes * 10"
    PRINT #1, "WRITE(706,"; CHR$(34); "SMH 1"; CHR$(34); ")"
    PRINT #1, "Pause (2)"
    PRINT #1, "IF MaxField < 5000 GOTO HiResMode1"
    PRINT #1, "WRITE(706,"; CHR$(34); "SMH 0"; CHR$(34); ")"
    PRINT #1, "Voltmeter = "; CHR$(34); "RVC 3"; CHR$(34)
    PRINT #1, "MagnRes = MagnRes / 10"

    PRINT #1, ": HiResMode1"
    PRINT #1, "WRITE(706,"; CHR$(34); "SMS 1"; CHR$(34); ")"
    PRINT #1, "Pause (7)"

    FOR Hl = Hlmax TO 10000 STEP -5000.01
    H = (Hl ^ 2 + Ht ^ 2) ^ .5
    theta = ATN(Ht / Hl) * 180 / 3.1415926#
    IF theta < 0 THEN theta = theta + 180
    dtheta = theta - theta0
    theta0 = theta
    steps = 94.9 * dtheta
    PRINT #1, "write(706, "; CHR$(34); "RTD "; steps; CHR$(34);
")"
    PRINT #1, "Field ="; H
    PRINT #1, "CALL stable"
    PRINT #1, "wait(temp)"
    PRINT #1, "measure(long)"
    PRINT #1, "clongemu(ml)"
```

```
    PRINT #1, "measure(trans)"
    PRINT #1, "ctransemu(mt)"
    PRINT #1, "h="; Hl
    PRINT #1, "ctemp(temperature)"
    PRINT #1, "time(t)"
    PRINT #1, "concat(h,"; CHR$(34); " "; CHR$(34); ")"
    PRINT #1, "concat(h,temperature)"
    PRINT #1, "concat(h,"; CHR$(34); " "; CHR$(34); ")"
    PRINT #1, "concat(h,ml)"
    PRINT #1, "concat(h,"; CHR$(34); " "; CHR$(34); ")"
    PRINT #1, "concat(h,mt)"
    PRINT #1, "concat(h,"; CHR$(34); " "; CHR$(34); ")"
    PRINT #1, "concat(h,t)"
    PRINT #1, "concat(h,"; CHR$(34); " "; CHR$(34); ")"
    PRINT #1, "concat(h,"; CHR$(34); theta; CHR$(34); ")"
    PRINT #1, "PRINT(h)"
    NEXT

    FOR Hl = 9500 TO 5000 STEP -500.01
    H = (Hl ^ 2 + Ht ^ 2) ^ .5
    theta = ATN(Ht / Hl) * 180 / 3.1415926#
    IF theta < 0 THEN theta = theta + 180
    dtheta = theta - theta0
    theta0 = theta
    steps = 94.9 * dtheta
    PRINT #1, "write(706, "; CHR$(34); "RTD "; steps; CHR$(34);
")"
```

```
PRINT #1, "Field ="; H
PRINT #1, "CALL stable"
PRINT #1, "wait(temp)"
PRINT #1, "measure(long)"
PRINT #1, "clongemu(ml)"
PRINT #1, "measure(trans)"
PRINT #1, "ctransemu(mt)"
PRINT #1, "h="; Hl
PRINT #1, "ctemp(temperature)"
PRINT #1, "time(t)"
PRINT #1, "concat(h,"; CHR$(34); " "; CHR$(34); ")"
PRINT #1, "concat(h,temperature)"
PRINT #1, "concat(h,"; CHR$(34); " "; CHR$(34); ")"
PRINT #1, "concat(h,ml)"
PRINT #1, "concat(h,"; CHR$(34); " "; CHR$(34); ")"
PRINT #1, "concat(h,mt)"
PRINT #1, "concat(h,"; CHR$(34); " "; CHR$(34); ")"
PRINT #1, "concat(h,t)"
PRINT #1, "concat(h,"; CHR$(34); " "; CHR$(34); ")"
PRINT #1, "concat(h,"; CHR$(34); theta; CHR$(34); ")"
PRINT #1, "PRINT(h)"
NEXT

FOR Hl = 4800 TO -Hlmax STEP -200.01
H = (Hl ^ 2 + Ht ^ 2) ^ .5
theta = ATN(Ht / Hl) * 180 / 3.1415926#
IF theta < 0 THEN theta = theta + 180
```

```
    dtheta = theta - theta0
    theta0 = theta
    steps = 94.9 * dtheta
    PRINT #1, "write(706, "; CHR$(34); "RTD "; steps; CHR$(34);
")"
    PRINT #1, "Field ="; H
    PRINT #1, "CALL stable"
    PRINT #1, "wait(temp)"
    PRINT #1, "measure(long)"
    PRINT #1, "clongemu(ml)"
    PRINT #1, "measure(trans)"
    PRINT #1, "ctransemu(mt)"
    PRINT #1, "h="; Hl
    PRINT #1, "ctemp(temperature)"
    PRINT #1, "time(t)"
    PRINT #1, "concat(h,"; CHR$(34); " "; CHR$(34); ")"
    PRINT #1, "concat(h,temperature)"
    PRINT #1, "concat(h,"; CHR$(34); " "; CHR$(34); ")"
    PRINT #1, "concat(h,ml)"
    PRINT #1, "concat(h,"; CHR$(34); " "; CHR$(34); ")"
    PRINT #1, "concat(h,mt)"
    PRINT #1, "concat(h,"; CHR$(34); " "; CHR$(34); ")"
    PRINT #1, "concat(h,t)"
    PRINT #1, "concat(h,"; CHR$(34); " "; CHR$(34); ")"
    PRINT #1, "concat(h,"; CHR$(34); theta; CHR$(34); ")"
    PRINT #1, "PRINT(h)"
    NEXT
```

```
    PRINT #1, "WRITE(706,"; CHR$(34); "SMS 0"; CHR$(34); ")"
    PRINT #1, "WRITE(706,"; CHR$(34); "SMH 1"; CHR$(34); ")"
    PRINT #1, "pause(15)"
    PRINT #1, "WRITE(706,"; CHR$(34); "SMC 0"; CHR$(34); ")"
    PRINT #1, "pause(120)"
    PRINT #1, "Write(706,Voltmeter)"
    PRINT #1, "Tmp1 = Read(706)"
    PRINT #1, "Tmp1 = Tmp1 / MagnRes"
    PRINT #1, "Tmp1 = Tmp1 * FTOCRAT"
    PRINT #1, "ActualField = Tmp1"
    PRINT #1, "Dec (Tmp1)"
    PRINT #1, "UpdMag (Tmp1)"
    PRINT #1, "WRITE(706,"; CHR$(34); "SMR 0"; CHR$(34); ")"
    PRINT #1, "WRITE(706,"; CHR$(34); "SMP 0"; CHR$(34); ")"

    PRINT #1, "write(706, "; CHR$(34); "RTD "; -(theta + 10) *
94.9; CHR$(34); ")"
    PRINT #1, "pause(120)"
    PRINT #1, "write(706, "; CHR$(34); "RTD "; 949; CHR$(34);
")"

    PRINT #1, "subroutine stable"
    PRINT #1, "TargetField = Field"
    PRINT #1, ": Stable"
    PRINT #1, "Tmp1 = TargetField / FTOCRAT"
```

```
PRINT #1, "Dec (Tmp1)"
PRINT #1, "Tmp2 = "; CHR$(34); "SMC "; CHR$(34)
PRINT #1, "Concat(Tmp2,Tmp1)"
PRINT #1, "WRITE(706,Tmp2)"
PRINT #1, "Tmp1 = 99999"
PRINT #1, ": NotStable"
PRINT #1, "Tmp2 = Tmp1"
PRINT #1, "Write(706,Voltmeter)"
PRINT #1, "Tmp1 = Read(706)"
PRINT #1, "Tmp1 = Tmp1 / MagnRes"
PRINT #1, "Tmp1 = Tmp1 * FTOCRAT"
PRINT #1, "ActualField = Tmp1"
PRINT #1, "Dec (Tmp1)"
PRINT #1, "UpdMag (Tmp1)"
PRINT #1, "Tmp3 = Tmp1 - Tmp2"
PRINT #1, "IF Tmp3 > 1 GOTO NotStable"
PRINT #1, "IF Tmp3 < -1 GOTO NotStable"
PRINT #1, "DeltaH = ActualField - Field"
PRINT #1, "TargetField = TargetField - DeltaH"
PRINT #1, "IF DeltaH > 1 GOTO Stable"
PRINT #1, "IF DeltaH < -1 GOTO Stable"
PRINT #1, "RETURN"
```

The above program produces the following output file: "10KHYST.EDC".

```
MaxField = 26925.82
FTOCRAT = 1534.916
MagnRes = -.21
SetMag(0,1,1)
Wait(mag)
Pause (4)
WRITE(706,"SMP 1")
WRITE(706,"SMR 1")
Voltmeter = "RVC 2"
MagnRes = MagnRes * 10
WRITE(706,"SMH 1")
Pause (2)
IF MaxField < 5000 GOTO HiResModel
WRITE(706,"SMH 0")
Voltmeter = "RVC 3"
MagnRes = MagnRes / 10
: HiResModel
WRITE(706,"SMS 1")
Pause (7)
write(706, "RTD  2068.954 ")
Field = 26925.82
CALL stable
wait(temp)
measure(long)
clongemu(ml)
measure(trans)
```

```
ctransemu(mt)
h= 25000
ctemp(temperature)
time(t)
concat(h," ")
concat(h,temperature)
concat(h," ")
concat(h,ml)
concat(h," ")
concat(h,mt)
concat(h," ")
concat(h,t)
concat(h," ")
concat(h," 21.80141 ")
PRINT(h)
write(706, "RTD  452.0706 ")
Field = 22360.67
CALL stable
wait(temp)
measure(long)
clongemu(ml)
measure(trans)
ctransemu(mt)
h= 19999.99
ctemp(temperature)
time(t)
concat(h," ")
```

```
concat(h,temperature)
concat(h," ")
concat(h,ml)
concat(h," ")
concat(h,mt)
concat(h," ")
concat(h,t)
concat(h," ")
concat(h," 26.56506 ")
PRINT(h)
```

Appendix C

The calculation presented in Fig. 4.3 was performed with the following Mathematica script.

```
s=100
Delta[i_,j_]:=If[i==j,1,0]

Do[{H=Table[(-i^2) Delta[i,j]+h2/2 (Sqrt[(s-i) (s+i+1)]
Delta[j,i+1] +
     Sqrt[(s+i) (s-i+1)] Delta[j,i-1]),{i,-s,s},{j,-s,s}];,
     evalues[h2]=Sort[Eigenvalues[H]];,
     splittings[h2]=Table[Part[evalues[h2],i+1]-
     Part[evalues[h2],i],{i,1,2s,2}];,
     emeans[h2] = Table[If[i==2s+1,Part[evalues[h2],2s+1],
     (Part[evalues[h2],i+1]+Part[evalues[h2],i])/2],{i,1,2s+1,2
}];},
{h2,0.,2. s,s/10}]

Do[{
     flag=0;,
     m=s+1;,
     Do[If[flag==0 && Part[splittings[h2],i]>.001,
          {m=i,flag=1},],{i,1,s}];,
     barrier[h2] = Part[emeans[h2],m]-Part[emeans[h2],1]},
{h2,0.,2. s,s/10}]

Table[{h2/2./s,barrier[h2]/s^2},{h2,0.,2. s,s/10}]

ListPlot[%]

Plot[(1-h1)^2,{h1,0,1}]

Show[%,%%]
```

Appendix D

Figs. 4.5 - 4.7 were generated with the following Mathematica script.

```
s=10

n=1

d=.6

h=0

beta=1/2.5

energy[q_]:= -d q^2+ h q

gamma[m_,q_]:= 5 10^6

deltatunnel[m_,H_]:= 3 10^10/1.44 2 d/((2m-1)!)^2 *
Sqrt[(s+m+n/2)!/(s-m+n/2)! (s+m-n/2)!/(s-m-n/2)!] *
(H/2/.46)^(2 m)

gammatunnel[m_,H_]:= deltatunnel[m,H]^2 gamma[m,m+1]/
(gamma[m,m+1]^2 + (3 10^10/1.44 (m+n/2) h)^2)

GGamma[H_]:= gamma[0,s-n/2] /2 *
(1+Exp[-beta (energy[s-n/2]-energy[-s-n/2])]) *
Exp[beta (energy[s-n/2]-energy[0])]+
Sum[1/2 (1+Exp[-beta (energy[s-n/2]-energy[-s-n/2])]) *
Exp[beta (energy[s-n/2]-energy[m])]/
(1/gamma[m,s-n/2] + 1/gammatunnel[m,H]),
{m,1/2+Mod[n+1,2]/2,s-n/2-1}]+ deltatunnel[s,H]

h=0
onres = Plot[Log[10,GGamma[H]],{H,.00001,1}]

h=-.1
offres=Plot[Log[10,GGamma[H]],{H,.00001,1}]

classical=Plot[Log[10,gamma[m,s] 1/2 *
(1+Exp[-beta (energy[s-n/2]-energy[-s-n/2])])*
Exp[-d (s-n/2)^2 beta (1-H/9.2)^2]],{H,.00001,1}]

Show[onres,offres,classical]

Show[Table[Plot[GGamma[H],{h,-.1,.1}],{H,.00001,.35,.05}],
PlotRange->All]
```

```
h=0
Show[Table[Plot[Log[10,GGamma[H]/gamma[1,s]],
{beta,0.1,2}],{H,.00001,1,.1}]]
```

Bibliography

1 A. O. Caldeira and A. J. Leggett, Phys. Rev. Lett. **46,** 211 (1981).

2 A. O. Caldeira and A. J. Leggett, Ann. Phys. (N.Y.) **149,** 374 (1983).

3 J. Clarke, A. N. Cleland, M. H. Devoret, D. Esteve, and J. M. Martinis, Science **239,** 992-997 (1988).

4 C. P. Bean and J. D. Livingston, J. Appl. Phys. **30,** 120S-129S (1959).

5 T. Egami, Phys. Status Solidi **A 20,** 157 (1973).

6 B. Barbara, G. Fillion, D. Gignoux, and R. Lemaire, Solid State Comm. **10,** 1149-1151 (1973).

7 O. Bostanjoglo and H. P. Gemund, Phys. Status Solidi **A 17,** 115 (1973).

8 O. Bostanjoglo and H. P. Gemund, Phys. Status Solidi **A 48,** 41 (1978).

9 J. A. Baldwin, F. Milstein, R. C. Wong, and J. L. West, J. Appl. Phys. **48,** 2612-2617 (1977).

10 W. Reihemann and E. Nembach, J. Appl. Phys. **55,** 1081-1091 (1984).

11 W. Reihemann and E. Nembach, J. Appl. Phys. **57,** 476 (1986).

12 E. M. Chudnovsky and L. Gunther, Phys. Rev. Lett. **60,** 661-664 (1988).

13 M. Enz and R. Schilling, J. Phys. C: Solid State Phys. **19,** 1765-1770 (1986).

14 J. L. van Hemmen and A. Süto, Europhys. Lett. **1,** 481 (1986).

15 D. D. Awschalom, D. P. DiVincenzo, and J. F. Smyth, Science **258,** 414-421 (1992).

16 J. Tejada, Science **272,** 424 (1996).

17 J. Tejada, X. X. Zhang, and E. M. Chudnovsky, Phys. Rev. B **47,** 14997 (1993).

18 J. Tejada and X. X. Zhang, J. Magn. Magn. Mater. **140-144,** 1815 (1995).

19 C. Paulsen, L. C. Sampaio, B. Barbara, R. Tucoulou-Tachoueres, D. Fruchard, A. Marchand, J. L. Tholence, and M. Uehara, Europhys. Lett. **19,** 643-648 (1992).

20 J. I. Arnaudas, A. del Moral, C. de la Fuente, and P. A. J. de Groot, Phys. Rev. B **47,** 11924-11934 (1993).

21 M. M. Ibrahim, S. Darwish, and M. S. Seehra, Phys. Rev. B **51,** 2955-2959 (1995).

22 L. Gunther, in *Qunatum Tunneling of Magnetization*, edited by L. Gunther and B. Barbara (Kluwer, Amsterdam, 1995), p. 413.

23 X. X. Zhang, J. Tejada, A. Roig, O. Nikolov, and E. Molins, J. Magn. Magn. Mater. **L235,** 137 (1994).

24 J. R. Friedman, M. P. Sarachik, J. Tejada, J. Maciejewski, and R. Ziolo, J. Appl. Phys. **79,** 6031-6033 (1996).

25 J. R. Friedman, M. P. Sarachik, J. Tejada, and R. Ziolo, Phys. Rev. Lett. **76,** 3830-3833 (1996).

26 J. M. Hernandez, X. X. Zhang, F. Luis, J. Bartolomé, J. Tejada, and R. Ziolo, Europhys. Lett. **35,** 301-306 (1996).

27 J. M. Hernandez, X. X. Zhang, F. Luis, J. Tejada, J. R. Friedman, M. P. Sarachik, and R. Ziolo, submitted to Phys. Rev. B (1996).

28 J. R. Friedman, M. P. Sarachik, J. M. Hernandez, X. X. Zhang, J. Tejada, E. Molins, and R. Ziolo, submitted to J. Appl. Phys. (1996).

29 L. Thomas, F. Lionti, R. Ballou, D. Gatteschi, R. Sessoli, and B. Barbara, Nature **383,** 145-147 (1996).

30 E. M. Chudnovsky, JETP **50,** 1035 (1980).

31 P. C. E. Stamp, E. M. Chudnovsky, and B. Barbara, Int. J. Mod. Phys. B **6,** 1355-1473 (1992).

32 R. Schilling, in *Quantum Tunneling of Magnetization*, edited by L. Gunther and B. Barbara (Kluwer, Amsterdam, 1995).

33 J. L. van Hemmen and A. Süto, in *Quantum Tunneling of Magnetization*, edited by L. Gunther and B. Barbara (Kluwer, Amsterdam, 1995).

[34] A. Garg and G. H. Kim, Phys. Rev. Lett. **63,** 2512 (1989).

[35] A. Garg and G. H. Kim, J. Appl. Phys. **67,** 5669-5671 (1990).

[36] B. Barbara, L. C. Sampaio, J. E. Wegrowe, B. A. Ratnam, A. Marchand, C. Paulsen, M. A. Novak, J. L. Tholence, M. Uehara, and D. Fruchart, J. Appl. Phys. **73,** 6703-6708 (1993).

[37] B. Barbara, W. Wernsdorfer, L. C. Sampaio, J. G. Park, C. Paulsen, M. A. Novak, R. Ferré, D. Mailly, R. Sessoli, A. Caneschi, K. Hasselbach, A. Benoit, and L. Thomas, Journal of Magnetism and Magnetic Materials **140-144,** 1825-1828 (1995).

[38] J. Tejada and X. X. Zhang, J. Appl. Phys. **73,** 6709 (1995).

[39] C. Paulsen, J.-G. Park, B. Barbara, R. Sessoli, and A. Caneschi, J. Magn. Magn. Mater. **140-144,** 379-380 (1995).

[40] C. Paulsen, J.-G. Park, B. Barbara, R. Sessoli, and A. Caneschi, J. Magn. Magn. Mater. **140-144,** 1891-1892 (1995).

[41] C. Paulsen and J.-G. Park, in *Quantum Tunneling of Magnetization*, edited by L. Gunther and B. Barbara (Kluwer, Amsterdam, 1995), p. 189-207.

[42] M. A. Novak and R. Sessoli, in *Quantum Tunneling of Magnetization*, edited by L. Gunther and B. Barbara (Kluwer, Amsterdam, 1995), p. 171-188.

[43] A. Caneschi, D. Gatteschi, R. Sessoli, A. L. Barra, L. C. Brunel, and M. Guillot, J. Am. Chem. Soc. **113,** 5873-5874 (1991).

[44] R. Sessoli, H.-L. Tsai, A. R. Schake, S. Wang, J. B. Vincent, K. Folting, D. Gatteschi, G. Christou, and D. N. Hendrickson, J. Am. Chem. Soc. **115,** 1804-1816 (1993).

[45] R. Sessoli, D. Gatteschi, A. Caneschi, and M. A. Novak, Nature **365,** 141-143 (1993).

[46] M. A. Novak, R. Sessoli, A. Caneschi, and D. Gatteschi, J. Magn. Magn. Mater. **146,** 211-213 (1995).

[47] R. Sessoli, Mol. Cryst. Liq. Cryst. **274,** A 145 (1995).

[48] J. Villain, F. Hartmann-Boutron, R. Sessoli, and A. Rettori, Europhys. Lett. **27,** 159-164 (1994).

49 P. Politi, A. Rettori, F. Hartmann-Boutron, and J. Villain, Phys. Rev. Lett. **75,** 537-540 (1995).

50 F. Hartmann-Boutron, P. Politi, and J. Villain, preprint (1996).

51 T. Lis, Acta Cryst. B **36,** 2042-2046 (1980).

52 J. C. Gallop, (Adam Hilger, Bristol, 1991).

53 M. B. Ketchen, D. D. Awschalom, W. J. Gallagher, A. W. Kleinsasser, R. L. Sandstrom, J. R. Rozen, and B. Bumble, IEEE Trans. Mag. **MAG-25,** 1212-1215 (1989).

54 S. Foner, (1996).

55 D. A. Garanin, J. Phys. A: Math. Gen. **24,** L61-L62 (1991).

56 A. Garg, Phys. Rev. B **51,** 15161-15168 (1995).

57 A. L. Burin, N. V. Prokof'ev, and P. C. E. Stamp, Phys. Rev. Lett. **76,** 3040 (1996).

58 A. Burin, (1996).

59 S. Aubin and S. Spagna, (1996).

60 N. V. Prokof'ev and P. C. E. Stamp, to be published in J. Low. Temp. Phys. (1996).

61 R. Rouse, S. Han, and J. E. Lukens, Phys. Rev. Lett. **75,** 1614 (1995).

62 S. Han, R. Rouse, and J. E. Lukens, Phys. Rev. Lett. **76,** 3404 (1996).

63 S. Foner, Y. Shapira, D. Heiman, P. Becla, R. Kershaw, K. Dwight, and A. Wold, Phys. Rev. B **39,** 11793-11799 (1989).

64 Y. Shapira, J. Appl. Phys. **67,** 5090-5095 (1990).

65 K. L. Taft, C. D. Delfs, G. C. Papaefthymiou, S. Foner, D. Gatteschi, and S. J. Lippard, J. Am. Chem. Soc. **116,** 823-832 (1994).

66 J. J. Smit, L. J. de Jongh, D. de Klerk, R. L. Carlin, and C. J. Conner, Physica **86-88B,** 1147 (1977).

67 F. Varret, Y. Allain, and A. Miedan-Gros, Solid State Comm. **14,** 17-20 (1974).

68 V. Bindilatti, A. N. Anisimov, N. F. Oliveira, Y. Shapira, M. Goiran, F. Yang, S. Isber, M. Averous, and M. Demianiuk, Phys. Rev. B **50,** 16464-16467 (1994).

69 M. Uehara, B. Barbara, B. Dieny, and P. C. E. Stamp, Physics Letters **114A,** 23-26 (1986).

70 A. Paduan-Filho, C. C. Becerra, V. B. Barbeta, Y. Shapira, J. Campo, and F. Palicio, J. Magn. Magn. Mater. **140-144,** 1925-1926 (1995).